Linear Elastic Fracture Mechanics in Anisotropic Solids: Application to Fluid-Driven Crack Propagation

by

Hadrien Hyacinthe Laubie

Ingénieur de l'École Polytechnique (X2008)

Submitted to the Department of Civil and Environmental Engineering
in partial fulfillment of the requirements for the degree of

Master of Science in Civil and Environmental Engineering

at the

MASSACHUSETTS INSTITUTE OF TECHNOLOGY

June 2013

Author .....
Department of Civil and Environmental Engineering
May 17, 2013

Certified by .....
Franz-Josef Ulm
Professor of Civil and Environmental Engineering
Thesis Supervisor

Accepted by .....
Heidi M. Nepf
Departmental Committee for Graduate Students

Linear Elastic Fracture Mechanics in Anisotropic Solids: Application to Fluid-Driven Crack Propagation

by

Hadrien Hyacinthe Laubie

Submitted to the Department of Civil and Environmental Engineering
on May 17, 2013, in partial fulfillment of the
requirements for the degree of
Master of Science in Civil and Environmental Engineering

Abstract

Fracture mechanics is a field of continuum mechanics with the objective to predict how cracks initiate and propagate in solids. It has a wide domain of application. While aerospace engineers want to make sure a defect in a structure will not grow and possibly lead to failure, petroleum engineers try to increase the permeability of gas shale rocks by fracturing it. In this context, we introduce some elements of linear elastic fracture mechanics in anisotropic solids. Notably, a special attention is paid to transverse isotropy, often used to model rocks but also some piezoelectric materials or fiber-reinforced composites. We focus on brittle materials, that is, we consider only elastic deformations; we thus ignore dissipative phenomena other than the one associated with the creation of crack surface.

This thesis aims at understanding and predicting how pressurized cracks propagate in anisotropic brittle solids, in the framework of linear elastic fracture mechanics. The elastic coefficients relevant to the study of a pressurized crack in such materials are identified. Interestingly, they are directly related to quantities easily measured in a lab at the macroscopic scale through indentation tests and acoustic measurements. As an application, the fluid-driven crack problem is addressed. It is shown that the classical tools of the isotropic fluid-driven crack model remain valid in anisotropy, provided the appropriate elastic constants are used. We introduce the concept of crack-shape adaptability: the ability of three-dimensional cracks to shape with the elastic content. This ability could be ruled by three criteria herein introduced. The first one is based on the maximum dissipation principle. The second one is based on Irwin's theory of fracture and the concept of stress intensity factors. As for the third one, it is based on Griffith's energetic theory. While the first criterion predicts that circular cracks are more favorable, the others predict that elliptical shapes are more likely to be seen.

This thesis could be valuable in the context of the stimulation of unconventional oil and gas from organic-rich shale.

Thesis Supervisor: Franz-Josef Ulm
Title: Professor of Civil and Environmental Engineering

Acknowledgments

I would like to express my sincere gratitude to my advisor, Prof. Franz-Josef Ulm. His knowledge in a wide range of disciplines and his enthusiasm guided me through the challenges of accomplishing this work. I am also thankful for the financial support provided through the Schoettler Scholarship, the X-Shale Project and the Concrete Sustainability Hub.

I wish to acknowledge the help provided by Brice Lecampion and Romain Prioul from the Schlumberger-Doll Research Center. Their expertise on the subject and their constructive recommendations were valuable assets to this thesis.

I am particularly grateful to all the members of the Hub. The excellent atmosphere in the group made my research work a lot more enjoyable. Special thanks go to Sina for the reading suggestions he gave me when I joined the group and to Siavash for giving a first proofreading to this thesis.

I would also like to thank Prof. Frédéric Bonnans, Attilio Frangi and Patrick Huerre from the École Polytechnique who helped me entering the Master of Science program at MIT.

I am thankful to my dear family who encouraged me to pursue my graduate studies abroad, even if it meant being far away for a long time.

I would like to express my great appreciation to Samy and Andrés never short of good advice.

Last but not least, life in Cambridge would not have been the same without the French gang: Julien, the 494 Mass Ave and of course the 784 Main St with whom I experienced my first bed-bug invasion, seen by one liked by none, earthquake, hurricane, blizzard... Merci.

Contents

List of Figures

List of Tables

Chapter 1

Introduction

1.1 Industrial context

Over the past decade, unconventional resources of energy such as gas shale have gained a specific attention from the oil and gas industry. Analysts from the United States Department of Energy predicted [46] that by 2035, the share of shale gas in the U.S. natural gas production could reach 49% while it represented only 23% in 2010.

Unlike more conventional resources, gas shale rock has a very low permeability. In order to fully recover the gas trapped in the nanopores of the rock, it became common practice to stimulate the rock by hydraulic fracturing. In fact, it is the only known method to stimulate a shale formation with an intrinsically low permeability. The technique consists of fluid injection in already existing cracks generated by means of explosives. The pressurized fluid makes the fractures propagate, and therefore increases the permeability of the rock.

In order to improve the well productivity but also to reduce the environmental footprint of the shale gas industry, a better understanding of crack propagation in anisotropic media is valuable.

1.2 Research objectives and approach

In this thesis, we intend to better understand and predict how a crack propagates in an elastically anisotropic brittle medium, the model we consider for rock-type materials.

To do so, we chose to first focus on two-dimensional crack propagation. This problem has been extensively studied in the case of cracks in isotropic media subjected to pure pressure

loading (see for instance Ref. [1, 10, 11, 15, 19, 21, 42]). For our part, we consider cracks in anisotropic media possibly subjected to shear conditions due to some stress anisotropy existing in the field conditions.

We then add one more dimension to the problem, by considering elliptical cracks. This raised an original, at least to our knowledge, question on the crack-shape adaptability due to elastic anisotropy.

The overall goal of this thesis is to identify the relevant elastic coefficients intervening in the pressurized crack problem, the most favorable directions for crack propagation and the preferred crack-shapes to be seen in the field.

1.3 Thesis outline

To meet the objectives presented here above, we first recall in Chapter 2 some relations of plane-strain problems in transverse isotropy and introduce relevant concepts of linear elastic fracture mechanics (LEFM). This Chapter thus provides the tools necessary to address a fracture mechanics problem under plane-strain conditions. The scratch testing of anisotropic materials illustrates the formalism introduced in the Chapter.

Chapter 3 provides the full solution of the plane-strain crack problem. The problem consists in obtaining the stress, strain and displacement fields in a cracked body subjected to loading conditions involving either prescribed stresses or prescribed displacements on the crack surface. To do so, we use the complex potential theory introduced by Muskhelishvili [35] in the isotropic case, and extended to the anisotropic case through Lekhnitskii's formalism [32].

In Chapter 4, the fluid-driven crack propagation problem is addressed. We show that the coupled fluid/solid problem can be broken into two weak coupling problems: a solid problem and a fluid problem. While the solid problem has been addressed in Chapter 3, the fluid problem is formulated in the context of the lubrication theory. A numerical method to solve the non-linear strong coupling between the solid and fluid phases is also introduced.

Chapter 5 then deals with three-dimensional flat ellipsoidal cracks subjected to uniform loadings. After summarizing Hoenig's main results [26], we apply them to the specific case of transverse isotropy. Different criteria aiming to find how a crack could adapt to the elasticity are introduced.

Finally, Chapter 6 provides conclusions with the main findings and recommendations of future work.

Chapter 2

The plane-strain problem in transverse isotropy

In this Chapter, we present the necessary tools to solve linear elastic fracture mechanics problems in transversely isotropic (TI) media, in the particular case of plane-strain state. As a warm-up, we study a specific fracture mechanics problem, the scratch test on a TI material. The study of this problem will allow us to introduce some basic concepts of fracture mechanics within the framework of plane-strain state.

We will first give the expression of the two-dimensional generalized Hooke's law for different orientations of the material's orthonormal basis. We will then write the governing equations of continuum mechanics in the specific case of generalized plane-strain and introduce the notion of complex potentials. After recalling some important features of linear elastic fracture mechanics, we will address the scratch problem in transverse isotropy.

2.1 Plane-strain Hooke's law in transverse isotropy

2.1.1 Three-dimensional Hooke's law in transverse isotropy

Consider an elastic material with elastic properties characterized by means of the fourth-order compliance tensor $\underline{\underline{\underline{\underline{S}}}}$. The stress-strain relationship is written as $\epsilon_{ij} = S_{ijkl}\sigma_{kl}$ (with $\underline{\underline{\epsilon}}$ the strain tensor, $\underline{\underline{\sigma}}$ the stress tensor and where we use Einstein summation convention). Since the stress and the strain tensors are symmetric ($\epsilon_{ij} = \epsilon_{ji}$ and $\sigma_{ij} = \sigma_{ji}$), the compliance tensor must satisfy the (minor) symmetries $S_{ijkl} = S_{jikl} = S_{ijlk}$. In addition, since the

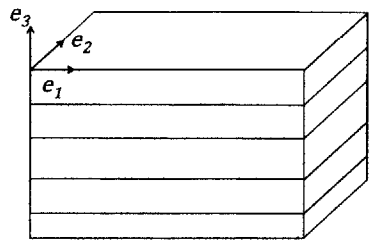

Figure 2-1: Definition of the material canonical basis of a TI medium.

strain energy density $\psi = \frac{1}{2}\underline{\underline{\sigma}} : \underline{\underline{\underline{\underline{S}}}} : \underline{\underline{\sigma}} = \frac{1}{2}\sigma_{ij}S_{ijkl}\sigma_{kl}$ should not change when interchanging subscripts ij and kl, the compliance tensor also satisfies the (major) symmetry $S_{ijkl} = S_{klij}$. From these symmetries, one deduces that the elastic properties of a material are fully characterized by means of twenty-one independent compliance constants.
Using Voigt notation, one can take advantage of these symmetries to simplify some notations. Indeed, one can reduce to two the number of subscripts of the compliance constants by regrouping into one subscript the first two and last two subscripts ($S_{\{ij\}\to\alpha,\{kl\}\to\beta}$) according to Table 2.1. Voigt notation is extensively used in e.g. finite-element method (see for instance [7]).

The particularity of TI materials is that their properties, and notably the *elastic* properties, are invariant by rotation about an axis. One can deduce that the number of independent elastic constants of such materials is reduced to five.

We introduce the orthonormal basis $(\underline{e}_1, \underline{e}_2, \underline{e}_3)$ where $\underline{e}_3$ is the axis of rotational symmetry. Any plane parallel to vect$(\underline{e}_1, \underline{e}_2)$ is then a plane of isotropy (see Fig. 2-1). The basis $(\underline{e}_1, \underline{e}_2, \underline{e}_3)$ will be referred to as the *material canonical* orthonormal basis in the sense that in this basis, the three-dimensional Hooke's law exhibits its simplest form. Specifically, in this basis, using the Voigt notation, the generalized Hooke's law for a TI material is written in terms of the compliance constants as:

Classical notation ij/kl	11	22	33	23	32	13	31	12	21
Voigt notation α/β	1	2	3	4	4	5	5	6	6

Table 2.1: From the classical notation to Voigt notation.

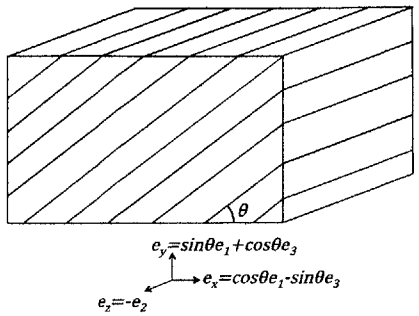

Figure 2-2: First rotation considered, $\underline{e}_2$ parallel to $\underline{e}_z$.

$$\begin{pmatrix} \epsilon_{11} \\ \epsilon_{22} \\ \epsilon_{33} \\ 2\epsilon_{23} \\ 2\epsilon_{13} \\ 2\epsilon_{12} \end{pmatrix} = \begin{bmatrix} S_{11} & S_{12} & S_{13} & 0 & 0 & 0 \\ S_{12} & S_{11} & S_{13} & 0 & 0 & 0 \\ S_{13} & S_{13} & S_{33} & 0 & 0 & 0 \\ 0 & 0 & 0 & S_{44} & 0 & 0 \\ 0 & 0 & 0 & 0 & S_{44} & 0 \\ 0 & 0 & 0 & 0 & 0 & 2(S_{11} - S_{12}) \end{bmatrix} \begin{pmatrix} \sigma_{11} \\ \sigma_{22} \\ \sigma_{33} \\ \sigma_{23} \\ \sigma_{13} \\ \sigma_{12} \end{pmatrix} \tag{2.1}$$

For the sake of simplicity, we chose here to express Hooke's law in terms of the five compliance constants $\{S_{11}, S_{12}, S_{13}, S_{33}, S_{44}\}$ instead of the stiffness constants $\{C_{11}, C_{12}, C_{13}, C_{33}, C_{44}\}$ or the set of elastic constants $\{E_1, E_3, \nu_{12}, \nu_{13}, G_{13}\}$. The relationships linking one set of constants to the others are given in Appendix B.

In general, the basis $(\underline{e}_1, \underline{e}_2, \underline{e}_3)$ is not be the most relevant one for the problems considered. For instance, if one wants to study the propagation of a crack in the plane $(\underline{e}_x, \underline{e}_z)$ that originally belongs to the plane $y = 0$ that makes an angle θ with the plane $x_3 = 0$, the basis $(\underline{e}_x, \underline{e}_y, \underline{e}_z)$ will be more relevant. We will then need a stress-strain relationship analogous to the previous one in the rotated basis $(\underline{e}_x, \underline{e}_y, \underline{e}_z)$. In what follows, we will consider two rotations; the first type of rotation will be such that $\underline{e}_2$ is parallel to $\underline{e}_z$ (see Fig. 2-2) while for the second one, $\underline{e}_2$ will be parallel to $\underline{e}_y$ (see Fig. 2-3).

Later on, we will consider structures or material systems in which the length in one direction (say, in the z-direction) is much greater than the others. It is readily understood that such a problems is two-dimensional, for which the strains ϵ_{xz}, ϵ_{yz} and ϵ_{zz} vanish. Under

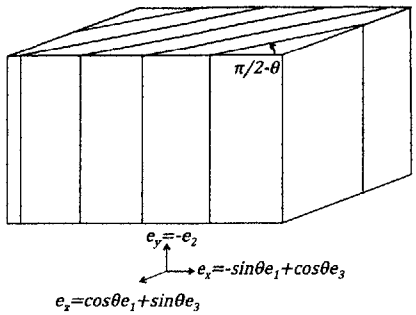

Figure 2-3: Second rotation considered, $\underline{e}_2$ parallel to $\underline{e}_y$.

these *generalized* plane-strain conditions, the only independent stress components are σ_{xx}, σ_{yy} and σ_{xy}, as shown here below. For this case, we will employ a two-dimensional Hooke's law of the form:

$$\{\epsilon\} = [f]\{\sigma\} \tag{2.2}$$

with $[f]$ a 3x3 symmetric matrix, $\{\epsilon\} = {}^t[\epsilon_{xx} \;\; \epsilon_{yy} \;\; 2\epsilon_{xy}]$, and $\{\sigma\} = {}^t[\sigma_{xx} \;\; \sigma_{yy} \;\; \sigma_{xy}]$.

2.1.2 Two-dimensional Hooke's law in transverse isotropy: first rotation considered

Consider the orthonormal basis $(\underline{e}_x, \underline{e}_y, \underline{e}_z)$ where $\underline{e}_2$ is parallel to $\underline{e}_y$ (see Fig. 2-2). From now on, roman subscripts (i, j) will refer to the material canonical basis while Greek subscripts (α, β) will refer to the basis $(\underline{e}_x, \underline{e}_y, \underline{e}_z)$. This basis is such that $\underline{e}_\alpha = \mathcal{P}_{\alpha i}\underline{e}_i$, where:

$$\mathcal{P} = \begin{bmatrix} \cos\theta & 0 & -\sin\theta \\ \sin\theta & 0 & \cos\theta \\ 0 & -1 & 0 \end{bmatrix} \tag{2.3}$$

The compliance tensor $\underline{\underline{S}}'$ in the basis $(\underline{e}_x, \underline{e}_y, \underline{e}_z)$ is deduced from the one in the material canonical basis using the transformation formula (for more details, the reader is directed to Appendix D or to Ref. [32]): $S'_{\alpha\beta} = (\mathcal{R}_\epsilon)_{\alpha i} S_{ij} \left({}^t\mathcal{R}_\epsilon\right)_{j\beta}$ for $(\alpha, \beta) \in [\![1, 6]\!]x[\![1, 6]\!]$[1] where the transformation matrix $[R_\epsilon]$ is defined as:

[1] $[\![a, b]\!] = \{j \in \mathbb{Z} | a \leq j \leq b\}$.

$$[R_\epsilon] = \begin{bmatrix} \cos^2\theta & 0 & \sin^2\theta & 0 & -\cos\theta\sin\theta & 0 \\ \sin^2\theta & 0 & \cos^2\theta & 0 & \cos\theta\sin\theta & 0 \\ 0 & 1 & 0 & 0 & 0 & 0 \\ 0 & 0 & 0 & -\cos\theta & 0 & -\sin\theta \\ 0 & 0 & 0 & \sin\theta & 0 & -\cos\theta \\ 2\sin\theta\cos\theta & 0 & -2\sin\theta\cos\theta & 0 & \cos^2\theta - \sin^2\theta & 0 \end{bmatrix} \tag{2.4}$$

Using Voigt notation, the compliance tensor $\underline{\underline{\underline{\underline{S'}}}}$ can then be written as (to simplify the writings, we used the following notations: while S_{ij} refers to the material canonical basis $(\underline{e}_1, \underline{e}_2, \underline{e}_3)$, S'_{ij} refers to the basis $(\underline{e}_x, \underline{e}_y, \underline{e}_z)$ so that $S'_{11} = S_{xx} \neq S_{11}$ etc.):

$$\left[S'\right](\theta) = \begin{bmatrix} S'_{11}(\theta) & S'_{12}(\theta) & S'_{13}(\theta) & 0 & 0 & S'_{16}(\theta) \\ S'_{12}(\theta) & S'_{22}(\theta) & S'_{23}(\theta) & 0 & 0 & S'_{26}(\theta) \\ S'_{13}(\theta) & S'_{23}(\theta) & S'_{33}(\theta) & 0 & 0 & S'_{36}(\theta) \\ 0 & 0 & 0 & S'_{44}(\theta) & S'_{45}(\theta) & 0 \\ 0 & 0 & 0 & S'_{45}(\theta) & S'_{55}(\theta) & 0 \\ S'_{16}(\theta) & S'_{26}(\theta) & S'_{36}(\theta) & 0 & 0 & S'_{66}(\theta) \end{bmatrix} \tag{2.5}$$

The three-dimensional Hooke's law in the rotated basis is then:

$$\left\{\epsilon'\right\} = \left[S'\right]\left\{\sigma'\right\} \tag{2.6}$$

where $\{\epsilon'\} = {}^t[\epsilon_{xx}\ \epsilon_{yy}\ \epsilon_{zz}\ 2\epsilon_{yz}\ 2\epsilon_{xz}\ 2\epsilon_{yz}]$ and $\{\sigma'\} = {}^t[\sigma_{xx}\ \sigma_{yy}\ \sigma_{zz}\ \sigma_{yz}\ \sigma_{xz}\ \sigma_{yz}]$.

Consider then the plane-strain conditions $\epsilon_{12} = \epsilon_{22} = \epsilon_{32} = 0$, which are strictly equivalent to letting $\epsilon_{xz} = \epsilon_{yz} = \epsilon_{zz} = 0$. Using the stress-strain relationship (2.6), these three equations can be rewritten as:

$$\begin{cases} 0 &= S'_{11}\sigma_{xx} + S'_{23}\sigma_{yy} + S'_{33}\sigma_{zz} + S'_{36}\sigma_{xy} \\ 0 &= S'_{44}\sigma_{yz} + S'_{45}\sigma_{xz} \\ 0 &= S'_{45}\sigma_{yz} + S'_{55}\sigma_{xz} \end{cases} \tag{2.7}$$

Considering only the last two equations in (2.7), the determinant Δ of the sub-system is: $\Delta = S'_{44}S'_{55} - S'^2_{45} = 2S_{44}(S_{11} - S_{12})$. For $\Delta \neq 0$, we thus deduce that:

$$\sigma_{xz} = \sigma_{yz} = 0 \tag{2.8}$$

Moreover, the first equation in (2.7) allows us to express σ_{zz} in terms of σ_{xx}, σ_{yy} and σ_{xy} as:

$$\sigma_{zz} = -\frac{1}{S'_{33}}\left[S'_{13}\sigma_{xx} + S'_{23}\sigma_{yy} + S'_{36}\sigma_{xy}\right] \tag{2.9}$$

where $S'_{33} = \frac{1}{E_1} \neq 0$ (the materials we consider are deformable).

Thus, under plane-strain conditions, Eq. (2.6) together with (2.9) and (2.8) gives the strain-stress relationship:

$$\begin{pmatrix} \epsilon_{xx} \\ \epsilon_{yy} \\ 2\epsilon_{xy} \end{pmatrix} = \begin{bmatrix} f_{11}(\theta) & f_{12}(\theta) & f_{13}(\theta) \\ f_{12}(\theta) & f_{22}(\theta) & f_{23}(\theta) \\ f_{13}(\theta) & f_{23}(\theta) & f_{33}(\theta) \end{bmatrix} \begin{pmatrix} \sigma_{xx} \\ \sigma_{yy} \\ \sigma_{xy} \end{pmatrix} \tag{2.10}$$

with:

$$\begin{cases} f_{11}(\theta) &= S'_{11} - \frac{S'^2_{13}}{S'_{33}} \\ f_{12}(\theta) &= S'_{12} - \frac{S'_{13}S'_{23}}{S'_{33}} \\ f_{13}(\theta) &= S'_{16} - \frac{S'_{13}S'_{36}}{S'_{33}} \\ f_{22}(\theta) &= S'_{22} - \frac{S'^2_{23}}{S'_{33}} \\ f_{23}(\theta) &= S'_{26} - \frac{S'_{23}S'_{36}}{S'_{33}} \\ f_{33}(\theta) &= S'_{66} \end{cases} \tag{2.11}$$

The three remaining stress components verify:

$$\begin{cases} \sigma_{yz} &= 0 \\ \sigma_{xz} &= 0 \\ \sigma_{zz} &= -\frac{1}{S'_{33}}\left[S'_{13}\sigma_{xx} + S'_{23}\sigma_{yy} + S'_{36}\sigma_{xy}\right] \end{cases} \tag{2.12}$$

2.1.3 Two-dimensional Hooke's law in transverse isotropy: second rotation considered

Consider now the orthonormal basis $(\underline{e}_x, \underline{e}_y, \underline{e}_z)$ where $\underline{e}_2$ is parallel to $\underline{e}_z$ (see Fig. 2-3). This basis is such that $\underline{e}_\alpha = \mathcal{P}_{\alpha i}\underline{e}_i$, with:

$$\mathcal{P} = \begin{bmatrix} -\sin\theta & 0 & \cos\theta \\ 0 & -1 & 0 \\ \cos\theta & 0 & \sin\theta \end{bmatrix} \tag{2.13}$$

The compliance tensor $\underline{\underline{\underline{\underline{S'}}}}$ in the basis $(\underline{e}_x, \underline{e}_y, \underline{e}_z)$ is deduced from the one in the material canonical basis using the transformation formula: $S'_{\alpha\beta} = (\mathcal{R}_\epsilon)_{\alpha i} S_{ij} \left({}^t\mathcal{R}_\epsilon\right)_{j\beta}$ for $(\alpha, \beta) \in [\![1, 6]\!]^2$ where the transformation matrix $[R_\epsilon]$ is given as:

$$[R_\epsilon] = \begin{bmatrix} \sin^2\theta & 0 & \cos^2\theta & 0 & -\cos\theta\sin\theta & 0 \\ 0 & 1 & 0 & 0 & 0 & 0 \\ \cos^2\theta & 0 & \sin^2\theta & 0 & \cos\theta\sin\theta & 0 \\ 0 & 0 & 0 & -\sin\theta & 0 & -\cos\theta \\ -2\cos\theta\sin\theta & 0 & 2\cos\theta\sin\theta & 0 & \cos^2\theta - \sin^2\theta & 0 \\ 0 & 0 & 0 & -\cos\theta & 0 & \sin\theta \end{bmatrix} \tag{2.14}$$

The derivation of the stress-strain relationship for the rotation studied in Part 2.1.2 applies step by step, *mutatis mutandis*, for the rotation studied here. The strain-stress relationship can then be written as:

$$\begin{pmatrix} \epsilon_{xx} \\ \epsilon_{yy} \\ 2\epsilon_{xy} \end{pmatrix} = \begin{bmatrix} f_{11}(\theta) & f_{12}(\theta) & 0 \\ f_{12}(\theta) & f_{22}(\theta) & 0 \\ 0 & 0 & f_{33}(\theta) \end{bmatrix} \begin{pmatrix} \sigma_{xx} \\ \sigma_{yy} \\ \sigma_{xy} \end{pmatrix} \tag{2.15}$$

with:

$$\begin{cases} f_{11}(\theta) &= S'_{11} + \frac{S'_{13}(S'_{35}S'_{15}-S'_{13}S'_{55})+S'_{15}(S'_{35}S'_{13}-S'_{33}S'_{15})}{S'_{33}S'_{55}-{S'_{35}}^2} \\ f_{12}(\theta) &= S'_{12} + \frac{S'_{13}(S'_{25}S'_{35}-S'_{23}S'_{55})+S'_{15}(S'_{23}S'_{35}-S'_{25}S'_{33})}{S'_{33}S'_{55}-{S'_{35}}^2} \\ f_{22}(\theta) &= S'_{22} + \frac{S'_{23}(S'_{35}S'_{25}-S'_{23}S'_{55})+S'_{25}(S'_{35}S'_{23}-S'_{33}S'_{25})}{S'_{33}S'_{55}-{S'_{35}}^2} \\ f_{33}(\theta) &= S'_{66} - \frac{{S'_{46}}^2}{S'_{44}} \end{cases} \tag{2.16}$$

The three remaining stress components verify:

$$\begin{cases} \sigma_{yz} &= -\frac{S'_{46}}{S'_{44}}\sigma_{xy} \\ \sigma_{xz} &= \frac{S'_{35}S'_{13}-S'_{33}S'_{15}}{S'_{33}S'_{55}-{S'_{35}}^2}\sigma_{xx} - \frac{S'_{35}S'_{23}-S'_{33}S'_{25}}{S'_{33}S'_{55}-{S'_{35}}^2}\sigma_{yy} \\ \sigma_{zz} &= \frac{S'_{35}S'_{15}-S'_{55}S'_{13}}{S'_{33}S'_{55}-{S'_{35}}^2}\sigma_{xx} - \frac{S'_{35}S'_{25}-S'_{55}S'_{23}}{S'_{33}S'_{55}-{S'_{35}}^2}\sigma_{yy} \end{cases} \tag{2.17}$$

2.2 Plane-strain governing equations

With the expressions of the three independent strains and the three independent stresses just derived, we try to expressiong the governing equations of continuum mechanics for the plane-strain state.

2.2.1 Potential method

Considering all the fields independent of the z coordinate and neglecting body forces, the equilibrium equation $\mathrm{div}\underline{\underline{\sigma}} = \underline{0}$ is written as:

$$\begin{cases} \sigma_{xx,x} + \sigma_{xy,y} &= 0 \\ \sigma_{xy,x} + \sigma_{yy,y} &= 0 \end{cases} \tag{2.18}$$

where $(.)_{,x_i} = \frac{\partial .}{\partial x_i}$.

Then, introduce the potential $\Psi = \Psi(x, y)$, and express the stresses in terms of the partial derivatives as follows:

$$\begin{cases} \sigma_{xx} &= \Psi_{,yy} \\ \sigma_{yy} &= \Psi_{,xx} \\ \sigma_{xy} &= -\Psi_{,xy} \end{cases} \tag{2.19}$$

Equation (2.19) ensures that for any stress function Ψ, the equilibrium condition $\mathrm{div}\underline{\underline{\sigma}} = \underline{0}$ is satisfied.

The potential Ψ must satisfy some constraints. Indeed it has to satisfy the compatibility condition which ensures that a displacement field $\underline{\xi}$ exists, such that $\underline{\underline{\epsilon}} = \frac{1}{2}\left(\underline{\underline{\nabla\xi}}(\underline{x}) + {}^t\underline{\underline{\nabla\xi}}(\underline{x})\right)$. In plane-strain, it merely consists in the single equation:

$$\epsilon_{xx,yy} + \epsilon_{yy,xx} - 2\epsilon_{xy,xy} = 0 \tag{2.20}$$

Using the stress-strain relationship (2.2) in Eq. (2.20), the strain tensor $\underline{\underline{\epsilon}}$ can be derived from a displacement field $\underline{\xi}$ if:

$$\begin{aligned} f_{11}(\theta)\Psi_{,4y} + f_{22}(\theta)\Psi_{,4x} + (f_{33}(\theta) + \ & 2f_{12}(\theta))\Psi_{,2x2y} \\ & -2f_{13}(\theta)\Psi_{,x3y} - 2f_{23}(\theta)\Psi_{,3xy} = 0 \end{aligned} \tag{2.21}$$

where, to simplify the notation, we used $\Psi_{,2x2y} = \Psi_{,xxyy}$ etc.

Let us introduce the linear operator $\mathcal{L}_\theta$ defined as:

$$\begin{aligned} \mathcal{L}_\theta(.) = f_{11}(\theta)(.)_{,4y} + f_{22}(\theta)(.)_{,4x} + \ & (f_{33}(\theta) + 2f_{12}(\theta))(.)_{,2x2y} \\ & -2f_{13}(\theta)(.)_{,x3y} - 2f_{23}(\theta)(.)_{,3xy} \end{aligned} \tag{2.22}$$

This allows us to rewrite the compatibility equation (2.21) in a simpler form:

$$\mathcal{L}_\theta(\Psi) = 0 \tag{2.23}$$

To solve any plane-strain problem, one has to find a potential Ψ satisfying the boundary conditions of the problem and the compatibility equation (2.23).

Remark 1 *In the case of an isotropic material, the compatibility equation expressed in terms of the stress components is known as the Beltrami equation. Furthermore, since* $f_{11}(\theta) = f_{22}(\theta) = \frac{1-\nu^2}{E}$, $f_{12}(\theta) = -\frac{\nu}{E}(1+\nu)$, $f_{13}(\theta) = f_{23}(\theta) = 0$ *and* $f_{33}(\theta) = \frac{2(1+\nu)}{E}$, *Eq. (2.23) can be simplified and gives the well-known equation:*

$$\Psi_{,4y} + \Psi_{,4x} + 2\Psi_{,2x2y} = \Delta\Delta\Psi = 0 \tag{2.24}$$

That is, Ψ *is biharmonic (the* $\mathcal{L}$ *operator is such that* $\mathcal{L} = \Delta\Delta$ *where* $\Delta(.) = (.)_{,xx} + (.)_{,yy}$ *is the two-dimensional Laplacian). In this sense, Eq.* (2.23) *is a mere generalization to the*

plane-strain anisotropic case.

2.2.2 Complex potential theory

We saw in the previous Section that solving an elasticity problem in plane-strain can be reduced to solving for a potential Ψ satisfying some constraints. The determination of such a potential is usually far from obvious. For elasticity problems in isotropy, Muskhelishvili [35] provides an expression of the (biharmonic) potential Ψ in terms of two analytic functions of the complex variable $z = x + iy$.

Lekhnitskii [32] proposed an analogous method that is summarized here below.

Given the two-dimensional compliance matrix $[f]$ defined by Eq. (2.2), introduce the fourth-order polynomial $P_{[f]}(X)$:

$$P_{[f]}(X) = f_{11}X^4 - 2f_{13}X^3 + (2f_{12} + f_{33})\,X^2 - 2f_{23}X + f_{22} \tag{2.25}$$

Let η be a complex number, possibly different from the imaginary unit i, and introduce a holomorphic function F of the complex variable $z = x + \eta y$. The $\mathcal{L}_\theta$ operator introduced in Eq. (2.22) applied to F gives:

$$\mathcal{L}_\theta(F(z)) = P_{[f]}(\eta).\frac{d^4F}{dz^4}(z) \tag{2.26}$$

The compatibility equation (2.23) will then be satisfied by any function $\Psi(z) = F(x + \eta y)$[2] if η is a root of $P_{[f]}$.

Lekhnitskii proved that the roots of $P_{[f]}$ are always complex. Let μ_1 and μ_2 be the roots of $P_{[f]}$ with a strictly positive imaginary part. Then, introduce the two complex variables $z_1 = x + \mu_1 y$ and $z_2 = x + \mu_2 y$, and the two complex potentials Φ_1 and Φ_2.
In the absence of body forces, and ignoring the rigid-body displacements, the general expressions of the stresses and displacements ensuring the equilibrium condition (2.19), com-

[2]Since the F function may be complex, one can define Ψ as $\Psi = \mathrm{Re}\,[F]$ to ensure that the stresses and strains be real valued functions.

patibility equation (2.23) and the constitutive equation (2.2) are given by the relationships:

$$\begin{cases} \sigma_{xx}(z) &= 2\,\mathrm{Re}\left[(\mu_1)^2\Phi_1'(z_1) + (\mu_2)^2\Phi_2'(z_2)\right] \\ \sigma_{yy}(z) &= 2\,\mathrm{Re}\left[\Phi_1'(z_1) + \Phi_2'(z_2)\right] \\ \sigma_{xy}(z) &= -2\,\mathrm{Re}\left[\mu_1\Phi_1'(z_1) + \mu_2\Phi_2'(z_2)\right] \\ \xi_x(z) &= 2\,\mathrm{Re}\left[p_1\Phi_1(z_1) + p_2\Phi_2(z_2)\right] \\ \xi_y(z) &= 2\,\mathrm{Re}\left[q_1\Phi_1(z_1) + q_2\Phi_2(z_2)\right] \end{cases} \tag{2.27}$$

where:

$$\begin{cases} p_i &= f_{11}(\mu_i)^2 + f_{12} - f_{13}\mu_i \\ q_i &= f_{12}\mu_i + \frac{f_{22}}{\mu_i} - f_{23} \end{cases} \tag{2.28}$$

for $i = 1$ or 2 and where $\Phi_i'(z_i) = \frac{d\Phi_i}{dz_i}(z_i)$.

Solving any problem then reduces to finding the complex potentials Φ_1 and Φ_2 satisfying the stress and/or displacement boundary conditions.

2.2.3 A reminder of Plemelj's formula and Hilbert's problem [31]

Some additional mathematical tools that will turn out usefule are briefly recalled.

The Plemelj formula

Consider $\mathcal{L}$ an oriented line, and h an analytic function defined and differentiable along $\mathcal{L}$. We define f the $\mathbb{C} \setminus \mathcal{L}$-analytic function of the complex variable $z = x + iy$ as:

$$f(z) = \frac{1}{2i\pi}\int_{\mathcal{L}} \frac{h(t)}{t - z}dt \tag{2.29}$$

This integral is often referred to as the *Cauchy integral.*

Plemelj's formula states that[3]:

$$f(t_0^+) - f(t_0^-) = h(t_0), \qquad \forall t_0 \in \mathcal{L} \tag{2.30}$$

[3]Here and in what follows, the notation $t^\pm$ stands for $t^\pm = t \pm i\epsilon$, $\epsilon \to 0$, $\epsilon > 0$.

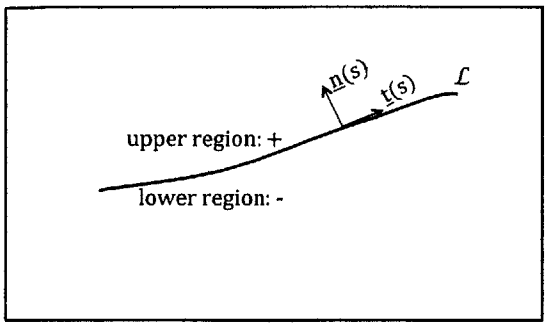

Figure 2-4: Two-dimensional crack.

The Hilbert problem

Given an oriented line $\mathcal{L}$ - whose boundaries in the complex plane are $a \in \mathbb{C}$ and $b \in \mathbb{C}$ - and given k, a function defined and differentiable on $\mathcal{L}$, Hilbert's problem consists of finding the analytic function f of complex variable z that vanishes when $|z| \to +\infty$, and that satisfies:

$$f(t_0^+) + f(t_0^-) = k(t_0), \qquad \forall t_0 \in \mathcal{L} \setminus \{a, b\} \tag{2.31}$$

The solution is given by:

$$f(z) = \frac{\mathcal{F}(z)}{2i\pi} \int_{t \in \mathcal{L}} \frac{k(t)dt}{\mathcal{F}(t^+)(t-z)} + C\mathcal{F}(z) \tag{2.32}$$

where C is a constant and $\mathcal{F}(z) = \frac{1}{\sqrt{(z-a)(z-b)}}$ ($\mathcal{F}$ is defined such that $\mathcal{F}(z) \sim \frac{1}{z}$ at infinity and its branch cut is $\mathcal{L}$).

2.3 Elements of linear elastic fracture mechanics

Since the theory of linear elastic fracture mechanics (LEFM) will be used extensively in the continuation, we here recall some elements of brittle fracture mechanics. For a general overview of the subject, the reader is referred to the first part of Leblond's review book [31].

2.3.1 The three fracture modes and stress intensity factors

In two-dimensions, a crack is defined as a line of discontinuity $\mathcal{L}$ parameterized by the curvilinear abscissa s. Let $\underline{n}(s)$ be the unit vector normal to $\mathcal{L}$ and pointing toward the upper surface; $\underline{t}(s)$ be the unit vector tangent to $\mathcal{L}$, and define $\underline{b} = \underline{t} \times \underline{n}$ (see Fig. 2-4). Let

s^+ and s^- refer to the upper and lower surfaces of the crack, respectively. The displacement jump $[\![\underline{\xi}]\!](s) = \underline{\xi}(s^+) - \underline{\xi}(s^-)$ can then be decomposed as (for more details, see for instance [45]):

$$[\![\underline{\xi}]\!](s) = \left([\![\underline{\xi}]\!](s).\underline{n}(s)\right)\underline{n}(s) + \left([\![\underline{\xi}]\!](s).\underline{t}(s)\right)\underline{t}(s) + \left([\![\underline{\xi}]\!](s).\underline{b}(s)\right)\underline{b}(s) \tag{2.33}$$

In isotropy this decomposition allows us to define three fracture modes:

- In isotropy, a crack is said to be loaded in Mode I, if the displacement jump reduces to a normal displacement discontinuity:

$$[\![\underline{\xi}]\!]_I(s) = \left([\![\underline{\xi}]\!](s).\underline{n}(s)\right)\underline{n}(s) \tag{2.34}$$

  This mode is often referred to as the *opening* mode.

- In isotropy, Mode II refers to loadings which lead to an in-plane tangential displacement discontinuity:

$$[\![\underline{\xi}]\!]_{II}(s) = \left([\![\underline{\xi}]\!](s).\underline{t}(s)\right)\underline{t}(s) \tag{2.35}$$

  This mode is referred to as the *sliding* mode.

- As for Mode III (still in isotropy), it refers to loadings which lead to an out-of-plane tangential displacement discontinuity:

$$[\![\underline{\xi}]\!]_{III}(s) = \left([\![\underline{\xi}]\!](s).\underline{b}(s)\right)\underline{b}(s) \tag{2.36}$$

  This mode is referred to as the *tearing* mode.

In the specific case of plane-strain, no displacement is allowed in the out-of-plane direction $\underline{b}$ so that only Modes I and II need to be considered.

Due to the displacement discontinuity that define a crack, stresses become singular at the crack tip(s). The dominant singular term at a crack tip is of the order $\sigma \propto r^{-1/2}$ where r is the distance to the tip. The Mode I, II and III stress intensity factors K_I, K_{II} and K_{III} quantify the *degree* of singularity of the normal, in plane and out of plane shear stresses, respectively. For a crack belonging to the plane $y = 0$ ($\underline{t} = \underline{e}_x$, $\underline{n} = \underline{e}_y$ and $\underline{b} = \underline{e}_z$), the stress

intensity factors are defined as:

$$\begin{cases} K_I &= \lim\limits_{r\to 0^+} \sqrt{2\pi r}\sigma_{yy}(x=r,y=0) \\ K_{II} &= \lim\limits_{r\to 0^+} \sqrt{2\pi r}\sigma_{xy}(x=r,y=0) \\ K_{III} &= \lim\limits_{r\to 0^+} \sqrt{2\pi r}\sigma_{yz}(x=r,y=0) \end{cases} \tag{2.37}$$

These stress intensity factors depend on the *geometry*, the *loading* and possibly the *elastic properties* of the solid studied.

Remark 2 *As we shall see in Section 3.4.4, the definition of the three fracture modes in terms of displacement discontinuities is actually valid only in isotropy and in some specific cases in anisotropy. Indeed, in anisotropy, the existence of a tangential displacement jump does not always ensure the singularity of the shear stress.*

2.3.2 Some crack-propagation criteria

Linear elastic fracture mechanics is not able to predict the coalescence of cracks. However, it is able to predict whether or not an already existing crack propagates. To do so, two criteria are often used. The first one is said to be *local* in the sense that it focuses on what happens at the crack tip. The relevant quantities are then the stress intensity factors introduced in Section 2.3.1. Another one is based on energy dissipation considerations. The link between the two approaches can be made through Irwin's formula introduced here below.

Irwin's criterion or the local approach [34]

Irwin's criterion applies to cracks in linear elastic brittle solids subjected to purely Mode I (opening) loadings. Irwin postulated the existence of a critical stress intensity factor that cannot be exceeded and below which a crack cannot propagate [29]. This critical value of the Mode I stress intensity factor is called *fracture toughness* and is written K_{Ic}. It is commonly considered as a material property, independent of the problem considered.
Irwin's propagation criterion can be summarized in three laws[4]:

[4]This propagation criterion was based on the Kuhn-Tucker complementary condition [23], extensively used in rate-independent plasticity:

- $\frac{d\bar{\epsilon}_p}{dt} \geq 0$
- $f \leq 0$
- $f\frac{d\bar{\epsilon}_p}{dt} = 0$

- Irreversibility: $\frac{dl}{dt} \geq 0$
- Threshold: $K_I \leq K_{Ic}$
- Propagation condition: $(K_I - K_{Ic})\frac{dl}{dt} = 0$

In other words, this criterion states that if $K_I < K_{Ic}$, the crack *cannot* propagate while if $K_I = K_{Ic}$, crack propagation is *possible*.

The drawback of Irwin's criterion is that it ignores any other loading than pure Mode I loading. According to this criterion, an existing crack subjected to a pure Mode II loading would never propagate since $0 = K_I < K_{Ic}$. Moreover, one can argue that Irwin's criterion is based on a mathematical construct, the Mode I stress intensity factor K_I, and that no real material can stand an infinite stress.

Griffith's criterion or the global approach [34]

While Irwin's criterion uses the notion of fracture toughness K_{Ic}, Griffith's criterion [22] makes use of the fracture energy $\mathcal{G}_c$, a material property characterizing a brittle material. When a crack propagates, surfaces are created and energy is dissipated. This energy is proportional to the area of the surfaces created, the proportionality factor being the *fracture energy* $\mathcal{G}_c$. If any other dissipative phenomenon (such as plasticity) is ignored, this energy should be equal to $2\gamma_s$ where γ_s is the surface energy and the factor *two* accounts for upper and lower surfaces associated with surface created during propagation.
We introduce $\mathcal{G}$ the energy release rate defined as:

$$\mathcal{G}(\Gamma) \equiv -\frac{\partial \mathcal{E}_p}{\partial \Gamma} \tag{2.38}$$

where $\mathcal{E}_p$ is the potential energy of the structure (the energy stored in the structure due to external loading) and Γ the crack area (length in 2-D). $\mathcal{G}$ is the amount of energy per unit of created surface required (and dissipated) to propagate a crack. It has to be equal to $\mathcal{G}_c$ if propagation occurs.

Griffith's criterion can then be summarized as follows:

- Irreversibility: $\frac{d\Gamma}{dt} \geq 0$

where f is the yield function and $\frac{d\bar{\varepsilon}_p}{dt}$ is the equivalent plastic strain rate.

- Threshold: $\mathcal{G} \leq \mathcal{G}_c$
- Energy balance: $(\mathcal{G} - \mathcal{G}_c)\frac{d\Gamma}{dt} = 0$

From the local approach to the global approach

So far, we introduced two propagation criteria: Irwin's criterion based on fracture toughness, and Griffith's criterion based on fracture energy. The handshake between the two criteria can be made through Irwin's formula [29]. This formula links the energy release rate to the stress intensity factors. In the case of two-dimensional plane-strain problems, it can be written as[5]:

$$\mathcal{G} = \pi^t\{K\}.[H].\{K\} \tag{2.39}$$

where $\{K\} = {}^t[K_I \ K_{II}]$ is a vector containing the stress intensity factors, and $[H]$, coined here the *Irwin matrix*, a 2x2 matrix that depends on the elastic properties of the material. The energy release rate $\mathcal{G}$ is quadratic fuction of the stress intensity factors. Its associated matrix is the Irwin matrix $[H]$. In plane-strain isotropy, $[H]$ is diagonal and is equal to:

$$[H] = \frac{1-\nu^2}{\pi E}\begin{bmatrix} 1 & 0 \\ 0 & 1 \end{bmatrix} \tag{2.40}$$

where E is the Young's modulus and ν the Poisson's ratio of the material.
Putting together Irwin's and Griffith's criteria for a crack subjected to a pure Mode I loading, one can relate the fracture energy $\mathcal{G}_c$ to the fracture toughness K_{Ic} through the formula:

$$\mathcal{G}_c = \frac{1-\nu^2}{E}K_{Ic}^2 \tag{2.41}$$

For mixed-mode loadings, one can extend the definition of fracture toughness by means of a generalized toughness defined as

$$K_c^2 = \frac{E}{1-\nu^2}\mathcal{G}_c \tag{2.42}$$

[5]This writing of Irwin's formula in a matrix form is not standard. However, we found it very convenient especially when it comes to anisotropic media where the Modes I and II are coupled. The name *Irwin matrix* is also not standard but since this matrix will play an important role is the continuation, it was convenient to have it named.

Provided that $\mathcal{G}_c$ is mode angle independent (the mode angle Θ is defined as $\tan\Theta = \frac{K_{II}}{K_I}$), the fracture toughness should also be mode angle independent.

In anisotropy, a generalized Irwin formula was proposed[6] by Sih et al. in Ref. [39]. We write it here in a matrix form (2.39), with the Irwin matrix given by:

$$[H] = \frac{f_{11}}{2\pi}\begin{bmatrix} -\frac{f_{22}}{f_{11}}\mathrm{Im}\left[\frac{\mu_1+\mu_2}{\mu_1\mu_2}\right] & \frac{1}{2}\mathrm{Im}\left[\mu_1\mu_2 - \frac{f_{22}}{f_{11}}\frac{1}{\mu_1\mu_2}\right] \\ \frac{1}{2}\mathrm{Im}\left[\mu_1\mu_2 - \frac{f_{22}}{f_{11}}\frac{1}{\mu_1\mu_2}\right] & \mathrm{Im}\left[\mu_1+\mu_2\right] \end{bmatrix} \tag{2.43}$$

where μ_i and f_{ij} were defined in Section 2.2.2. In contrast to the isotropic case (2.40), this matrix is no more diagonal, which means that there exists some coupling between the Modes.

2.3.3 On the direction of crack propagation

So far, the energy release rate was determined assuming that the crack-propagation was symmetrical and collinear to the original crack. The first hypothesis is reasonable if we restrict ourselves to symmetrical loadings; and - at least in isotropy - the second one should also be reasonable in the case of pure Mode I loading.

For an isotropic material, the typical argument reads as follows [31]:

- If there is propagation, it will be done in the direction such that $K_{II}^{\star} = 0$ where $K_{II}^{\star}$ is the Mode II stress intensity factor at the crack tip of an infinitesimal crack kink.
- $\begin{cases} \mathcal{G} < \mathcal{G}_c & \text{no crack propagation is possible} \\ \mathcal{G} = \mathcal{G}_c & \text{crack propagation is possible} \end{cases}$

This propagation criterion (propagation such that $K_{II}^{\star} = 0$) is known as the *principle of local symmetry*. Other criteria such as the maximal hoop stress and maximal energy release rate criteria also exist. They predict that the crack propagation should occur in the direction that either maximizes the hoop stress or the energy release rate.

In isotropy, these three criteria all agree in one point, nomely that in pure Mode I no branching should occur. As we will see in Section 3.4.5, this is true only for some specific crack orientations in anisotropy.

[6] A proof of this formula shall also be given in the continuation.

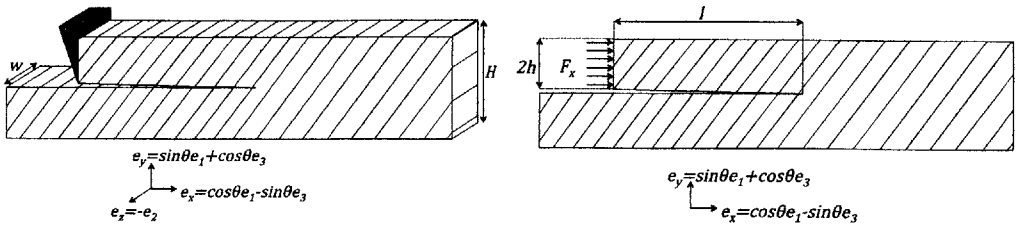

(a) Three-dimensional scratch test. (b) Two-dimensional scratch test.

Figure 2-5: Scratch test on a TI material.

2.4 Application: Scratch-test on a transversely isotropic material

Consider a scratch test performed on a transversely isotropic (TI) material (for more details on the scratch test as a fracture characterization method, see [2]). The scratch tool (e.g. a blade) is moved along the x-direction that makes an angle θ with the direction $\underline{e}_1$ of the material (Fig. 2-5a). We can consider this problem as two-dimensional. In addition, if the width w is large compared to the height H of the scratched sample, plane-strain equations can be used. Let us hypothesize the existence of a pre-existing horizontal crack at the tip of the blade (Fig. 2-5b). If the initial crack-length l is long compared to the depth of scratching $2h$, the upper left part of the structure can be considered as a beam loaded on its left end by a transversal force.

The aim of this Section is to use the tools introduced in the previous Sections to determine the *scratch toughness* of a brittle TI material. We will first give a possible approximation of the solution of the simple beam problem in transverse isotropy using the governing equations introduced in Section 2.2. From this approximation, we will use the concepts presented in Section 2.3 to derive the expression of the *scratch toughness*.

2.4.1 The rectangular beam problem

If the initial crack-length, l, is long enough, the upper left part of the scratched material can be considered as a beam loaded at its left end by a transversal force F_x. We will make some approximations of the stress, strain and displacement fields in a TI beam subjected to a transversal force.

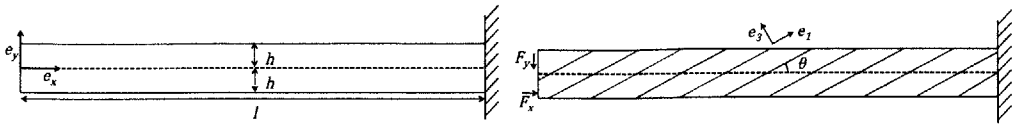

(a) Rectangular beam. (b) TI beam with end-load.

Figure 2-6: Two-dimensional beam problem.

Problem statement

Consider the two-dimensional problem of an elastic rectangular beam of height $2h$ and length $l >> h$ (Fig. 2-6a) made of a TI material.

Introduce the orthonormal basis $(\underline{e}_x, \underline{e}_y, \underline{e}_z)$ such that $\widehat{(\underline{e}_x, \underline{e}_1)} = \theta$, $\widehat{(\underline{e}_y, \underline{e}_3)} = \theta$, $\widehat{(\underline{e}_z, \underline{e}_2)} = \pi$.

The beam is loaded on its left end by a horizontal force F_x, a vertical force F_y and is fixed at its right end (Fig. 2-6b).

We saw in Section 2.2.1 that solving a plane-strain problem reduces to finding a potential Ψ satisfying the compatibility equation (2.23) and the boundary conditions of the problem considered.

Following a method used in isotropy [5], let us try to find Ψ of the form:

$$\Psi(x,y) = \sum_{k=0}^{4} \sum_{l=0}^{k} \alpha_{kl} x^l y^{k-l}$$

so that:

$$\begin{cases} \sigma_{xx} = \Psi_{,yy} = \sum_{k=0}^{4} \sum_{l=0}^{k} \alpha_{kl}(k-l-1)(k-l-2) x^l y^{k-l-2} \\ \sigma_{yy} = \Psi_{,xx} = \sum_{k=0}^{4} \sum_{l=0}^{k} \alpha_{kl} l(l-1) x^{l-2} y^{k-l} \\ \sigma_{xy} = -\Psi_{,xy} = -\sum_{k=0}^{4} \sum_{l=0}^{k} \alpha_{kl} l(k-l) x^{l-1} y^{k-l-1} \end{cases} \tag{2.44}$$

Using Eq. (2.44) and the compatibily equation (2.23), we deduce:

$$6f_{11}(\theta)\alpha_{40} - 3f_{23}(\theta)\alpha_{41} + (f_{33}(\theta) + 2f_{12}(\theta))\alpha_{42} - 3f_{13}(\theta)\alpha_{43} + 6f_{22}(\theta)\alpha_{44} = 0 \tag{2.45}$$

We then enforce the boundary conditions (in a strong sense) on the surface $y = \pm h$ as:

$$\begin{cases} \sigma_{xy}(x, y = \pm h) &= 0 \quad \forall x \in [0, l] \\ \sigma_{yy}(x, y = \pm h) &= 0 \quad \forall x \in [0, l] \end{cases} \tag{2.46}$$

Using Eq. (2.44), the first condition in (2.46) can be rewritten as:

$$\sigma_{yy}(x, \pm h) = \sum_{l=0}^{2} \left\{ x^l (l+2)(l+1) \sum_{k=l+2}^{4} \alpha_{kl+2} (\pm h)^{k-l-2} \right\} = 0 \tag{2.47}$$

and the second one as:

$$\sigma_{xy}(x, \pm h) = -\sum_{l=0}^{2} \left\{ x^l (l+1) \sum_{k=l+2}^{4} \alpha_{kl+1} (\pm h)^{k-l-2} \right\} = 0 \tag{2.48}$$

The two polynomials of degree two in x appearing in Eq. (2.47) and (2.48), vanishing in the segment $[0, l]$, are equal to the trivial polynomial. All their coefficients are then null; thus we have:

$$\begin{cases} \sum_{k=2}^{4} \alpha_{k2} (\pm h)^{k-2} &= \alpha_{22} \pm \alpha_{32} h + \alpha_{42} h^2 &= 0 \\ \sum_{k=3}^{4} \alpha_{k3} (\pm h)^{k-3} &= \alpha_{33} \pm \alpha_{43} h &= 0 \\ \sum_{k=4}^{4} \alpha_{k4} (\pm h)^{k-4} &= \alpha_{44} &= 0 \end{cases} \tag{2.49}$$

and:

$$\begin{cases} \sum_{k=2}^{4} \alpha_{k1} (k-1) (\pm h)^{k-2} &= \alpha_{21} \pm 2\alpha_{31} h + 3\alpha_{41} h^2 &= 0 \\ \sum_{k=3}^{4} \alpha_{k2} (k-2) (\pm h)^{k-3} &= \alpha_{32} \pm 2\alpha_{42} h &= 0 \\ \sum_{k=4}^{4} \alpha_{k3} (k-3) (\pm h)^{k-4} &= \alpha_{43} &= 0 \end{cases} \tag{2.50}$$

Equation (2.49) together with (2.50) give:

$$\begin{cases} 0 &= \alpha_{32} = \alpha_{33} = \alpha_{42} = \alpha_{43} = \alpha_{44} = \alpha_{22} \\ 0 &= \alpha_{21} \pm 2\alpha_{31} h + 3\alpha_{41} h^2 \end{cases} \tag{2.51}$$

so that we finally have:

$$\Psi(x, y) = \alpha_{20} y^2 + \alpha_{21} xy + \alpha_{30} y^3 + \alpha_{31} xy^2 + \alpha_{40} y^4 + \alpha_{41} xy^3 \tag{2.52}$$

(the terms in $k = 0, 1$ have been omitted since they lead to a trivial stress field). The

compatibility equation (2.45) then reduces to:

$$6f_{11}(\theta)\alpha_{40} - 3f_{23}(\theta)\alpha_{41} = 0 \tag{2.53}$$

Furthermore, we have to impose the boundary conditions (this time in a weak sense) on the left end of the rectangular beam, that is:

$$\begin{cases} F_x = -\int_{-h}^{h} \sigma_{xx}(0,y)wdy = -\frac{4hw}{3}(3\alpha_{20} + 4\alpha_{40}h^2) \\ F_y = \int_{-h}^{h} \sigma_{xy}(0,y)wdy = -2hw(\alpha_{21} + \alpha_{41}h^2) \end{cases} \tag{2.54}$$

and the weak boundary condition on the right end of the beam:

$$F_y l = -\int_{-h}^{h} y\sigma_{xx}(l,y)wdy = 4(\alpha_{30} + l\alpha_{41})wh^3 \tag{2.55}$$

Conclusion: A stress field satisfying the equilibrium equations, the compatibility equations, the strong boundary conditions on the surfaces $y = \pm h$ and the weak boundary conditions on the left and right ends of the beam can be derived from a potential $\Psi(x,y)$ of the form (2.52) with its coefficients α_{ij} satisfying Eq. (2.51), (2.53), (2.54) and (2.55). We define $[M]$, a 6x6 matrix, as:

$$[M] = \begin{bmatrix} -4wh & 0 & 0 & 0 & -\frac{4}{3}wh^3 & 0 \\ 0 & -2wh & 0 & 0 & 0 & -2wh^3 \\ 0 & 0 & 4wh^3 & 0 & 0 & 4lwh^3 \\ 0 & 1 & 0 & 2h & 0 & 3h^2 \\ 0 & 1 & 0 & -2h & 0 & 3h^2 \\ 0 & 0 & 0 & 0 & 6f_{11}(\theta) & -3f_{23}(\theta) \end{bmatrix} \tag{2.56}$$

It satisfies $[M].\{\alpha\} = \{F\}$ with $\{\alpha\} = {}^t[\alpha_{20}\ \alpha_{21}\ \alpha_{30}\ \alpha_{31}\ \alpha_{40}\ \alpha_{41}]$ and $\{F\} = {}^t[F_x\ F_y\ F_y l\ 0\ 0\ 0]$. Since $\det[M] \propto h^8 f_{11}(\theta)$, $[M]$ can be inverted provided that $f_{11}(\theta) \neq 0$ (which is always true). Finally, the stress function Ψ is completely determined by the coefficients α_{ij} deduced from:

$$\{\alpha\} = [M]^{-1}.\{F\} \tag{2.57}$$

Stress, strain and displacement fields in the case of a transverse loading

For the specific case of a transversal loading ($F_y = 0$), we obtain from Eq. (2.57) $\{\alpha\} = {}^t\left[-\frac{F_x}{4wh}\ 0\ 0\ 0\ 0\ 0\right]$ so that $\Psi(x,y) = -\frac{F_x}{4wh}y^2$ and thus:

$$\begin{cases} \sigma_{xx} &= -\frac{F_x}{2hw} \\ \sigma_{yy} &= 0 \\ \sigma_{xy} &= 0 \end{cases} \tag{2.58}$$

Using the stress-strain relationship, we deduce:

$$\begin{cases} \epsilon_{xx} &= \xi_{x,x} &= -f_{11}(\theta)\frac{F_x}{2wh} \\ \epsilon_{yy} &= \xi_{y,y} &= -f_{12}(\theta)\frac{F_x}{2wh} \\ 2\epsilon_{xy} &= \xi_{x,y} + \xi_{y,x} &= -f_{13}(\theta)\frac{F_x}{2wh} \end{cases} \tag{2.59}$$

Integrating the first two equations in (2.59), we find:

$$\begin{cases} \xi_x(x,y) &= f_{11}(\theta)(a(y) - \frac{F_x}{2wh}x) \\ \xi_y(x,y) &= f_{12}(\theta)(b(x) - \frac{F_x}{2wh}y) \end{cases} \tag{2.60}$$

Substituting these expressions in (2.59_3), one gets:

$$f_{11}(\theta)a'(y) = -f_{12}b'(x) - \frac{F_x}{2wh}f_{13}(\theta) \tag{2.61}$$

While the left-hand term in Eq. (2.61) depends only on the variable y, the right-hand term depends only on x. Those two terms are then equal to a constant C independent of x and y. This leads to the following displacement field:

$$\begin{cases} \xi_x(x,y) &= a_0 - \frac{f_{11}(\theta)F_x}{2wh}x + Cy \\ \xi_y(x,y) &= b_0 - \frac{F_x f_{13}(\theta) + 2hC}{2wh}x - \frac{f_{12}(\theta)F_x}{2wh}y \end{cases} \tag{2.62}$$

with a_0, b_0 and C three constants to be determined. To find a_0, b_0 and C, let us consider the displacement boundary conditions on the right end of the beam. Ideally, we would like to have:

$$\xi_x(x = l, y) = \xi_y(x = l, y) = 0 \ \ \forall y \in [-h, h] \tag{2.63}$$

which is clearly impossible here. Instead, we enforce the following weak boundary conditions:

$$\left\{\begin{array}{rcrcl} 0 &=& -\int_{-h}^{h}\xi_x(l,y)dy &=& (a_0 - \frac{f_{11}(\theta)F_x}{2wh}l)2h \\ 0 &=& -\int_{-h}^{h}\xi_y(l,y)dy &=& (b_0 - \frac{f_{13}(\theta)F_x+2hC}{2wh}l)2h \\ 0 &=& -\int_{-h}^{h}y\xi_x(l,y)dy &=& 2C\frac{h^3}{3} \end{array}\right. \tag{2.64}$$

The first two equations in (2.64) impose a null average horizontal and vertical displacement, while the third one imposes a null average slope of the right end of the beam. Equation (2.64) then gives: $C = 0$, $a_0 = \frac{f_{11}(\theta)F_x}{2wh}l$ and $b_0 = \frac{f_{13}(\theta)F_x}{2wh}l$.

Conclusion: The problem of a rectangular TI beam whose plane of isotropy makes an angle θ with the plane $(\underline{e}_x, \underline{e}_z)$ and loaded by an horizontal force F_x to its left extremity has been solved in a weak sense. This solution leads to the following stress, strain and displacement fields:

$$\left\{\begin{array}{rcl} \sigma_{xx} &=& -\frac{F_x}{2wh} \\ \sigma_{yy} &=& 0 \\ \sigma_{xy} &=& 0 \\ \\ \epsilon_{xx} &=& -f_{11}(\theta)\frac{F_x}{2wh} \\ \epsilon_{yy} &=& -f_{12}(\theta)\frac{F_x}{2wh} \\ 2\epsilon_{xy} &=& -f_{13}(\theta)\frac{F_x}{2wh} \\ \\ \xi_x(x,y) &=& \frac{f_{11}(\theta)F_x}{2wh}(l-x) \\ \xi_y(x,y) &=& \frac{f_{13}(\theta)F_x}{2wh}(l-x) - \frac{f_{12}(\theta)F_x}{2wh}y \end{array}\right. \tag{2.65}$$

2.4.2 Determination of the scratch toughness

We introduces in Section 2.3.2 a quantity of interest, the energy release rate, $\mathcal{G} = -\frac{\partial \mathcal{E}_p}{\partial \Gamma}$, where $\mathcal{E}_p$ is the potential energy of the structure and $\Gamma = wl$ is the crack area. The determination of $\mathcal{G}$ generally requires the knowledge of the stress, strain and displacement fields in the whole volume of the structure, including in the near-tip region. An available technique to avoid the calculation of the (singular) fields associated with the near-tip region is the use of the J-integral, introduced by Rice [38]. The J-integral for a crack propagating along the

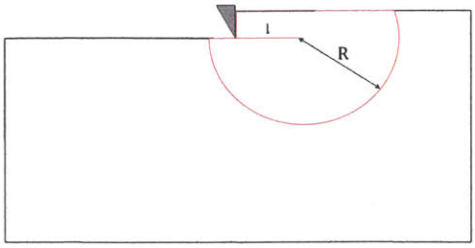

Figure 2-7: Contour $\partial\mathcal{D}$ (in red) for the computation of the J-integral.

direction $\underline{e}_x$ is defined as:

$$J = \int_{\partial\mathcal{D}} \left(\frac{1}{2}(\underline{\underline{\sigma}} : \underline{\underline{\epsilon}})(\underline{n}.\underline{e}_x) - (\underline{\underline{\sigma}}.\underline{n}).\underline{\xi}_{,x} \right) ds \tag{2.66}$$

where $\partial\mathcal{D}$ is any contour enclosing the crack tip and $\underline{n}$ the outward unit vector normal to the surface $\partial\mathcal{D}$. Provided that the crack surfaces are traction-free, it can be shown that $J = w\mathcal{G}$ in our problem.

We restrict ourselves to the cases where:

- The initial crack is long enough and horizontal, so that the beam approximation applies;
- The crack propagates collinearly to its original orientation, so that the J-integral can be used to estimate the energy release rate;
- The crack surfaces are traction-free (i.e. no crack closure), so that again, the J-integral can be used to estimate the energy release rate.

Considering the contour $\partial\mathcal{D}$ drawn on Fig. 2-7 with $R \gg l$, the only contribution to the J-integral will come from the contact surface between the blade and the material, $x = 0$, $y \in [-h, h]$. Indeed, all the other surfaces are traction-free; and if the radius R is taken big enough, the material points intersected by the contour do not *feel* the loading. The J-integral is then equal to:

$$J = \int_{-h}^{h} \left(\frac{1}{2} \left(\frac{F_x}{2wh} \right)^2 f_{11}(\theta)(-1) + \left(\frac{F_x}{2wh} \right)^2 f_{11}(\theta) \right) w dy \tag{2.67}$$

so that:

$$J = \frac{F_x^2}{4wh} f_{11}(\theta) \tag{2.68}$$

We then deduce:

$$\mathcal{G} = \frac{J}{w} = \frac{F_x^2}{4w^2 h} f_{11}(\theta) \tag{2.69}$$

Using Irwin's formula (2.39) and Griffith's propagation criterion introduced in Section 2.3.2, we deduce that when the crack propagates, the transversal force F_x should satisfy:

$$\left.\frac{\mathrm{F}_x}{2w\sqrt{h}}\right|_{F_x \text{ at propagation}} = \sqrt{\frac{\mathcal{G}_c}{f_{11}(\theta)}} = \left.\sqrt{\frac{\pi^t \{K\} . [H(\theta)] . \{K\}}{f_{11}(\theta)}}\right|_{\{K\} \text{ at propagation}} \tag{2.70}$$

The right-hand side of Eq. (2.70) could be defined as a *scratch toughness* K_s:

$$K_s \equiv \left.\sqrt{\frac{\pi^t \{K\} . [H(\theta)] . \{K\}}{f_{11}(\theta)}}\right|_{\{K\} \text{ at propagation}} \tag{2.71}$$

and could be measured through the transversal force F_x.

Specifically, for a crack in the bedding plane, we would have:

$$K_s(\theta = 0) = \left.\sqrt{\pi \mathcal{H}_1 \frac{C_{11}C_{33} - C_{13}^2}{C_{33}} \left(K_I^2 + \sqrt{\frac{C_{33}}{C_{11}}} K_{II}^2 \right)}\right|_{\{K\} \text{ at propagation}} \tag{2.72}$$

while for a crack normal to the bedding plane, we would have:

$$K_s(\theta = \frac{\pi}{2}) = \left.\sqrt{\pi \mathcal{H}_1 \frac{C_{11}C_{33} - C_{13}^2}{C_{11}} \left(\sqrt{\frac{C_{33}}{C_{11}}} K_I^2 + K_{II}^2 \right)}\right|_{\{K\} \text{ at propagation}} \tag{2.73}$$

with $\mathcal{H}_1 = \frac{1}{2\pi} \sqrt{\frac{C_{11}}{C_{11}C_{33} - C_{13}^2}} \left(\frac{1}{C_{44}} + \frac{2}{\sqrt{C_{33}C_{11}} + C_{13}} \right)$.

The drawback of the *scratch* toughness definition (2.71) is that even if the fracture energy was isotropic (if $\mathcal{G}_c$ was independent of θ), the *scratch* toughness would be anisotropic. Indeed, we would have:

$$K_s(\theta = 0) = \sqrt{\frac{C_{11}}{C_{33}}} K_s(\theta = \pi/2) \tag{2.74}$$

A way to correct this drawback would be to define another scratch toughness K_s' as:

$$K_s' = \sqrt{\frac{f_{11}(\theta)}{f_{11}(0)}} K_s \tag{2.75}$$

with K_s defined by (2.71).

With the help of Eq. (2.70), we then would have:

$$K'_s = \sqrt{\frac{f_{11}(\theta)}{f_{11}(0)}} \left. \frac{\mathrm{F}_x}{2w\sqrt{h}} \right|_{F_x \text{ at propagation}} \tag{2.76}$$

For an isotropic material (see Section 2.3.2), $f_{11}(\theta) = \frac{1-\nu^2}{E}$ and $H_{11} = H_{22} = \frac{1-\nu^2}{\pi E}$ so that the *scratch* toughness is strictly equivalent to the *generalized fracture* toughness K_c defined in Section 2.3.2, Eq. (2.42):

$$K_s^{iso} \equiv K_c^{iso} = \sqrt{\frac{E}{1-\nu^2}\mathcal{G}_c} \tag{2.77}$$

2.5 Chapter summary

We introduced in this Chapter the tools necessary to address a fracture mechanics problem in the specific case of plane-strain state conditions. This allowed us to identify some specificities of anisotropic media such as the fracture modes coupling. We also showed that the scratch-test model could be extended to the anisotropic case, provided some hypotheses are verified and that a *scratch* toughness is properly defined.

Chapter 3

Plane-strain cracks in anisotropic media

In the previous Chapter, we introduced the necessary tools to study anisotropic fracture mechanics problems under plane-strain conditions. We will now apply these tools to study the problem of a straight crack subjected to an external loading. As it is custom in continuum mechanics, we consider that these external solicitations can be either in the form of prescribed stresses or prescribed displacements.

We first introduce the two types of boundary conditions that will turn out relevant for the fluid-driven crack propagation problem (addressed in Chapter 4). For these boundary conditions, the stress and displacement fields are derived using the complex potentials theory. The crack shape induced by an imposed stress field is also studied, and the question of crack propagation is addressed.

While England and Green [16] - using the potential theory - and Sneddon and Lowengrub [41] - using the Hankel transform - studied this problem for isotropic materials, we consider here anisotropic solids, and specifically TI solids. Hoenig [27] already considered this problem but only focused on the near-tip behavior under uniform loading conditions. Barnett and Asaro [6] also considered this problem - using dislocation theory - but did not give the actual crack shape induced.

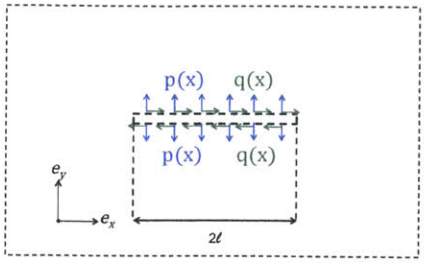

Figure 3-1: Boundary-stress method.

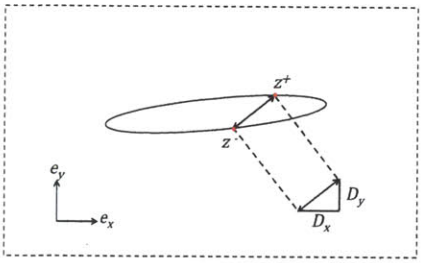

Figure 3-2: Displacement-jump method.

3.1 Problem statement

We consider a two-dimensional (plane-strain) crack in a linear elastic anisotropic brittle material. The crack belongs to the plane $y = 0$ and has a half-length l ; the crack initially belongs to the segment:

$$\mathcal{L} = \{z = x + iy | (x, y) \in [-l, l] \, \mathrm{x} \, \{-\epsilon l, \epsilon l\}, \epsilon \to 0\} \tag{3.1}$$

where ϵ is a dimensionless parameter. Two types of external loadings are considered: normal and shear *stresses* on the crack (see Fig. 3-1); normal and transverse *displacement jumps* on the crack surface (see Fig. 3-2).

3.1.1 Boundary-stress method

The first case considered consists of crack surfaces loaded[1] by a normal stress $-p$ and a shear stress $-q$ defined and differentiable on $\mathcal{L}$.

Given the pressure and shear fields p and q acting on the faces of the line crack $\mathcal{L}$, we aim at finding the crack shape and the stress and displacement fields induced in the cracked body.

In an *anisotropic medium*, we have to find the complex potentials Φ_1 and Φ_2 introduced in Section 2.2.2 that satisfies the following boundary conditions:

$$\begin{cases} \sigma_{yy}(z) &= -p(x), & z = x + iy \in \mathcal{L} \setminus \{-l, l\} \\ \sigma_{xy}(z) &= -q(x), & z = x + iy \in \mathcal{L} \setminus \{-l, l\} \\ |\underline{\underline{\sigma}}|(z) &\to 0, & |z| \to +\infty \end{cases} \tag{3.2}$$

3.1.2 The displacement-jump method

The second load scenario considers normal and tangential displacement jumps defined by the functions D_y and D_x, respectively, imposed on the crack surface. The functions D_y and D_x are defined and differentiable on $\mathcal{L}$.

Given the displacement jumps imposed on a line crack $\mathcal{L}$, we aim at finding the traction $\underline{T} = -p\underline{n} - q\underline{t}$ acting on the crack lips and the stress and displacement fields induced in the body.

In an *anisotropic medium*, we have to find the complex potentials Φ_1 and Φ_2 introduced in Section 2.2.2 that satisfy the following boundary conditions:

$$\begin{cases} [\![\xi_z]\!](x) &= D_x(x), & z = x + iy \in \mathcal{L} \setminus \{-l, l\} \\ [\![\xi_z]\!](x) &= D_y(x), & z = x + iy \in \mathcal{L} \setminus \{-l, l\} \\ [\![\sigma_{yy}]\!](z) &= 0, & z = x + iy \in \mathcal{L} \setminus \{-l, l\} \\ [\![\sigma_{xy}]\!](z) &= 0, & z = x + iy \in \mathcal{L} \setminus \{-l, l\} \\ |\underline{\underline{\sigma}}|(z) &\to 0, & |z| \to +\infty \\ |\underline{\xi}|(z) &\to 0, & |z| \to +\infty \end{cases} \tag{3.3}$$

[1] We consider that the pressure acts normally to the initial crack surface and not to the deformed one: $\underline{\underline{\sigma}}.\underline{n} = -p\underline{n} - q\underline{t} = \pm p\underline{e}_y \pm q\underline{e}_x$.

Remark 3 *Contrary to the boundary-stress method, the displacement-jump method is a mixed-boundary value problem. Indeed, while the boundary conditions of the boundary-stress method involve only the stress tensor* $\underline{\underline{\sigma}}$*, the ones of the displacement-jump method involve stress and displacement components.*

Remark 4 *In isotropic media, if one knows the displacement jump* D_i *(*$i = x$ *or* y*) on the crack, one can deduce the displacement on the top and lower surfaces of the crack; indeed, by symmetry of the problem,* $\xi_i = D_i/2$*. This formula obviously does not apply in anisotropic media.*

3.2 On the determination of the complex potentials

3.2.1 Complex potentials for the boundary-stress method

We introduce the complex potentials Ω_1 and Ω_2 such that:

$$\left\{ \begin{array}{rcl} \Phi_1(z_1) & = & \frac{2}{\mu_2-\mu_1}\left(\mu_2\Omega_1(z_1)+\Omega_2(z_1)\right) \\ \Phi_2(z_2) & = & \frac{-2}{\mu_2-\mu_1}\left(\mu_1\Omega_1(z_2)+\Omega_2(z_2)\right) \end{array} \right. \tag{3.4}$$

(for $\mu_1 \neq \mu_2$). These new potentials will allow us to separate the normal and shear stresses. According to Eq. (2.27), the normal and shear stresses σ_{yy} and σ_{xy} can then be written as:

$$\left\{ \begin{array}{rcl} \sigma_{yy}(z) & = & 4\,\mathrm{Re}\left\{\frac{1}{\mu_2-\mu_1}\left[\mu_2\Omega_1'(z_1)-\mu_1\Omega_1'(z_2)\right]\right\} \\ & & \qquad +4\,\mathrm{Re}\left\{\frac{1}{\mu_2-\mu_1}\left[\Omega_2'(z_1)-\Omega_2'(z_2)\right]\right\} \\ \sigma_{xy}(z) & = & -4\,\mathrm{Re}\left\{\frac{\mu_1\mu_2}{\mu_2-\mu_1}\left[\Omega_1'(z_1)-\Omega_1'(z_2)\right]\right\} \\ & & \qquad -4\,\mathrm{Re}\left\{\frac{1}{\mu_2-\mu_1}\left[\mu_1\Omega_2'(z_1)-\mu_2\Omega_2'(z_2)\right]\right\} \end{array} \right. \tag{3.5}$$

Remark 5 *The reasoning here is valid only if the material's elastic properties and the crack orientation are such that* $\mu_1 \neq \mu_2$*, which is not always true. For instance, isotropic materials are such that* $\mu_1 = \mu_2 = i$*. However, one can overcome this restriction by replacing* $\mu_1 = i$ *and* $\mu_2 = i$ *by* $\hat{\mu}_1 = \epsilon + \mu_1$ *and* $\hat{\mu}_2 = -\epsilon + \mu_1$*, respectively, and by letting* ϵ *go to* 0 *(this ensures that* $\mu_1 + \mu_2 \in i\mathbb{R}$ *and that* $\mu_1\mu_2 \in \mathbb{R}$*, a property of cracks belonging to a plane of material symmetry - see Appendix E).*

More specifically, on the crack (for $z_c^{\pm} = x_c \pm iy_c \in \mathcal{L} \setminus \{-l, l\}$) [2,3]:

$$\left\{ \begin{array}{rcl} \sigma_{yy}(z_c^{\pm}) & = & 4\,\mathrm{Re}\left[\Omega_1'(z_c^{\pm})\right] = 2\left[\Omega_1'(z_c^{\pm}) + \bar{\Omega}_1'(z_c^{\mp})\right] \\ \sigma_{xy}(z_c^{\pm}) & = & 4\,\mathrm{Re}\left[\Omega_2'(z_c^{\pm})\right] = 2\left[\Omega_2'(z_c^{\pm}) + \bar{\Omega}_2'(z_c^{\mp})\right] \end{array} \right. \tag{3.6}$$

The boundary conditions (3.2) then lead to:

$$\left\{ \begin{array}{rcl} -w_i(x_c) & = & 2\left[\Omega_i'(z_c^{+}) + \bar{\Omega}_i'(z_c^{-})\right] \\ -w_i(x_c) & = & 2\left[\Omega_i'(z_c^{-}) + \bar{\Omega}_i'(z_c^{+})\right] \end{array} \right. \tag{3.7}$$

for $i = 1$ or 2 with $w_1 = p$ and $w_2 = q$.

Taking the difference of the two equations in (3.7), one obtains:

$$\left[\Omega_i' - \bar{\Omega}_i'\right](z_c^{+}) - \left[\Omega_i' - \bar{\Omega}_i'\right](z_c^{-}) = 0 \quad \forall z_c \in \mathcal{L} \setminus \{-l, l\} \tag{3.8}$$

close to a constant, $\Omega_i' - \bar{\Omega}_i'$ is then given by the Cauchy integral (see Section 2.2.3) with $k = 0$; and we deduce:

$$\Omega_i'(z) = \bar{\Omega}_i'(z) \tag{3.9}$$

(we take the constant $C = 0$ so that $\Omega_i' - \bar{\Omega}_i'$ vanishes at infinity). Using Eq. (3.9) in (3.7), we have to find Ω_i' such that:

$$\Omega_i'(z_c^{+}) + \Omega_i'(z_c^{-}) = -\frac{w_i(x_c)}{2} \quad \forall z_c \in \mathcal{L} \setminus \{-l, l\} \tag{3.10}$$

One recognizes here a Hilbert's problem in which $k = -\frac{w_i}{2}$ (see Section 2.2.3). We then have:

$$\Omega_i'(z) = -\frac{\mathcal{F}(z)}{4i\pi} \int_{t=-l}^{l} \frac{w_i(t)dt}{\mathcal{F}(t^{+})(t-z)} = \frac{1}{4\pi\sqrt{z^2 - l^2}} \int_{t=-l}^{l} w_i(t) \frac{\sqrt{l^2 - t^2}}{z - t} dt \tag{3.11}$$

Again, we take $C = 0$ since Ω_i' has to be $O(1/z^2)$ as $|z| \to +\infty$ [31].

More specifically, on the plane $y = 0$, we have:

$$\Omega_i'(x) = \frac{\mathrm{sgn}(x)}{4\pi\sqrt{x^2 - l^2}} \int_{t=-l}^{l} w_i(t) \frac{\sqrt{l^2 - t^2}}{x - t} dt \tag{3.12}$$

[2] One should remember that $\mathrm{Im}\,\mu_i > 0$ for $i = 1$ or 2 so that $\lim_{y \to 0^{\pm}} z_i = \lim_{y \to 0^{\pm}} z = z^{\pm}$.

[3] For f analytic, we use Muskhelishvili conjugate $\bar{f}$ defined as: $\bar{f}(z) = \overline{f(\bar{z})}$ [35].

Remark 6 *What is interesting here is that the functions Ω_i', for $i = 1$ or 2, are independent of the elastic properties of the material.*

Ignoring the rigid body translation along the x-direction, the primitives Ω_i given by England and Green [16] are equal to:

$$\Omega_i(z) = \int_{t=0}^{l} \frac{F_i(t) + zG_i(t)}{\sqrt{z^2 - t^2}} dt \tag{3.13}$$

with:

$$\begin{cases} F_i(t) &= -\frac{t}{2\pi} \int_{u=0}^{t} \frac{f_i(u)}{\sqrt{t^2-u^2}} du \\ G_i(t) &= -\frac{1}{2\pi t} \int_{u=0}^{t} \frac{u g_i(u)}{\sqrt{t^2-u^2}} du \end{cases} \tag{3.14}$$

where f_i and g_i are the projections of w_i on the vector space of even and odd functions, respectively. They are differentiable and defined on $[-l, l]$ as $f_i(x) = \frac{w_i(x)+w_i(-x)}{2}$ and $g_i(x) = \frac{w_i(x)-w_i(-x)}{2}$ so that we trivially have $w_i = f_i + g_i$.

Remark 7 *On the crack - for $z_c = x_c + iy_c \in \mathcal{L} \setminus \{-l, l\}$ - we have:*

$$\Omega_i(z_c^{\pm}) = sgn(x_c) \int_{t=0}^{|x_c|} \frac{F_i(t) + x_c G_i(t)}{\sqrt{x_c^2 - t^2}} dt \mp i \int_{t=|x_c|}^{l} \frac{F_i(t) + x_c G_i(t)}{\sqrt{t^2 - x_c^2}} dt \tag{3.15}$$

Now that we have the expressions of Ω_i and Ω_i' in terms of the loading w_i, the stress and displacement fields are known in the whole domain:

$$
\left\{
\begin{array}{rcl}
\sigma_{xx}(z) & = & 4\,\mathrm{Re}\left\{\frac{\mu_1\mu_2}{\mu_2-\mu_1}\left[\mu_1\Omega_1'(z_1)-\mu_2\Omega_1'(z_2)\right]\right\} \\
 & & \qquad +4\,\mathrm{Re}\left\{\frac{1}{\mu_2-\mu_1}\left[\mu_1^2\Omega_2'(z_1)-\mu_2^2\Omega_2'(z_2)\right]\right\} \\
\sigma_{yy}(z) & = & 4\,\mathrm{Re}\left\{\frac{1}{\mu_2-\mu_1}\left[\mu_2\Omega_1'(z_1)-\mu_1\Omega_1'(z_2)\right]\right\} \\
 & & \qquad +4\,\mathrm{Re}\left\{\frac{1}{\mu_2-\mu_1}\left[\Omega_2'(z_1)-\Omega_2'(z_2)\right]\right\} \\
\sigma_{xy}(z) & = & -4\,\mathrm{Re}\left\{\frac{\mu_1\mu_2}{\mu_2-\mu_1}\left[\Omega_1'(z_1)-\Omega_1'(z_2)\right]\right\} \\
 & & \qquad -4\,\mathrm{Re}\left\{\frac{1}{\mu_2-\mu_1}\left[\mu_1\Omega_2'(z_1)-\mu_2\Omega_2'(z_2)\right]\right\} \\
\xi_x(z) & = & 4\,\mathrm{Re}\left\{\frac{1}{\mu_2-\mu_1}\left[p_1\mu_2\Omega_1(z_1)-p_2\mu_1\Omega_1(z_2)\right]\right\} \\
 & & \qquad +4\,\mathrm{Re}\left\{\frac{1}{\mu_2-\mu_1}\left[p_1\Omega_2(z_1)-p_2\Omega_2(z_2)\right]\right\} \\
\xi_y(z) & = & 4\,\mathrm{Re}\left\{\frac{1}{\mu_2-\mu_1}\left[q_1\mu_2\Omega_1(z_1)-q_2\mu_1\Omega_1(z_2)\right]\right\} \\
 & & \qquad +4\,\mathrm{Re}\left\{\frac{1}{\mu_2-\mu_1}\left(q_1\Omega_2(z_1)-q_2\Omega_2(z_2)\right]\right\}
\end{array}
\right. \tag{3.16}
$$

3.2.2 Complex potentials for the displacement-jump method

In the displacement-jump method (see Eq. (3.3)), we consider that the displacement jumps are given along the crack surface. Furthermore, we impose the stresses to be the same on both crack surfaces.

Introduce two new complex potentials, Ψ_1 and Ψ_2, such that:

$$
\left\{
\begin{array}{rcl}
\Phi_1(z_1) & = & \frac{1}{p_1q_2-p_2q_1}\left(q_2\Psi_1(z_1)-p_2\Psi_2(z_1)\right) \\
\Phi_2(z_2) & = & \frac{-1}{p_1q_2-p_2q_1}\left(q_1\Psi_1(z_2)+p_1\Psi_2(z_2)\right)
\end{array}
\right. \tag{3.17}
$$

(for $p_1q_2 \neq p_2q_1$). This will allow us to separate the normal and transverse displacement jumps. The normal and transverse displacements ξ_y and ξ_x can then be written as:

$$
\left\{
\begin{array}{rcl}
\xi_x(z) & = & 2\,\mathrm{Re}\left\{\frac{1}{p_1q_2-p_2q_1}\left[p_1q_2\Psi_1(z_1)-p_2q_1\Psi_1(z_2)\right]\right\} \\
 & & \qquad +2\,\mathrm{Re}\left\{\frac{p_1p_2}{p_1q_2-p_2q_1}\left[-\Psi_2(z_1)+\Psi_2(z_2)\right]\right\} \\
\xi_y(z) & = & 2\,\mathrm{Re}\left\{\frac{q_1q_2}{p_1q_2-p_2q_1}\left[\Psi_1(z_1)-\Psi_1(z_2)\right]\right\} \\
 & & \qquad +2\,\mathrm{Re}\left\{\frac{1}{p_1q_2-p_2q_1}\left[-p_2q_1\Psi_2(z_1)+p_1q_2\Psi_2(z_2)\right]\right\}
\end{array}
\right. \tag{3.18}
$$

Remark 8 *The reasoning conducted here should be valid only if the material elastic properties and the crack orientation are such that $p_1 q_2 \neq p_2 q_1$; which is not always true. For instance, isotropic materials are such that $\mu_1 = \mu_2 = i$ so that $p_1 = p_2$ and $q_1 = q_2$. However, this restriction can be overcome just as in Remark 5.*

More specifically, on the crack (for $z_c^{\pm} = x_c \pm i y_c \in \mathcal{L} \setminus \{-l, l\}$):

$$\left\{ \begin{array}{rcl} \xi_x(z_c^{\pm}) & = & 2\,\mathrm{Re}\left[\Psi_1'(z_c^{\pm})\right] \;=\; \Psi_1'(z_c^{\pm}) + \bar{\Psi}_1'(z_c^{\mp}) \\ \xi_y(z_c^{\pm}) & = & 2\,\mathrm{Re}\left[\Psi_2'(z_c^{\pm})\right] \;=\; \Psi_2'(z_c^{\pm}) + \bar{\Psi}_2'(z_c^{\mp}) \end{array} \right. \tag{3.19}$$

To satisfy the boundary conditions (3.3), we must have: $[\![\xi_i]\!](x_c) = D_i$ where $i = x$ of y so that Eq. (3.19) gives:

$$\left[\Psi_i - \bar{\Psi}_i\right](z_c^+) - \left[\Psi_i - \bar{\Psi}_i\right](z_c^-) \;=\; D_i(z_c) \quad \forall z_c \in \mathcal{L} \setminus \{-l, l\} \tag{3.20}$$

$\Psi_i - \bar{\Psi}_i$ is then given, close to a constant, by the Cauchy integral (see Section 2.2.3) with $h = D_i$, resulting in:

$$\Psi_i(z) - \bar{\Psi}_i(z) = \frac{1}{2i\pi} \int_{\mathcal{L}} \frac{D_i(t)}{t - z} dt \tag{3.21}$$

(we take the constant $C = 0$ in order to have the ξ_i vanish at infinity).
Furthermore, the normal and shear stresses are given by:

$$\left\{ \begin{array}{rcl} \sigma_{yy}(z) & = & 2\,\mathrm{Re}\left\{\frac{1}{p_1 q_2 - p_2 q_1}\left[q_2 \Psi_1'(z_1) - q_1 \Psi_1'(z_2)\right]\right\} \\ & & \quad +2\,\mathrm{Re}\left\{\frac{1}{p_1 q_2 - p_2 q_1}\left[-p_2 \Psi_2'(z_1) + p_1 \Psi_2'(z_2)\right]\right\} \\ \sigma_{xy}(z) & = & 2\,\mathrm{Re}\left\{\frac{1}{p_1 q_2 - p_2 q_1}\left[-\mu_1 q_2 \Psi_1(z_1) + \mu_2 q_1 \Psi_1(z_2)\right]\right\} \\ & & \quad +2\,\mathrm{Re}\left\{\frac{1}{p_1 q_2 - p_2 q_1}\left[\mu_1 p_2 \Psi_2(z_1) - \mu_2 p_1 \Psi_2(z_2)\right]\right\} \end{array} \right. \tag{3.22}$$

On the crack - for $z_c^{\pm} = x_c \pm i y_c \in \mathcal{L} \setminus \{-l, l\}$ - we have:

$$\left\{ \begin{array}{rcl} \sigma_{yy}(z_c^{\pm}) & = & 2\,\mathrm{Re}\left\{\frac{q_2 - q_1}{p_1 q_2 - p_2 q_1} \Psi_1'(z_c^{\pm})\right\} + 2\,\mathrm{Re}\left\{\frac{p_1 - p_2}{p_1 q_2 - p_2 q_1} \Psi_2'(z_c^{\pm})\right\} \\ \sigma_{xy}(z_c^{\pm}) & = & 2\,\mathrm{Re}\left\{\frac{-\mu_1 q_2 + \mu_2 q_1}{p_1 q_2 - p_2 q_1} \Psi_1'(z_c^{\pm})\right\} + 2\,\mathrm{Re}\left\{\frac{\mu_1 p_2 - \mu_2 p_1}{p_1 q_2 - p_2 q_1} \Psi_2'(z_c^{\pm})\right\} \end{array} \right. \tag{3.23}$$

which can be rewritten as:

$$\sigma_{iy}(z_c^{\pm}) = 2\,\mathrm{Re}\left\{\alpha_{ij} \Psi_j'(z_c^{\pm})\right\} \tag{3.24}$$

where $i = x$ or y and :

$$[\alpha] = \frac{1}{p_1 q_2 - p_2 q_1} \begin{bmatrix} q_2 - q_1 & p_1 - p_2 \\ -\mu_1 q_2 + \mu_2 q_1 & \mu_1 p_2 - \mu_2 p_1 \end{bmatrix} \tag{3.25}$$

The stress-boundary conditions in Eq. (3.3) then lead to:

$$\left[\alpha_{ij}\Psi'_j - \bar{\alpha}_{ij}\bar{\Psi}'_j\right](z_c^+) - \left[\alpha_{ij}\Psi'_j - \bar{\alpha}_{ij}\bar{\Psi}'_j\right](z_c^-) = 0 \tag{3.26}$$

$\alpha_{ij}\Psi'_j - \bar{\alpha}_{ij}\bar{\Psi}'_j$ is then given, close to a constant, by the Cauchy integral (see Section 2.2.3) with $h = 0$; resulting in:

$$\alpha_{ij}\Psi'_j - \bar{\alpha}_{ij}\bar{\Psi}'_j = 0 \tag{3.27}$$

(we take the constant $C = 0$ so that the stresses vanish at infinity).

This leads to:

$$\alpha_{ij}\Psi_j - \bar{\alpha}_{ij}\bar{\Psi}_j = c \tag{3.28}$$

where c is a constant.

Together, Eq. (3.28) and (3.21) give:

$$(\alpha_{ij} - \bar{\alpha}_{ij})\,\Psi_j(z) = -\frac{\bar{\alpha}_{ij}}{2i\pi}\int_{\mathcal{L}} \frac{D_j(t)}{t - z}dt + c \tag{3.29}$$

or:

$$\mathrm{Im}\{\alpha_{ij}\}\,\Psi_j(z) = \frac{\bar{\alpha}_{ij}}{4\pi}\int_{\mathcal{L}} \frac{D_j(t)}{t - z}dt + \frac{c}{2i} \tag{3.30}$$

Provided that $\det[\mathrm{Im}\{\alpha\}] \neq 0$, we can introduce $[\beta] = [\mathrm{Im}\{\alpha\}]^{-1}$, and deduce:

$$\Psi_i(z) = \frac{\beta_{ij}\bar{\alpha}_{jk}}{4\pi}\int_{\mathcal{L}} \frac{D_k(t)}{t - z}dt + \beta_{ij}\frac{c}{2i} \tag{3.31}$$

Again, we take the constant c equal to zero since there should be no displacement for $|z| \to \infty$.

We finally have:

$$\Psi_i(z) = \frac{\beta_{ij}\bar{\alpha}_{jk}}{4\pi}\int_{\mathcal{L}} \frac{D_k(t)}{t - z}dt \tag{3.32}$$

Now that we have the expression of Ψ_i in terms of the loading conditions, the stress and

displacement fields are known in the whole domain:

$$\left\{\begin{array}{rcl}
\sigma_{xx}(z) & = & 2\,\mathrm{Re}\left\{\frac{1}{p_1q_2-p_2q_1}\left[(\mu_1)^2 q_2\Psi_1'(z_1)-(\mu_2)^2 q_1\Psi_1'(z_2)\right]\right\} \\
& & +2\,\mathrm{Re}\left\{\frac{1}{p_1q_2-p_2q_1}\left[-(\mu_1)^2 p_2\Psi_2'(z_1)+(\mu_2)^2 p_1\Psi_2'(z_2)\right]\right\} \\
\sigma_{yy}(z) & = & 2\,\mathrm{Re}\left\{\frac{1}{p_1q_2-p_2q_1}\left[q_2\Psi_1'(z_1)-q_1\Psi_1'(z_2)\right]\right\} \\
& & +2\,\mathrm{Re}\left\{\frac{1}{p_1q_2-p_2q_1}\left[-p_2\Psi_2'(z_1)+p_1\Psi_2'(z_2)\right]\right\} \\
\sigma_{xy}(z) & = & 2\,\mathrm{Re}\left\{\frac{1}{p_1q_2-p_2q_1}\left[-\mu_1q_2\Psi_1'(z_1)+\mu_2q_1\Psi_1'(z_2)\right]\right\} \\
& & +2\,\mathrm{Re}\left\{\frac{1}{p_1q_2-p_2q_1}\left[\mu_1p_2\Psi_2'(z_1)-\mu_2p_1\Psi_2'(z_2)\right]\right\} \\
\xi_x(z) & = & 2\,\mathrm{Re}\left\{\frac{1}{p_1q_2-p_2q_1}\left[p_1q_2\Psi_1(z_1)-p_2q_1\Psi_1(z_2)\right]\right\} \\
& & +2\,\mathrm{Re}\left\{\frac{p_1p_2}{p_1q_2-p_2q_1}\left[-\Psi_2(z_1)+\Psi_2(z_2)\right]\right\} \\
\xi_y(z) & = & 2\,\mathrm{Re}\left\{\frac{q_1q_2}{p_1q_2-p_2q_1}\left[\Psi_1(z_1)-\Psi_1(z_2)\right]\right\} \\
& & +2\,\mathrm{Re}\left\{\frac{1}{p_1q_2-p_2q_1}\left[-p_2q_1\Psi_2(z_1)+p_1q_2\Psi_2(z_2)\right]\right\}
\end{array}\right. \tag{3.33}$$

3.3 Analysis of the displacement fields

3.3.1 On the deformed crack-shapes

We found in Section 3.2.1 the stress and displacement fields induced by a normal stress $-p$ and a shear stress $-q$ acting on the crack surfaces. From the displacement field, the crack shape induced by this loading can be deduced.

As the principle of superposition applies, we can study separately the normal stress $-p$ (derived from the complex potential Ω_1) and the shear stress $-q$ (derived from the complex potential Ω_2). To deduce the crack shape induced by the loading, one needs the displacement field $\xi_{x,i}(z_c)$ and $\xi_{y,i}(z_c)$ induced by the potential Ω_i ($i = 1$ or 2) for $z_c \in \mathcal{L} \setminus \{-l, l\}$.

Crack shape induced by the normal stress

By setting $\Omega_2 = 0$ in Eq. (3.16), one obtains[4]:

$$\left\{ \begin{array}{rcl} \xi_{x,1}(z_c^{\pm}) & = & 4\,\mathrm{Re}\left[\frac{p_1\mu_2 - p_2\mu_1}{\mu_2-\mu_1}\Omega_1(z_c^{\pm})\right] \\ \xi_{y,1}(z_c^{\pm}) & = & 4\,\mathrm{Re}\left[\frac{q_1\mu_2 - q_2\mu_1}{\mu_2-\mu_1}\Omega_1(z_c^{\pm})\right] \end{array} \right. \tag{3.34}$$

Since $p_1\mu_2 - p_2\mu_1 = -(\mu_2-\mu_1)(f_{11}\mu_1\mu_2 + f_{12})$ and $q_1\mu_2 - q_2\mu_1 = (\mu_2-\mu_1)(f_{22}\frac{\mu_1+\mu_2}{\mu_1\mu_2} - f_{23})$, we deduce that:

$$\left\{ \begin{array}{rcl} \xi_{x,1}(z_c^{\pm}) & = & -4\left(f_{11}\,\mathrm{Re}\left[\mu_1\mu_2\right] + f_{12}\right)\mathrm{Re}\left[\Omega_1(z_c^{+})\right] \\ & & \pm 4 f_{11}\,\mathrm{Im}\left[\mu_1\mu_2\right]\mathrm{Im}\left[\Omega_1(z_c^{+})\right] \\ \xi_{y,1}(z_c^{\pm}) & = & 4\left(f_{22}\,\mathrm{Re}\left[\frac{\mu_1+\mu_2}{\mu_1\mu_2}\right] - f_{23}\right)\mathrm{Re}\left[\Omega_1(z_c^{+})\right] \\ & & \mp 4 f_{22}\,\mathrm{Im}\left[\frac{\mu_1+\mu_2}{\mu_1\mu_2}\right]\mathrm{Im}\left[\Omega_1(z_c^{+})\right] \end{array} \right. \tag{3.35}$$

or:

$$\left\{ \begin{array}{rcl} \xi_{x,1}(x^{\pm}) & = & 8\pi\left(\mathcal{X}\mathrm{sgn}(x)\int_{t=0}^{|x|}\frac{F_1(t)+xG_1(t)}{\sqrt{x^2-t^2}}dt \;\pm\; \mathcal{K}\int_{t=|x|}^{l}\frac{F_1(t)+xG_1(t)}{\sqrt{t^2-x^2}}dt\right) \\ \xi_{y,1}(x^{\pm}) & = & 8\pi\left(\mathcal{Z}\mathrm{sgn}(x)\int_{t=0}^{|x|}\frac{F_1(t)+xG_1(t)}{\sqrt{x^2-t^2}}dt \;\mp\; \mathcal{H}\int_{t=|x|}^{l}\frac{F_1(t)+xG_1(t)}{\sqrt{t^2-x^2}}dt\right) \end{array} \right. \tag{3.36}$$

where we introduced the first set of *plane-strain elastic constants*:

$$\left\{ \begin{array}{rcl} \mathcal{X} & = & \frac{-1}{2\pi}\left(f_{11}\,\mathrm{Re}\left[\mu_1\mu_2\right] + f_{12}\right) \\ \mathcal{K} & = & \frac{-1}{2\pi} f_{11}\,\mathrm{Im}\left[\mu_1\mu_2\right] \\ \mathcal{Z} & = & \frac{1}{2\pi}\left(f_{22}\,\mathrm{Re}\left[\frac{\mu_1+\mu_2}{\mu_1\mu_2}\right] - f_{23}\right) \\ \mathcal{H} & = & \frac{-1}{2\pi} f_{22}\,\mathrm{Im}\left[\frac{\mu_1+\mu_2}{\mu_1\mu_2}\right] \end{array} \right. \tag{3.37}$$

Remark 9 *If the crack belongs to a plane of material symmetry, it can be shown (see Appendix E) that* $\mu_1 + \mu_2 \in i\mathbb{R}$, $\mu_1\mu_2 \in \mathbb{R}$ *and* $f_{23} = 0$ *so that* $\mathcal{K} = \mathcal{Z} = 0$ *and:*

$$\left\{ \begin{array}{rcl} \xi_{x,1}^{sym}(x^{\pm}) & = & 8\pi\mathcal{X}\,sgn(x)\int_{t=0}^{|x|}\frac{F_1(t)+xG_1(t)}{\sqrt{x^2-t^2}}dt \\ \xi_{y,1}^{sym}(x^{\pm}) & = & \mp 8\pi\mathcal{H}\int_{t=|x|}^{l}\frac{F_1(t)+xG_1(t)}{\sqrt{t^2-x^2}}dt \end{array} \right. \tag{3.38}$$

[4]One should remember that on the crack surface, $y_c = 0^{\pm}$ so that, since $\mathrm{Im}\,\mu_i > 0$, $z_1^{\pm} = z_2^{\pm} = z_c^{\pm}$.

Crack shape induced by the shear stress

By setting $\Omega_1 = 0$ in Eq. (3.16), one gets:

$$\left\{ \begin{array}{rcl} \xi_{x,2}(z_c^{\pm}) & = & 4\,\mathrm{Re}\left[\frac{p_1-p_2}{\mu_2-\mu_1}\Omega_2(z_c^{\pm})\right] \\ \xi_{y,2}(z_c^{\pm}) & = & 4\,\mathrm{Re}\left[\frac{q_1-q_2}{\mu_2-\mu_1}\Omega_2(z_c^{\pm})\right] \end{array} \right. \tag{3.39}$$

As $p_1 - p_2 = (\mu_2 - \mu_1)(f_{13} - f_{11}(\mu_1 + \mu_2))$ and $q_1 - q_2 = (\mu_2 - \mu_1)(\frac{f_{22}}{\mu_1\mu_2} - f_{12})$, we deduce that:

$$\left\{ \begin{array}{rcl} \xi_{x,2}(z_c^{\pm}) & = & 4\left(f_{13} - f_{11}\,\mathrm{Re}\left[\mu_1+\mu_2\right]\right)\mathrm{Re}\left[\Omega_2(z_c^{+})\right] \\ & & \pm 4 f_{11}\,\mathrm{Im}\left[\mu_1+\mu_2\right]\mathrm{Im}\left[\Omega_2(z_c^{+})\right] \\ \xi_{y,2}(z_c^{\pm}) & = & 4\left(f_{22}\,\mathrm{Re}\left[\frac{1}{\mu_1\mu_2}\right] - f_{12}\right)\mathrm{Re}\left[\Omega_2(z_c^{+})\right] \\ & & \mp 4 f_{22}\,\mathrm{Im}\left[\frac{1}{\mu_1\mu_2}\right]\mathrm{Im}\left[\Omega_2(z_c^{+})\right] \end{array} \right. \tag{3.40}$$

or:

$$\left\{ \begin{array}{rcl} \xi_{x,2}(x^{\pm}) & = & 8\pi\left(\mathcal{Z}'\mathrm{sgn}(x)\int_{t=0}^{|x|}\frac{F_2(t)+xG_2(t)}{\sqrt{x^2-t^2}}dt\right. \\ & & \left. \mp\,\mathcal{H}'\int_{t=|x|}^{l}\frac{F_2(t)+xG_2(t)}{\sqrt{t^2-x^2}}dt\right) \\ \xi_{y,2}(x^{\pm}) & = & 8\pi\left(-\mathcal{X}'\mathrm{sgn}(x)\int_{t=0}^{|x|}\frac{F_2(t)+xG_2(t)}{\sqrt{x^2-t^2}}dt\right. \\ & & \left. \pm\,\mathcal{K}\int_{t=|x|}^{l}\frac{F_2(t)+xG_2(t)}{\sqrt{t^2-x^2}}dt\right) \end{array} \right. \tag{3.41}$$

where we introduced the second set of *plane-strain elastic constants*:

$$\left\{ \begin{array}{rcl} \mathcal{Z}' & = & \frac{1}{2\pi}\left(f_{13} - f_{11}\,\mathrm{Re}\left[\mu_1+\mu_2\right]\right) \\ \mathcal{H}' & = & \frac{1}{2\pi} f_{11}\,\mathrm{Im}\left[\mu_1+\mu_2\right] \\ \mathcal{X}' & = & \frac{1}{2\pi}\left(f_{12} - f_{22}\,\mathrm{Re}\left[\frac{1}{\mu_1\mu_2}\right]\right) \\ \mathcal{K} & = & \frac{1}{2\pi} f_{22}\,\mathrm{Im}\left[\frac{1}{\mu_1\mu_2}\right] = \frac{-1}{2\pi} f_{11}\,\mathrm{Im}\left[\mu_1\mu_2\right] \end{array} \right. \tag{3.42}$$

Remark 10 *If the crack belongs to a plane of material symmetry, $\mathcal{K} = \mathcal{Z}' = 0$ and:*

$$\left\{ \begin{array}{rcl} \xi_{x,2}^{sym}(x^{\pm}) & = & \mp 8\pi\mathcal{H}'\int_{t=|x_c|}^{l}\frac{F_2(t)+xG_2(t)}{\sqrt{t^2-x_c^2}}dt \\ \xi_{y,2}^{sym}(x^{\pm}) & = & -8\pi\mathcal{X}'sgn(x)\int_{t=0}^{|x|}\frac{F_2(t)+xG_2(t)}{\sqrt{c^2-t^2}}dt \end{array} \right. \tag{3.43}$$

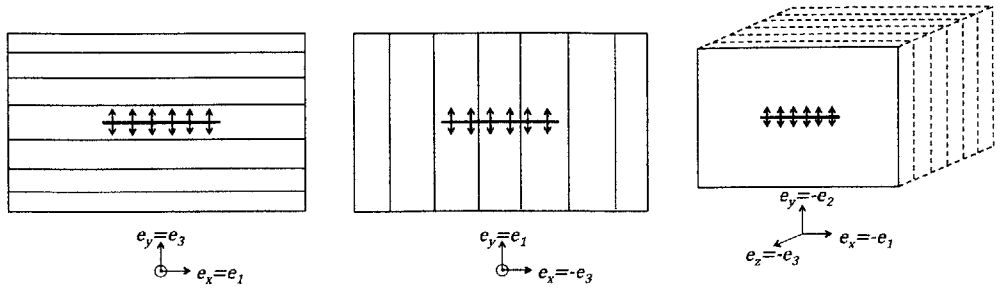

(a) Crack in bedding plane: $\underline{e}_y = \underline{e}_3$. (b) Crack normal to bedding plane: $\underline{e}_x = -\underline{e}_3$. (c) Transverse crack: $\underline{e}_z = -\underline{e}_3$.

Figure 3-3: Three crack orientations considered.

Crack displacement-jump induced by normal and shear stresses

From Eq. (3.36) and (3.41), one deduces the following normal and tangential displacement jumps, $[\![\xi_n]\!](x) = [\![\xi_y]\!](x)$ and $[\![\xi_t]\!](x) = [\![\xi_x]\!](x)$, respectively:

$$[\![\begin{pmatrix} \xi_n \\ \xi_t \end{pmatrix}]\!](x) = -16\pi \begin{bmatrix} \mathcal{H} & -\mathcal{K} \\ -\mathcal{K} & \mathcal{H}' \end{bmatrix} \int_{t=|x|}^{l} \frac{1}{\sqrt{t^2-x^2}} \begin{pmatrix} F_1(t)+xG_1(t) \\ F_2(t)+xG_2(t) \end{pmatrix} dt \qquad (3.44)$$

where the constants $\mathcal{H}$, $\mathcal{H}'$ and $\mathcal{K}$ are defined by Eq. (3.37) and (3.42). We will see shorlty that the square matrix involving these three constants will play an important role in the continuation.

3.3.2 Specification for transverse isotropy

Displacement field induced

We now focus on TI materials (as in the previous parts, $\underline{e}_3$ is the direction normal to the plane of isotropy). Let us introduce the stiffness constant[5] $C_{31} \equiv \sqrt{C_{11}C_{33}}$. As the strain energy must be positive: $\psi = \frac{1}{2}\underline{\underline{\epsilon}} : \underline{\underline{\underline{\underline{C}}}} : \underline{\underline{\epsilon}} \geqslant 0$, the stiffness tensor is positive definite. We then deduce that $\det[f] = \frac{1}{C_{44}(C_{31}^2 - C_{13}^2)} \geqslant 0$ (where the matrix $[f]$ was taken in the principal base $(\underline{e}_1, \underline{e}_2, \underline{e}_3)$), so that $C_{31}^2 > C_{13}^2$.

Let us first consider a crack belonging to the planes of material symmetry. For a TI material, the study of these special cracks reduces to the study of three crack orientations: 1) cracks in bedding plane (Fig. 3-3a), 2) cracks normal to bedding plane (Fig. 3-3b), 3)

[5]One should pay attention that this is a *definition* of C_{31}. C_{31} is different from C_{3311}: $C_{13} = C_{1133} = C_{3311} \neq C_{31}$.

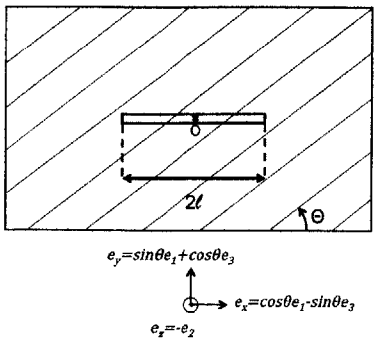

Figure 3-4: Rotated crack: $\widehat{(\underline{e}_z, \underline{e}_2)} = \pi$ and $\widehat{(\underline{e}_x, \underline{e}_1)} = \theta$.

transverse cracks (Fig. 3-3c). We can introduce the *plane-strain* elastic constants $\mathcal{X}_i$, $\mathcal{X}'_i$, $\mathcal{H}_i$ and $\mathcal{H}'_i$ introduced in Eq. (3.37) and (3.42) (where subscript $i = 1$, 2 or 3 stands for the crack orientation):

$$\left\{\begin{array}{rcccl} & \mathcal{X}_1 & = & \mathcal{X}_2 & = \frac{1}{2\pi}\frac{1}{C_{31}-C_{13}} \\ & & & \mathcal{X}_3 & = \frac{1}{2\pi}\frac{1}{C_{11}-C_{12}} \\ & \mathcal{X}'_1 & = & \mathcal{X}'_2 & = \frac{1}{2\pi}\frac{1}{C_{31}+C_{13}} \\ & & & \mathcal{X}'_3 & = \frac{1}{2\pi}\frac{1}{C_{11}+C_{12}} \\ & \mathcal{H}_1 & = & \mathcal{H}'_2 & = \frac{1}{2\pi}\sqrt{\frac{C_{11}}{C_{31}^2-C_{13}^2}\left(\frac{1}{C_{44}}+\frac{2}{C_{13}+C_{31}}\right)} \\ \mathcal{H}_2 = & \mathcal{H}'_1 & = & \sqrt{\frac{C_{33}}{C_{11}}}\mathcal{H}_1 & = \frac{1}{2\pi}\sqrt{\frac{C_{33}}{C_{31}^2-C_{13}^2}\left(\frac{1}{C_{44}}+\frac{2}{C_{13}+C_{31}}\right)} \\ & \mathcal{H}_3 & = & \mathcal{H}'_3 & = \frac{1}{\pi}\frac{C_{11}}{C_{11}^2-C_{12}^2} \end{array}\right. \tag{3.45}$$

A crack of type i will then have the following displacement field/pressure field relationships:

$$\left\{\begin{array}{rcl} \xi_x^i(x^\pm) & = & 8\pi\left(\mathcal{X}_i \mathrm{sgn}(x)\int_{t=0}^{|x|}\frac{F_1(t)+xG_1(t)}{\sqrt{x^2-t^2}}dt \right. \\ & & \left. \mp \mathcal{H}'_i\int_{t=|x|}^{l}\frac{F_2(t)+xG_2(t)}{\sqrt{t^2-x^2}}dt\right) \\ \xi_y^i(x^\pm) & = & 8\pi\left(-\mathcal{X}'_i \mathrm{sgn}(x)\int_{t=0}^{|x|}\frac{F_2(t)+xG_2(t)}{\sqrt{x^2-t^2}}dt \right. \\ & & \left. \mp \mathcal{H}_i\int_{t=|x|}^{l}\frac{F_1(t)+xG_1(t)}{\sqrt{t^2-x^2}}dt\right) \end{array}\right. \tag{3.46}$$

Let us consider cracks in a TI material such that $\widehat{(\underline{e}_z, \underline{e}_2)} = \pi$ and $\widehat{(\underline{e}_x, \underline{e}_1)} = \theta$ (see Fig. 3-4). $\hat{\mu}_1$ and $\hat{\mu}_2$ are the roots of $P_{[f](\theta=0)}(X)$ (see Section 2.2.2). It can be shown that $P_{[f](\theta)}\left(\frac{\sin\theta+X\cos\theta}{\cos\theta-X\sin\theta}\right) = P_{[f](\theta=0)}(X)$. As $\mathrm{Im}\left[\frac{\sin\theta+\hat{\mu}_i\cos\theta}{\cos\theta-\hat{\mu}_i\sin\theta}\right] > 0$ for $i = 1$ or 2, one deduces that $\mu_i(\theta) = \frac{\sin\theta+\hat{\mu}_i\cos\theta}{\cos\theta-\hat{\mu}_i\sin\theta}$.

The plane-strain elastic constants $\mathcal{X}$, $\mathcal{X}'$, $\mathcal{K}$, $\mathcal{Z}$, $\mathcal{Z}'$, $\mathcal{H}$ and $\mathcal{H}'$ defined in Eq. (3.37) and (3.42) then depend on θ and are given by:

$$\begin{cases} \mathcal{X}(\theta) &= \mathcal{X}_1\left(\cos^4\theta + \sin^4\theta\right) + 2\mathcal{X}_4\cos^2\theta\sin^2\theta \\ \mathcal{X}'(\theta) &= \mathcal{X}'_1 \\ \mathcal{K}(\theta) &= (\mathcal{H}_1 - \mathcal{H}_2)\cos\theta\sin\theta \\ \mathcal{Z}(\theta) &= 0 \\ \mathcal{Z}'(\theta) &= 0 \\ \mathcal{H}(\theta) &= \mathcal{H}_1\cos^2\theta + \mathcal{H}_2\sin^2\theta \\ \mathcal{H}'(\theta) &= \mathcal{H}_2\cos^2\theta + \mathcal{H}_1\sin^2\theta \end{cases} \tag{3.47}$$

where $\mathcal{X}_4 = \frac{1}{2\pi}\left(\frac{1}{C_{44}} + \frac{1}{C_{31}+C_{13}} - \frac{C_{11}+C_{33}}{C_{31}^2-C_{13}^2}\right)$.

On the *normal opening* elastic constants $\mathcal{H}_i$

The elastic constants $\mathcal{H}_i$ depend on the five (independent) characteristic constants of the TI material considered. These coefficients can be related to the first Thomsen parameter $\epsilon = \frac{C_{11}-C_{33}}{2C_{33}}$, accessible through accoustic measurements [44], and the indentation moduli[6] in the horizontal and vertical directions M_1 and M_3, respectively, accessible through indentation tests. Their expressions in terms of the stiffness constants C_{ij} can be found in Ref. [14]. Using these expressions, one obtains:

$$\begin{cases} \mathcal{H}_1 &= & \frac{1}{\pi M_3} \\ \mathcal{H}_2 &= \frac{1}{\pi}\sqrt{\frac{C_{33}}{C_{11}}}\frac{1}{M_3} &= \frac{1}{\pi\sqrt{1+2\epsilon}}\frac{1}{M_3} \\ \mathcal{H}_3 &\simeq \frac{1}{\pi}\sqrt{\frac{C_{11}}{C_{33}}}\frac{M_3}{M_1^2} &\simeq \frac{\sqrt{1+2\epsilon}}{\pi}\frac{M_3}{M_1^2} \end{cases} \tag{3.49}$$

For typical stiffness values of shales, we usually have (see Appendix C, Table C.3):

$$\mathcal{H}_1 > \mathcal{H}_2 > \mathcal{H}_3 \tag{3.50}$$

[6] "*The indentation modulus [in direction i] is defined from the unloading branch of an indentation test [...] [as]:*

$$\frac{dP_i}{dh} = \frac{2}{\sqrt{\pi}}M_i\sqrt{A} \tag{3.48}$$

where P_i is the applied load [in direction i], h is the rigid-body displacement of the indenter relative to the half-space [and] A is the projected area of contact."[14]

3.3.3 Crack geometry induced by uniform loading

The simplest case to study is the case of uniform loading $w_1^0 = p_0$, $w_2^0 = q_0$. We then have: $f_i(z) = w_i^0$, $g_i(z) = 0$, $i = 1$ or 2, so that, according to Eq. (3.15), the complex potentials Ω_i reduce to:

$$\Omega_i^0(z_c^+) = \frac{w_i^0}{4}\left(-x + i\sqrt{l^2 - x^2}\right) \tag{3.51}$$

The displacement field on the crack is then given by:

$$\begin{cases} \xi_x^0(z_c^\pm) &= A(p_0, q_0)x \;\pm\; B(p_0, q_0)\sqrt{l^2 - x^2} \\ \\ \xi_y^0(z_c^\pm) &= C(p_0, q_0)x \;\pm\; D(p_0, q_0)\sqrt{l^2 - x^2} \end{cases} \tag{3.52}$$

where

$$\begin{cases} A(p_0, q_0) &= -2\pi(\mathcal{X}p_0 + \mathcal{Z}'q_0) \\ B(p_0, q_0) &= -2\pi(\mathcal{K}p_0 - \mathcal{H}'q_0) \\ C(p_0, q_0) &= -2\pi(\mathcal{Z}p_0 - \mathcal{X}'q_0) \\ D(p_0, q_0) &= \;\; 2\pi(\mathcal{H}p_0 - \mathcal{K}q_0) \end{cases} \tag{3.53}$$

Initially, the crack is defined as $\Gamma = \{z = x \pm i\epsilon, x \in]-l, l[, \epsilon \to 0^+\}$. Let $z^\pm \in \Gamma$ be a point belonging to the initial crack. Define $s^\pm = z^\pm/l$ the dimensionless abscissa. The deformed crack shape is then defined as: $\Gamma' = \{z(s^\pm) = x(s^\pm) + iy(s^\pm), s \in]-1, 1[\}$ with:

$$\begin{cases} x(s^\pm) &= (1 + A(p_0, q_0))\, ls \pm B(p_0, q_0) l\sqrt{1 - s^2} \\ \\ y(s^\pm) &= C(p_0, q_0) ls \pm D(p_0, q_0) l\sqrt{1 - s^2} \end{cases} \tag{3.54}$$

The crack volume is then given by:

$$\mathcal{V}^0 = \mathcal{I}^+ - \mathcal{I}^- \tag{3.55}$$

where:

$$\mathcal{I}^\pm = \int_{x'(-1^\pm)}^{x'(1^\pm)} y'^\pm(x'^\pm)dx'^\pm \tag{3.56}$$

Since $dx^{\pm} = l\left[(1 + A(p_0, q_0)) \mp B(p_0, q_0)\frac{s}{\sqrt{1-s^2}}\right] ds$, we have:

$$\begin{aligned}\mathcal{I}^{\pm} &= l^2 \int_{-1}^{1} \left[C(p_0, q_0)s \pm D(p_0, q_0)\sqrt{1-s^2}\right] \left[(1 + A(p_0, q_0)) \mp B(p_0, q_0)\frac{s}{\sqrt{1-s^2}}\right] ds \\ &= \pm l^2 \frac{\pi}{2} \left[D(p_0, q_0)\left(1 + A(p_0, q_0)\right) - B(p_0, q_0)C(p_0, q_0)\right] \end{aligned} \tag{3.57}$$

so that the crack volume is given by:

$$\mathcal{V}^0 = \pi l^2 \left[D(p_0, q_0)\left(1 + A(p_0, q_0)\right) - B(p_0, q_0)C(p_0, q_0)\right] \tag{3.58}$$

It can be shown from Eq. (3.54) that:

- A crack subjected only to an uniform normal stress has always an elliptical deformed shape.
  - If the crack belongs to a plane of material symmetry, its principal axes are collinear to $\underline{e}_x$ and $\underline{e}_y$,
  - If the crack is in a TI material such that $\widehat{(\underline{e}_z, \underline{e}_2)} = \pi$ and $\widehat{(\underline{e}_x, \underline{e}_1)} = \theta$, its principal axes belong to the plane $z = 0$.
- The deformed shape of a crack subjected only to an uniform shear stress is an ellipse whose principal axes belong to the plane $z = 0$, *only* if the crack belongs to a plane of material symmetry .

3.4 On crack propagation

3.4.1 Energy release rate for a symmetrical and collinear crack propagation

A quantity of interest for fracture propagation is the energy release rate $\mathcal{G}(l)$, where l is the crack half-length (see Section 2.3).

We consider here that both crack tips propagate symmetrically and in a direction collinear to the initial crack (see Fig. 3-5). Furthermore, we consider that the pressure p and the shear stress q immediately after the crack propagation are null for $|x| \in]l, l + dl[$ and remain the same as before the propagation for $|x| \in [0, l + dl[$. For a crack filled with a

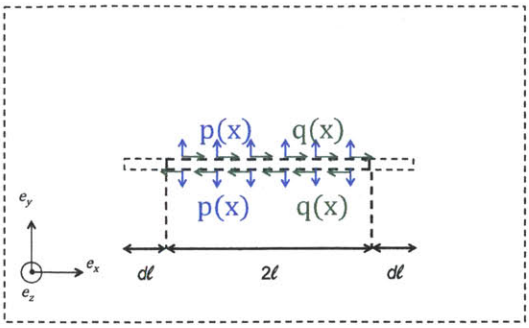

Figure 3-5: Symmetrical and collinear crack propagation.

fluid, this means that the fluid does not propagate as the crack tip does.

For our problem, using Clapeyron's formula [45], we have[7]:

$$\mathcal{E}_p(l) = -\frac{1}{2}\int_{x=-l}^{l} (p(x)[\![\xi_y]\!](x) + q(x)[\![\xi_x]\!](x))\, dx \tag{3.59}$$

The definition (2.38) of the energy release rate can be rewritten as:

$$\mathcal{G}(l) = -\lim_{dl\to 0} \frac{\mathcal{E}_p(l+dl) - \mathcal{E}_p(l)}{2dl} \tag{3.60}$$

so that:

$$\begin{aligned}\mathcal{G}(l) = 4\Big\{ & \mathcal{H}\left[l\left(\int_{u=0}^{l}\frac{f_1(u)du}{\sqrt{l^2-u^2}}\right)^2 + \frac{1}{l}\left(\int_{u=0}^{l}\frac{ug_1(u)du}{\sqrt{l^2-u^2}}\right)^2\right] \\ & +\mathcal{H}'\left[l\left(\int_{u=0}^{l}\frac{f_2(u)du}{\sqrt{l^2-u^2}}\right)^2 + \frac{1}{l}\left(\int_{u=0}^{l}\frac{ug_2(u)du}{\sqrt{l^2-u^2}}\right)^2\right] \\ & -2\mathcal{K}\left[l\int_{u=0}^{l}\frac{f_1(u)du}{\sqrt{l^2-u^2}}\int_{u=0}^{l}\frac{f_2(u)du}{\sqrt{l^2-u^2}} + \frac{1}{l}\int_{u=0}^{l}\frac{ug_1(u)du}{\sqrt{l^2-u^2}}\int_{u=0}^{l}\frac{ug_2(u)du}{\sqrt{l^2-u^2}}\right]\Big\}\end{aligned} \tag{3.61}$$

If we introduce the fracture energy (or critical energy release rate) $\mathcal{G}_c$, the propagation will be possible only if $\mathcal{G}(l) = \mathcal{G}_c$.

3.4.2 The local approach

In the previous Section, we used an energy (global) approach: we derived the energy release rate from the potential energy of the whole structure. In linear elastic fracture mechanics, another approach focuses on what happens at the crack tip. Relevant quantities are then

[7] A detailed computation of the energy release rate is given in Appendix F.

the stress intensity factors (see Section 2.3.2).

From the complex potentials Ω_i' found in Part 3.2.1, we can quantify the strength of the singularity of the stress fields at each crack tip by computing the Mode I and Mode II stress intensity factors.

For the left-hand crack tip, we define $K_I^\ell(l)$ and $K_{II}^\ell(l)$ the Mode I and Mode II stress intensity factors:

$$\left\{ \begin{array}{rcl} K_I^\ell(l) & = & \lim\limits_{r\to 0^+} \sqrt{2\pi r}\sigma_{yy}(z=-l-r) \\ K_{II}^\ell(l) & = & \lim\limits_{r\to 0^+} \sqrt{2\pi r}\sigma_{xy}(z=-l-r) \end{array} \right. \tag{3.62}$$

For the right-hand crack tip, we define $K_I^r(l)$ and $K_{II}^r(l)$ the Mode I and Mode II stress intensity factors:

$$\left\{ \begin{array}{rcl} K_I^r(l) & = & \lim\limits_{r\to 0^+} \sqrt{2\pi r}\sigma_{yy}(z=l+r) \\ K_{II}^r(l) & = & \lim\limits_{r\to 0^+} \sqrt{2\pi r}\sigma_{xy}(z=l+r) \end{array} \right. \tag{3.63}$$

On the plane $y=0$, putting together Eq. (3.12) and (3.16), we have:

$$\left\{ \begin{array}{rcl} \sigma_{yy}(x) & = & \frac{\mathrm{sgn}(x)}{\pi\sqrt{x^2-l^2}} \int_{t=-l}^{l} p(t)\frac{\sqrt{l^2-t^2}}{x-t}dt \\ \sigma_{xy}(x) & = & \frac{\mathrm{sgn}(x)}{\pi\sqrt{x^2-l^2}} \int_{t=-l}^{l} q(t)\frac{\sqrt{l^2-t^2}}{x-t}dt \end{array} \right. \tag{3.64}$$

Remark 11 *It is worth mentioning that since σ_{yy} and σ_{xy} do not depend (at least on the plane $y=0$) on the elastic properties of the material, the stress intensity factors will also be independent of the elastic properties.*

One deduces from Eq. (3.64) the following expressions for the left-hand and right-hand stress intensity factors:

$$\left\{ \begin{array}{rcl} K_I^\ell(l) & = & \frac{1}{\sqrt{\pi l}} \int_{t=-l}^{l} p(t)\sqrt{\frac{l-t}{l+t}}dt \\ & = & 2\left\{ \sqrt{\frac{l}{\pi}} \int_{t=0}^{l} \frac{f_1(t)dt}{\sqrt{l^2-t^2}} - \frac{1}{\sqrt{\pi l}} \int_{t=0}^{l} \frac{tg_1(t)dt}{\sqrt{l^2-t^2}} \right\} \\ K_{II}^\ell(l) & = & \frac{1}{\sqrt{\pi l}} \int_{t=-l}^{l} q(t)\sqrt{\frac{l-t}{l+t}}dt \\ & = & 2\left\{ \sqrt{\frac{l}{\pi}} \int_{t=0}^{l} \frac{f_2(t)dt}{\sqrt{l^2-t^2}} - \frac{1}{\sqrt{\pi l}} \int_{t=0}^{l} \frac{tg_2(t)dt}{\sqrt{l^2-t^2}} \right\} \end{array} \right. \tag{3.65}$$

and:

$$\left\{\begin{array}{rcl} K_I^r(l) & = & \frac{1}{\sqrt{\pi l}}\int_{t=-l}^{l} p(t)\sqrt{\frac{l+t}{l-t}}dt \\ & = & 2\left\{\sqrt{\frac{l}{\pi}}\int_{t=0}^{l}\frac{f_1(t)dt}{\sqrt{l^2-t^2}} + \frac{1}{\sqrt{\pi l}}\int_{t=0}^{l}\frac{tg_1(t)dt}{\sqrt{l^2-t^2}}\right\} \\ K_{II}^r(l) & = & \frac{1}{\sqrt{\pi l}}\int_{t=-l}^{l} q(t)\sqrt{\frac{l+t}{l-t}}dt \\ & = & 2\left\{\sqrt{\frac{l}{\pi}}\int_{t=0}^{l}\frac{f_2(t)dt}{\sqrt{l^2-t^2}} + \frac{1}{\sqrt{\pi l}}\int_{t=0}^{l}\frac{tg_2(t)dt}{\sqrt{l^2-t^2}}\right\} \end{array}\right. \tag{3.66}$$

If the loading is symmetrical (i.e. if $g_i = 0$, $i = 1$ or 2), the left-hand and right-hand stress intensity factors are obviously the same ($K_j^\ell(l) = K_j^r(l)$, $j = I$ or II).

3.4.3 Generalized Irwin's formula

Let us write the stress intensity vector $\{K\} = {}^t[K_I, K_{II}]$. For any crack problem in mixed-modes I and II, the generalized Irwin formula for an anisotropic material containing a crack propagating collinearly (i.e. without branching) is given by Eq. (2.39), which we recall:

$$\mathcal{G}(l) = \pi^t\{K\}.[H].\{K\} \tag{3.67}$$

where the Irwin matrix $[H]$ is given by Eq. (2.43). It can actually be rewritten in terms of the *plane-strain* elastic constants introduced in Eq. (3.37) as:

$$[H] = \begin{bmatrix} \mathcal{H} & -\mathcal{K} \\ -\mathcal{K} & \mathcal{H}' \end{bmatrix} \tag{3.68}$$

The Irwin matrix only depends on the crack orientation and the elastic properties of the material.

This is consistent with the energy release rate expression computed previously - Eq. (3.61) - from $\mathcal{G}(l) = -\frac{\partial \mathcal{E}_p}{2\partial l}(l)$. Indeed as we consider that the two crack tips propagate

symmetrically and without branching, Irwin's formula gives:

$$\begin{aligned}
\mathcal{G}(l) &= \frac{\mathcal{G}^\ell(l)+\mathcal{G}^r(l)}{2} \\
&= \frac{\pi}{2}\left\{\mathcal{H}\left(\left[K_I^\ell(l)\right]^2+[K_I^r(l)]^2\right)+\mathcal{H}'\left(\left[K_{II}^\ell(l)\right]^2+[K_{II}^r(l)]^2\right)\right. \\
&\qquad \left.-2\mathcal{K}\left(K_I^\ell(l)K_{II}^\ell(l)+K_I^r(l)K_{II}^r(l)\right)\right\} \\
&= 4\left\{\mathcal{H}\left[l\left(\int_{u=0}^{l}\frac{f_1(u)du}{\sqrt{l^2-u^2}}\right)^2+\frac{1}{l}\left(\int_{u=0}^{l}\frac{ug_1(u)du}{\sqrt{l^2-u^2}}\right)^2\right]\right. \\
&\quad +\mathcal{H}'\left[l\left(\int_{u=0}^{l}\frac{f_2(u)du}{\sqrt{l^2-u^2}}\right)^2+\frac{1}{l}\left(\int_{u=0}^{l}\frac{ug_2(u)du}{\sqrt{l^2-u^2}}\right)^2\right] \\
&\quad \left.-2\mathcal{K}\left[l\int_{u=0}^{l}\frac{f_1(u)du}{\sqrt{l^2-u^2}}\int_{u=0}^{l}\frac{f_2(u)du}{\sqrt{l^2-u^2}}+\frac{1}{l}\int_{u=0}^{l}\frac{ug_1(u)du}{\sqrt{l^2-u^2}}\int_{u=0}^{l}\frac{ug_2(u)du}{\sqrt{l^2-u^2}}\right]\right\}
\end{aligned} \tag{3.69}$$

3.4.4 On the near-tip displacement jump

Using Eq. (3.44), the near-tip normal and tangential displacement jumps, $[\![\xi_n]\!](r) = [\![\xi_y]\!](r)$ and $[\![\xi_t]\!](r) = [\![\xi_x]\!](r)$ (where $x = \pm(l-r)$), respectively, can be written in terms of the stress intensity factors as (a proof is given in Appendix G):

$$[\![\begin{pmatrix}\xi_n\\ \xi_t\end{pmatrix}]\!](r) \underset{r\to 0}{\sim} 8\pi\sqrt{\frac{r}{2\pi}}\,[H].\{K\} \tag{3.70}$$

where the matrix $[H]$ is the 2x2 the symmetric Irwin matrix introduced in Eq. (2.43).

In isotropy, we saw in Part 2.3.2 that the matrix $[H]$ was diagonal and equal to $[H] = \frac{1-\nu^2}{\pi E}\mathbb{1}$ so that a crack subjected to loading conditions inducing only a hoop (respectively shear) stress singularity will only have a normal (respectively tangential) displacement jump on its surface.

In anisotropy, unless under specific conditions[8], the Irwin matrix is not diagonal. This means that a crack subjected to loading conditions inducing only a hoop stress singularity ($K_I > 0$, $K_{II} = 0$) will have not only a normal displacement jump $[\![\xi_n]\!](r) \underset{r\to 0}{\sim} 8\pi\sqrt{\frac{r}{2\pi}}\mathcal{H}K_I$ but also a tangential displacement jump $[\![\xi_t]\!](r) \underset{r\to 0}{\sim} -8\pi\sqrt{\frac{r}{2\pi}}\mathcal{K}K_I$ on its surface. Similarly, a crack subjected to loading conditions inducing only a shear stress singularity ($K_I = 0$, $K_{II} \neq 0$) will have not only a tangential displacement jump $[\![\xi_t]\!](r) \underset{r\to 0}{\sim} 8\pi\sqrt{\frac{r}{2\pi}}\mathcal{H}'K_I$ but also a normal displacement jump $[\![\xi_n]\!](r) \underset{r\to 0}{\sim} -8\pi\sqrt{\frac{r}{2\pi}}\mathcal{K}K_{II}$ on its surface.

[8]Notably, when the crack belongs to a plane of material symmetry, it is shown in Appendix E that $\mu_1\mu_2 \in \mathbb{R}$ so that $\mathcal{K} = H_{12} = H_{21} = 0$.

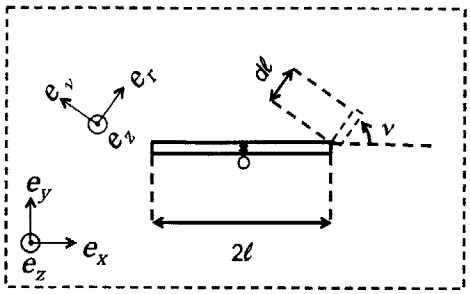

Figure 3-6: Crack kink, definition of the angle ν.

To be consistent with the denomination of Mode I and Mode II stress intensity factors, the definition of the fracture modes should be given in terms of stresses instead of displacement jumps as it is usually the case in isotropic media (see Section 2.3.1).

Remark 12 *In the specific case of plane strain, a definition of the fracture modes in terms of the stresses would also be confusing. Indeed, as we have seen in Eq.* (2.17)*, for some crack orientations, the out of plane shear stress σ_{yz} is proportional to the in plane shear stress σ_{xy}. This infers that the Modes II and III cannot be separated, meaning that it would be possible to be in presence of Mode III even in a two-dimensional plane-strain problem. However, since the third Mode shall not contribute to the energy release rate ($[\![\xi_b]\!] = [\![\xi_z]\!] = 0$), it can be disregarded.*

3.4.5 On the direction of crack propagation

Until now, we have considered only collinear crack propagation. If we were dealing with isotropic materials, this would be perfectly legitimate if the loading prescribed on the crack was a pure Mode I loading (see Section 2.3.3). However, we will see in the continuation that in anisotropy, crack-kinking can be more favorable than collinear crack extension even in pure Mode I, depending on the propagation criterion chosen.

Irwin's formula for a kinked crack

Let us now consider that the crack does not propagate collinearly. Instead, it propagates by an amount dl with an angle ν with respect to its original orientation (see Fig. 3-6). It is legitimate to consider that for a very small extension $dl \to 0$ and for a small kink angle ν, the

stress field at the crack tip will be similar to the stress field derived in Section 3.2. We can then introduce the new stress intensity factors $K_I^{\star r,l}(l,\nu)$ and $K_{II}^{\star r,l}(l,\nu)$ for an infinitesimal small kink and for a small kink angle:

$$\left\{\begin{array}{rcl} K_I^{\star r,l}(l,\nu) & = & \lim\limits_{dl\to 0^+} \sqrt{2\pi dl}\sigma_{\nu\nu}\left(z^{r,l}(dl,\nu)\right) \\ K_{II}^{\star r,l}(l,\nu) & = & \lim\limits_{dl\to 0^+} \sqrt{2\pi dl}\sigma_{r\nu}\left(z^{r,l}(dl,\nu)\right) \end{array}\right. \tag{3.71}$$

where $z_i^r(dl,\nu) = l + dl\cos\nu + \mu_i dl\sin\nu$ and $z_i^l(dl,\nu) = -z_i^r(dl,\nu)$ are the coordinates of the left-hand and right-hand crack tips, and:

$$\left\{\begin{array}{rcl} \sigma_{\nu\nu} & = & \left(\underline{\underline{\sigma}}.\underline{e}_\nu\right).\underline{e}_\nu = \sigma_{xx}\sin^2\nu + \sigma_{yy}\cos^2\nu - 2\sigma_{xy}\sin\nu\cos\nu \\ \sigma_{r\nu} & = & \left(\underline{\underline{\sigma}}.\underline{e}_\nu\right).\underline{e}_r = \sigma_{xy}\left(\sin^2\nu - \cos^2\nu\right) + \left(\sigma_{xx} - \sigma_{yy}\right)\sin\nu\cos\nu \end{array}\right. \tag{3.72}$$

are the hoop and shear stresses in the new local crack-tip polar coordinates (r,ν).

Noting that:

$$\left\{\begin{array}{rcl} \lim\limits_{dl\to 0^+} \sqrt{2\pi dl}\Omega_1'\left(z_i(dl,\nu)\right) & = & \frac{1}{\sqrt{\cos\nu+\mu_i\sin\nu}}K_I(l) \\ \lim\limits_{dl\to 0^+} \sqrt{2\pi dl}\Omega_2'\left(z_i(dl,\nu)\right) & = & \frac{1}{\sqrt{\cos\nu+\mu_i\sin\nu}}K_{II}(l) \end{array}\right. \tag{3.73}$$

where the Ω_i' are those of Eq. (3.12), we have:

$$\{K^\star(l,\nu)\} = [F(\nu)].\{K(l)\} \tag{3.74}$$

where [4]:

$$\left\{\begin{array}{rcl} F_{I,I}(\nu) & = & 4\,\mathrm{Re}\left[\frac{\mu_2}{\mu_2-\mu_1}\left(\mu_1\sin\nu+\cos\nu\right)^{3/2}\right. \\ & & \left. -\frac{\mu_1}{\mu_2-\mu_1}\left(\mu_2\sin\nu+\cos\nu\right)^{3/2}\right] \\ F_{I,II}(\nu) & = & 4\,\mathrm{Re}\left[\frac{1}{\mu_2-\mu_1}\left(\mu_1\sin\nu+\cos\nu\right)^{3/2}\right. \\ & & \left. -\frac{1}{\mu_2-\mu_1}\left(\mu_2\sin\nu+\cos\nu\right)^{3/2}\right] \\ F_{II,I}(\nu) & = & 4\,\mathrm{Re}\left[\frac{\mu_2}{\mu_2-\mu_1}\sqrt{\mu_1\sin\nu+\cos\nu}\left(-\mu_1\cos\nu+\sin\nu\right)\right. \\ & & \left. -\frac{\mu_1}{\mu_2-\mu_1}\sqrt{\mu_2\sin\nu+\cos\nu}\left(-\mu_2\cos\nu+\sin\nu\right)\right] \\ F_{II,II}(\nu) & = & 4\,\mathrm{Re}\left[\frac{1}{\mu_2-\mu_1}\sqrt{\mu_1\sin\nu+\cos\nu}\left(-\mu_1\cos\nu+\sin\nu\right)\right. \\ & & \left. -\frac{1}{\mu_2-\mu_1}\sqrt{\mu_2\sin\nu+\cos\nu}\left(-\mu_2\cos\nu+\sin\nu\right)\right] \end{array}\right. \tag{3.75}$$

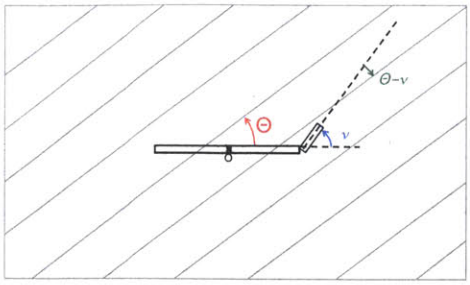

Figure 3-7: Definition of the θ and ν angles.

A possible expression for the energy release rate of a (single) crack tip kinking with an angle ν with respect to the initial crack direction would then be [4]:

$$\mathcal{G}^\star(l,\nu) = \pi^t\{K^\star(l,\nu)\}\,.\,[H^\star(\nu)]\,.\,\{K^\star(l,\nu)\} \tag{3.76}$$

where $[H^\star(\nu)]$ is the Irwin matrix $[H]$ introduced in Section 3.4.3 for a crack having the same orientation as the kink. For instance, if we consider a crack in a TI material such that $\widehat{(\underline{e}_z,\underline{e}_2)} = \pi$ and $\widehat{(\underline{e}_x,\underline{e}_1)} = \theta$, we have $[H^\star(\nu,\theta)] = [H(\theta-\nu)]$ (see Fig. 3-7).

As $F_{I,I}(0) = F_{II,II}(0) = 1$ and $F_{II,I}(0) = F_{I,II}(0) = 0$, we obviously have $\mathcal{G}^\star(l,\nu=0) = \mathcal{G}(l)$.

Some propagation criteria in anisotropy

Possible generalizations to anisotropy of the crack-propagation criterion introduced for isotropic materials in Section2.3.2 could be as follows:

- If there is propagation, it will be done at a kink angle ν_{kink} such that:
  - $\nu_{kink} = \arg\max_\nu \frac{\mathcal{G}^\star(\nu)}{\mathcal{G}_c(\nu)}$ (maximum energy release rate criterion) or,
  - $\nu_{kink} = \arg\max_\nu K_I^\star(\nu)$ (maximum hoop stress criterion) or,
  - ν_{kink} such that $K_{II}^\star(\nu_{kink}) = 0$ (principle of local symmetry)
- $\begin{cases} \mathcal{G}^\star(\nu_{kink}) & < & \mathcal{G}_c(\nu_{kink}) & \text{no crack propagation} \\ \mathcal{G}^\star(\nu_{kink}) & = & \mathcal{G}_c(\nu_{kink}) & \text{possible crack propagation} \end{cases}$

where $\mathcal{G}_c$ is the fracture energy for a crack propagating in the direction of the kink. This quantity is considered to be a material property independent of the geometry and of the

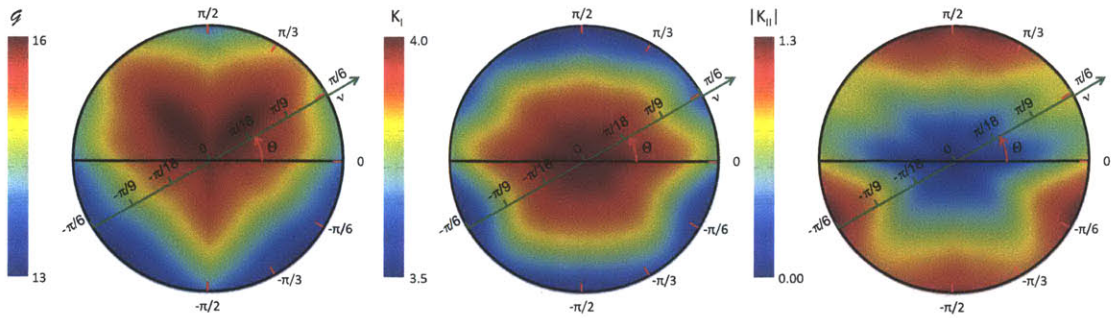

Figure 3-8: $\bar{\mathcal{G}}(\theta,\nu)$, $\bar{K}_I^\star(\nu,\theta)$ and $|\bar{K}_{II}^\star(\nu,\theta)|$ in the polar coordinates (ν,θ) for a TI clay model [37] subjected to a pure Mode I loading.

applied load. In an anisotropic material, it could depend on the direction of the crack propagation.

Remark 13 *As* $\frac{\partial K_I^\star}{\partial \nu}(\nu) \propto K_{II}^\star(\nu)$, *the last two criteria should be equivalent.*

Considering $\mathcal{G}_c$ independent of the crack orientation, we can define the functions $\bar{\mathcal{G}}$, $\bar{K}_I^\star$ and $|\bar{K}_{II}^\star$ as:

$$\begin{cases} \bar{\mathcal{G}}(\nu) &= \frac{{}^t\{K\}.{}^t[F(\nu)].[H^*(\nu)].[F(\nu)].\{K\}}{{}^t\{K\}.[H].\{K\}} \\ \bar{K}_I^\star(\nu) &= F_{I,I}(\nu) + F_{I,II}(\nu)\frac{K_{II}}{K_I} \\ |\bar{K}_{II}^\star(\nu)| &= |F_{II,I}(\nu) + F_{II,II}(\nu)\frac{K_{II}}{K_I}| \end{cases} \tag{3.77}$$

Depending on the chosen criterion, these functions should tell us at which kink angle the propagation should be the most favorable.

For a crack in a TI material such that $\widehat{(\underline{e}_z, \underline{e}_2)} = \pi$ and $\widehat{(\underline{e}_x, \underline{e}_1)} = \theta$ (Fig. 2-2) subjected to a pure Mode I loading, we plot in Fig. 3-8 and 3-9 *kink diagrams* showing $\bar{\mathcal{G}}(\theta,\nu)$, $\bar{K}_I^\star(\nu,\theta)$ and $|\bar{K}_{II}^\star(\nu,\theta)|$ in the polar coordinates (ν,θ) for a TI clay model [37] and for a reference[9] TI medium.

Figures 3-10 and 3-11 show ν_{kink} as a function of the crack orientation θ for the clay model [37] and the reference TI material, respectively. The fracture energy $\mathcal{G}_c$ is taken independent of the crack orientation and the loading is a pure Mode I loading. For a crack belonging to a plane of material symmetry ($\theta \equiv 0\left[\frac{\pi}{2}\right]$), the kinking angle is null so that, as

[9]This reference material is such that $E_1 = 1$ GPa, $E_3 = 2$ GPa, $\nu_{12} = 0$, $\nu_{13} = 0.4$ and $G_{23} = 1$ GPa, see Table C.4.

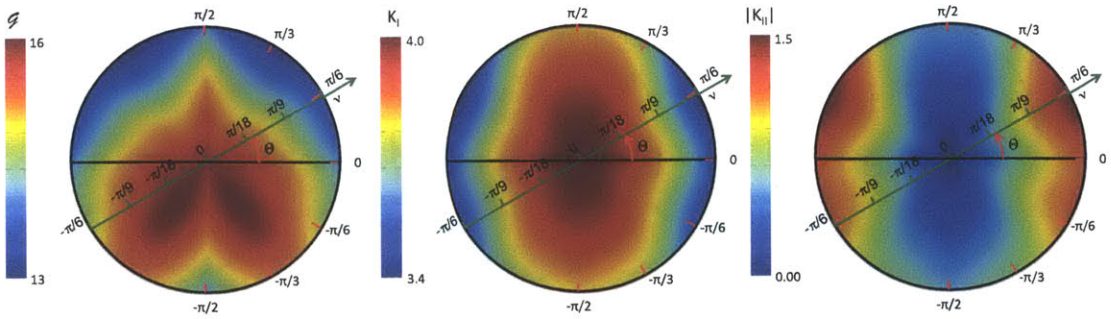

Figure 3-9: $\bar{\mathcal{G}}(\theta,\nu)$, $\bar{K}_I^\star(\nu,\theta)$ and $|\bar{K}_{II}^\star(\nu,\theta)|$ in the polar coordinates (ν,θ) for the reference TI material subjected to a pure Mode I loading.

in isotropy, no kinking should occur for a pure Mode I loading. However, if the initial crack does not belong to a plane of material symmetry and if we consider the maximum energy release rate criterion, ν_{kink} does not vanish anymore so that kinking should occur even for a pure Mode I loading. If the zero-$K_{II}^\star$ and the max-$K_I^\star$ criteria are consistent, the max-$\bar{\mathcal{G}}$ criterion diverges from the two others. While in Mode I the zero-$K_{II}^\star$ and max-$K_I^\star$ predict a collinear crack propagation, the max-$\mathcal{G}$ predicts a crack-kinking.

If one opts for the max-$\mathcal{G}$ criterion, a *stability*[10] analysis predicts that a crack belonging to the plane of material symmetry for which the $\mathcal{H}$ coefficient is the greater, will be more stable. By way of example, for the clay model for which $\mathcal{H}(\theta=\pi/2)=\mathcal{H}_2<\mathcal{H}_1=\mathcal{H}(\theta=0)$, if the initial crack has an orientation $\theta=\pm\epsilon$ with ϵ positive and close to zero, the kinked angle ν will have the same sign as θ so that the crack tip will eventually go back to the *stable* plane $\theta=0$. However, if the initial crack has an orientation $\theta=\pi/2\pm\epsilon$ with ϵ positive and close to zero, the kinked angle ν will have an opposit sign as $\theta-\pi/2$ so that the crack tip will move away from the plane $\theta=\pi/2$. The same kind of argument can be made for the reference TI material for which $\mathcal{H}(\theta=\pi/2)=\mathcal{H}_2>\mathcal{H}_1=\mathcal{H}(\theta=0)$; for this one, the *stable* plane is the plane $\theta=\pi/2$.

If we now consider the third type of cracks (Fig. 3-3c), the functions $F_{I,I}^{(3)}(\nu)$ and $F_{II,I}^{(3)}(\nu)$ are ill defined since $\mu_1=\mu_2=i$. A trick to overcome this problem is to set $\mu_1=\epsilon+i$ and

[10] In LEFM, a crack is said to be *stable* if $\frac{\partial\mathcal{G}}{\partial l}\leq 0$. The term *stability* is used here in a different context.

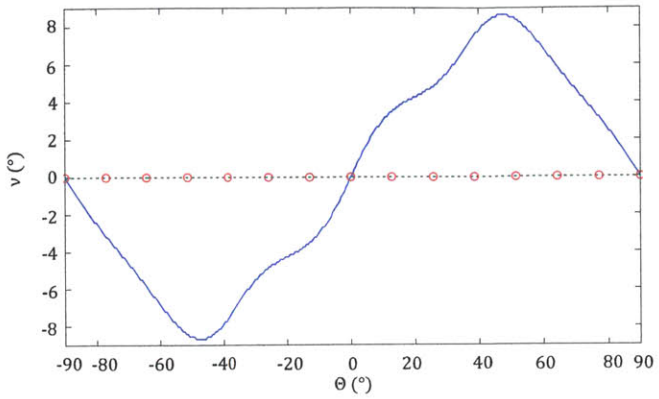

Figure 3-10: Comparison of the three criteria for the clay model subjected to a pure Mode I loading (in solid blue: max-$\mathcal{G}$, in dashed green: max-$K_I^\star$ and in red circle: zero-$K_{II}^\star$).

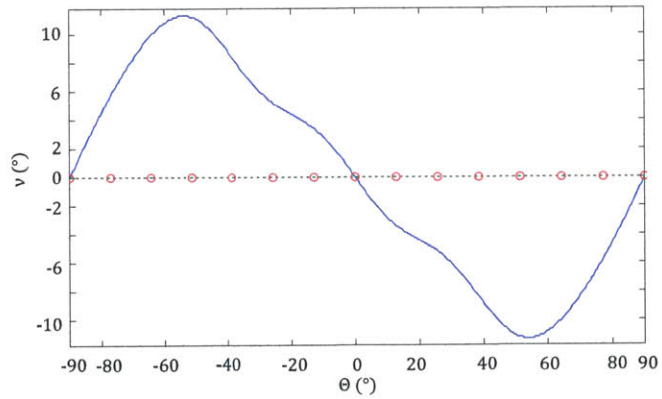

Figure 3-11: Comparison of the three criteria for the reference TI material subjected to a pure Mode I loading (in solid blue: max-$\mathcal{G}$, in dashed green: max-$K_I^\star$ and in red circle: zero-$K_{II}^\star$).

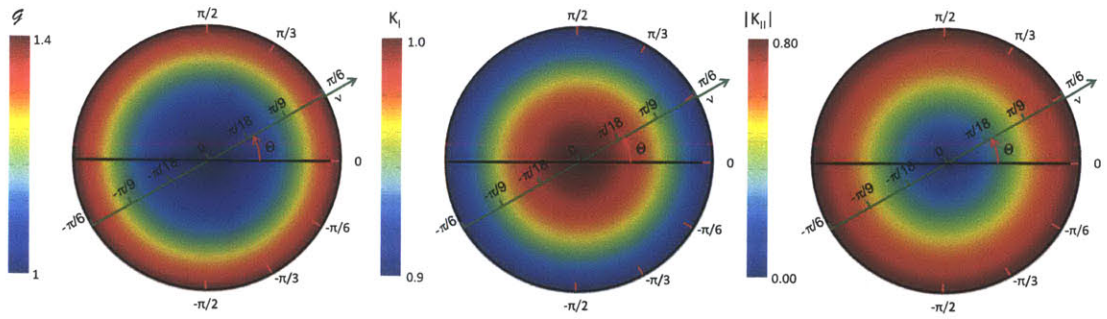

Figure 3-12: $\bar{\mathcal{G}}(\theta,\nu)$, $\bar{K}_I^\star(\nu,\theta)$ and $|\bar{K}_{II}^\star(\nu,\theta)|$ in the polar coordinates (ν,θ) for a crack of the third type subjected to a pure Mode I loading.

$\mu_2 = -\epsilon + i$. A Taylor series at the first order in ϵ of $F_{i,j}^{(3)}$ gives us:

$$\left\{\begin{array}{rcl} F_{I,I}^{(3)}(\nu) & = & \cos\nu\cos\frac{\nu}{2} + \frac{1}{2}\sin\nu\sin\frac{\nu}{2} \\ F_{II,I}^{(3)}(\nu) & = & \frac{1}{2}\sin\nu\cos\frac{\nu}{2} \\ F_{I,II}^{(3)}(\nu) & = & -\frac{3}{2}\sin\nu\cos\frac{\nu}{2} \\ F_{II,II}^{(3)}(\nu) & = & \cos\nu\cos\frac{\nu}{2} - \frac{1}{2}\sin\nu\sin\frac{\nu}{2} \end{array}\right. \tag{3.78}$$

These are the classical terms for isotropic materials (see Ref. [12]). For this type of cracks, $\bar{\mathcal{G}}(\theta,\nu)$, $K_I^\star(\theta,\nu)$ and $|K_{II}^\star(\theta,\nu)|$ are independent of θ but also independent of the elastic properties of the material since the crack kink *sees* the same elasticity as the main crack ($[H^\star(\nu)] = [H]$). These quantities are plotted for a pure Mode I loading on Fig. 3-12.

Remark 14 *At high kink angles, one can put in question the legitimacy of the use of the functions $F_{i,j}(\nu)$ from Eq. (3.75) (derived from the stress field before kinking). However, if we restrict ourselves to Mode I dominant loadings, the three criteria seem to agree that the most favorable kink angle should be small so that the $F_{i,j}(\nu)$ functions from Eq. (3.75) should be accurate. If Mode I is not dominant, a way to compute numerically the functions $F_{i,j}(\nu)$ at high kink angle is given in Ref. [36]. In Ref. [4], it is shown that the max-$K_I^\star$ (or zero-$K_{II}^\star$) criterion where $K_I^\star$ is derived from the functions $F_{i,j}(\nu)$ introduced in Eq. (3.75) predicts similar kink angles compared to max-$K_I^\star$, where $K_I^\star$ is derived from the numerical functions $F_{i,j}(\nu)$ from Ref. [36].*

Remark 15 *As Azhdari mentions in his paper [4], we are aware of the fact that even if*

we did not account here for the fracture energy anisotropy, it should play an even more important role than the elastic anisotropy. A possible way to assess the fracture anisotropy at the scale of elementary constituents would be to perform molecular simulations such as in [8].

3.5 Chapter summary

We applied Muskhelishvili's formalism to Lekhnitskii's anisotropic complex potentials and we derived the solution of the plane-strain crack problem, for both prescribed stress and prescribed displacement boundary conditions. The solution of this last type of boundary conditions is of interest, notably for the implementation of a boundary element method algorithm such as the one proposed by Crouch et al. for isotropic media [13].

We were able to identify a symmetric-square matrix, the so-called *Irwin matrix* that links the crack displacement jumps to the loading or the stress intensity factors. It also relates the energy release rate, the driving force of fracture propagation, to the stress intensity factors. This matrix depends on the elastic properties of the material through which the crack propagates and on the crack orientation. Interestingly, the coefficients appearing in this matrix are directly related to the indentation moduli accessible through macro-scale indentations and the first Thomsen parameter available by ultra-sonic measurements.

Contrary to the isotropic case, when a crack does not belong to a plane of material symmetry, the fracture Modes are not directly correlated to the normal and tangential crack displacement jumps (due to the existence of non diagonal terms in the Irwin matrix). Another difference with the isotropic case is the discrepancy between the three possible criteria ruling the direction of crack kinking, even for pure pressure loadings. If one uses the maximum energy release rate criterion, a *stable* plane of crack propagation can be identified.

Chapter 4

Fluid-driven crack propagation

We now consider a two-dimensional plane-strain crack in a linear elastic transversely isotropic brittle material of stiffness tensor $\underline{\underline{\underline{\underline{C}}}}$, and fracture energy $\mathcal{G}_c$ that may depend on the crack orientation. The crack, of half-length l, is possibly inclined with respect to the plane of symmetry of the material considered. It is subjected to a far-field stress $\underline{\underline{\sigma}} = \sigma_i \underline{e}_i \otimes \underline{e}_i$ (stresses positive in traction) and pressurized through fluid injection at a constant volumetric rate, Q_0, from a line source located on the plane $x = 0$ (the origin of coordinates is taken at the center of the initial crack). The fluid pressure is defined by the function p_f acting normally to the crack lips (in the reference configuration). Our goal is to find at any time t the crack opening (i.e. the crack shape), the fluid pressure and the crack half-length, given the initial conditions, the fluid and solid properties and the injection rate. This problem involves a strong coupling between the fluid and solid phases that can be broken into two weak couplings.

The first weak coupling can be reformulated as follows: *given the crack half-length, the crack opening and the fluid injection rate, determine the fluid pressure.*

As for the second weak coupling, it can be reformulated as follows: *given a fluid pressure field, determine the crack half-length and crack opening.* We start with the first weak coupling, relative to the fluid problem. We then apply the results of Chapter 3 to the fluid-driven crack propagation problem. The two weak problems will then be put together in a dimensionless form.

The same kind of problem has been extensively studied in the case of cracks in isotropic

media subjected to a normal stress. The interested reader is referred to the review paper from Detournay [15]. For more details on the *small and large toughness regimes*, the reader is referred to Ref. [20] and [19], respectively. We consider here cracks in anisotropic media possibly undergoing some shear. This will mainly modify the equations of the solid problem.

The fluid/solid coupled problem is strongly non-linear and we propose in this Chapter a numerical method to solve it while others introduced self-similar solutions for some specific *regimes* (see, for instance, Ref. [42] or [1]). Comparisons between the self-similar and numerical solutions were given in Ref. [11] in the *small toughness regime*. Herein we suggest a way to numerically solve the solid problem (second weak coupling), that is to find numerically the crack opening induced by an arbitrary pressure field. Finally the strong coupling problem will be tackled using a numerical method, and some simulation results are presented.

4.1 The first weak coupling: Fluid problem

We consider here that the crack geometry is known. We thus look for the pressure of the fluid injected in the crack. To do so, we will use the conservation of mass and momentum equations.

Remark 16 *Note that this first weak coupling is physically impossible since the injection of an incompressible fluid into a crack will inevitably lead to changing the crack opening.*

4.1.1 Conservation of momentum

We consider that the fluid is *Newtonian* so that we have the following relationship between the shear stress τ and the velocity gradient perpendicular to the shear direction $\frac{\partial u_x}{\partial y}$:

$$\tau = \eta \frac{\partial u}{\partial y} \tag{4.1}$$

where η is the fluid dynamic viscosity.

The conservation of momentum for an *incompressible Newtonian fluid* is then equivalent to the *Navier-Stokes equation* (see, for instance, Ref. [28]). Considering that the flow is two dimensional (we have *a priori* $\underline{u} = u_x(x,y)\underline{e}_x + u_y(x,y)\underline{e}_y$ and $p_f(x,y)$), the projection along x and y of the Navier-Stokes equation can be written as:

$$\begin{cases} \rho\left(\frac{\partial}{\partial t}+u_x\frac{\partial}{\partial x}+u_y\frac{\partial}{\partial y}\right)u_x &= -\frac{\partial p_f}{\partial x}+\eta\left(\frac{\partial^2}{\partial x^2}+\frac{\partial^2}{\partial y^2}\right)u_x \\ \rho\left(\frac{\partial}{\partial t}+u_x\frac{\partial}{\partial x}+u_y\frac{\partial}{\partial y}\right)u_y &= -\frac{\partial p_f}{\partial y}+\eta\left(\frac{\partial^2}{\partial x^2}+\frac{\partial^2}{\partial y^2}\right)u_y \end{cases} \tag{4.2}$$

Let us write the fluid velocities in the x and y directions, U_x^0 and U_y^0, at $x=0$ and w^0 and p_f^0, the opening and pressure at $x=0$. Now we introduce the dimensionless parameters:

$$\begin{cases} \bar{u}_x = \frac{u_x}{U_x^0} \\ \bar{u}_y = \frac{u_y}{U_y^0} \\ \bar{x} = \frac{x}{l} \\ \bar{y} = \frac{y}{w^0} \\ \bar{p} = \frac{p_f - p_f^0}{\rho {U_x^0}^2} \\ \bar{t} = \frac{tU_x^0}{l} \end{cases} \tag{4.3}$$

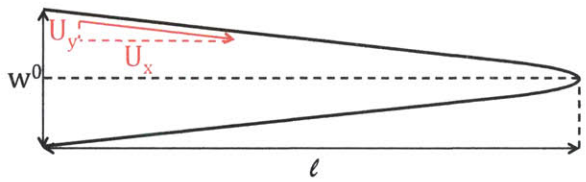

Figure 4-1: Simplified geometry: $\frac{U_y^0}{U_x^0} \sim \frac{w^0}{l}$.

Using those parameters and the relationship $U_y^0 \sim \frac{w^0}{l}U_x^0$ (Fig. 4-1), the Navier-Stokes equation (4.2) can be rewritten in a dimensionless form:

$$\begin{cases} \frac{\partial}{\partial t}\bar{u}_x+\bar{u}_x\frac{\partial \bar{u}_x}{\partial \bar{x}}+\bar{u}_y\frac{\partial \bar{u}_x}{\partial \bar{y}} &= -\frac{\partial \bar{p}}{\partial \bar{x}}+\frac{1}{R_e}\left(\frac{w^0}{l}\frac{\partial^2 \bar{u}_x}{\partial \bar{x}^2}+\frac{l}{w^0}\frac{\partial^2 \bar{u}_x}{\partial \bar{y}^2}\right) \\ \frac{\partial}{\partial t}\bar{u}_y+\bar{u}_x\frac{\partial \bar{u}_y}{\partial \bar{x}}+\bar{u}_y\frac{\partial \bar{u}_y}{\partial \bar{y}} &= -\left(\frac{l}{w^0}\right)^2\frac{\partial \bar{p}}{\partial \bar{y}}+\frac{1}{R_e}\left(\frac{l}{w^0}\frac{\partial^2 \bar{u}_y}{\partial \bar{x}^2}+\frac{w^0}{l}\frac{\partial^2 \bar{u}_y}{\partial \bar{y}^2}\right) \end{cases} \tag{4.4}$$

where $R_e = \frac{\rho U_x^0 w^0}{\eta}$ is the Reynolds number.

At low Reynolds numbers and neglecting the inertial terms, considering that the crack opening is small compared to the half-crack length ($w^0 \ll l$) - these are the hypotheses of lubrication theory [24]-, we have:

$$\begin{cases} \frac{\partial^2 u_x}{\partial y^2} &= \frac{1}{\eta}\frac{\partial p}{\partial x} \\ \frac{\partial p}{\partial y} &= 0 \end{cases} \tag{4.5}$$

Integrating Eq. (4.5) and taking into account the fact that the velocity u_x must vanish on the walls at $y = \pm \frac{w(x)}{2}$, we deduce that:

$$u_x(x,y) = -\frac{w(x)^2}{8\eta}\frac{\partial p_f}{\partial x}(x)\left(1 - 4\left(\frac{y}{w(x)}\right)^2\right) \tag{4.6}$$

Since the opening is small compared to the crack length, the mean value of the velocity over the plane of abscissa x, $\langle u_x \rangle$, defined as:

$$\langle u_x \rangle (x) = \frac{1}{w(x)} \int_{y=-\frac{w(x)}{2}}^{\frac{w(x)}{2}} u(x,y)dy \tag{4.7}$$

is representative of the flow velocity. This mean value is equal to:

$$\langle u_x \rangle (x) = -\frac{w^2(x)}{12\eta}\frac{\partial p_f}{\partial x}(x) \tag{4.8}$$

The mean flow $\langle Q \rangle (x)$ is then equal to:

$$\langle Q \rangle (x) = -\frac{w^3(x)}{12\eta}\frac{\partial p_f}{\partial x}(x) \tag{4.9}$$

The flow must also satisfy the condition of no flow at the crack tip, which can be written as:

$$\langle Q \rangle (x = l(t)) = 0 \tag{4.10}$$

4.1.2 Conservation of mass

Let us consider a slice of a fluid contained between x and $x + dx$. The mass conservation between the moments of time t and $t + dt$ can be written as:

$$\begin{aligned}(\rho.w)(x,t)dx = \; & (\rho.w)(x,t+dt)dx \\ & +(\rho.w.\langle u_x \rangle)(x+dx,t+dt)dt - (\rho.w.\langle u_x \rangle)(x,dt)dt\end{aligned} \tag{4.11}$$

so that:

$$\frac{(\rho.w)(x,t+dt) - (\rho.w)(x,t)}{dt} + \frac{(\rho.w.\langle u_x \rangle)(x+dx,t+dt) - (\rho.w.\langle u_x \rangle)(x,dt)}{dx} = 0 \tag{4.12}$$

Thus, a first order expansion in dx and dt leads to:

$$\frac{\partial \rho w}{\partial t}(x,t) + \frac{\partial \rho \langle Q \rangle}{\partial x}(x,t) = 0 \tag{4.13}$$

Considering an *incompressible* fluid ($\frac{\partial \rho}{\partial x} = 0$ and $\frac{\partial \rho}{\partial t} = 0$) we then deduce that:

$$\frac{\partial w}{\partial t}(x,t) + \frac{\partial \langle Q \rangle}{\partial x}(x,t) = 0 \tag{4.14}$$

Moreover, we must have[1] at $x = 0$:

$$\langle Q \rangle (x = 0, t) = \frac{Q_0}{2}. \tag{4.16}$$

Integrating the relationship (4.14) between $x = 0$ and l and taking into account relationship (4.16), we get:

$$\frac{\partial \mathcal{V}}{\partial t}(t) + \langle Q \rangle (l,t) - \langle Q \rangle (0,t) = 0 \tag{4.17}$$

so that:

$$\frac{\partial \mathcal{V}}{\partial t}(t) = \frac{Q_0}{2} \tag{4.18}$$

where $\mathcal{V}(t)$ is the volume of fluid contained in half the crack at time t.

4.1.3 First weak coupling equations

Combining the previous equations, we deduce a new system of equations linking the fluid pressure to the crack opening:

$$\left\{ \begin{array}{rcl} \frac{\partial w}{\partial t}(x,t) - \frac{\partial}{\partial x}\left(\frac{w^3(x,t)}{12\eta}\frac{\partial p_f}{\partial x}(x,t)\right)(x,t) & = & 0 \\ -\left(\frac{w^3}{12\eta}\frac{\partial p_f}{\partial x}\right)(x=0,t) & = & \frac{Q_0}{2} \\ -\left(\frac{w^3}{12\eta}\frac{\partial p_f}{\partial x}\right)(x=l,t) & = & 0 \\ p_f(x,t=0) & = & p_f^0(x) \\ \frac{\partial}{\partial t}\int_{x=0}^{l} w(x,t)dx & = & \frac{Q_0}{2} \end{array} \right. \tag{4.19}$$

We then deduce that, given a crack opening and a flow rate Q_0, we can compute the

[1] Rigorously, we should write:

$$\frac{\partial w}{\partial t}(x,t) + \frac{\partial \langle Q \rangle}{\partial x}(x,t) = \frac{Q_0}{2}\delta(x) \tag{4.15}$$

where $\delta(x)$ is the Dirac delta function. This expression contains both Eq. (4.14) and (4.16) but it is also more difficult to be numerically implemented.

fluid pressure field - close to a constant - using Eq. (4.19).

4.2 The second weak coupling: Solid problem

This Section aims at solving the second weak coupling of the fluid-driven crack problem. It consists of finding the crack-geometry induced by any fluid-pressure field acting on the surfaces of the crack. As we saw in the previous section, we will consider only one dimensional flow so that the only relevant information for the crack geometry are the crack length $2l$ and the crack opening w.

4.2.1 Crack opening induced by the pressure field

Let us consider for a moment uniform fluid pressure field. In the case of hydraulic fracturing, the coefficients defined in Eq. (3.53) are such that

$$\epsilon \equiv A(p_0, q_0) \sim B(p_0, q_0) \sim C(p_0, q_0) \sim D(p_0, q_0) \tag{4.20}$$

with $\epsilon \ll 1$ (typically, $\epsilon \simeq 10^{-5}$ for $\mathcal{H} \sim 10^{-11}\text{Pa}^{-1}$, $p_0 \sim 10^5\text{Pa}$) so that the deformed crack shape (3.54) can be approximated by:

$$\begin{cases} x^0(s^\pm) & \simeq & ls \\ \\ y^0(s^\pm) & \simeq & C(p_0, q_0)ls \pm D(p_0, q_0)l\sqrt{1-s^2} \end{cases} \tag{4.21}$$

where we recall that s is the dimensionless abscissa.

We introduce the new set base vectos $(\underline{e}'_x, \underline{e}'_y)$ such that:

$$\begin{cases} \underline{e}_x & = & \cos\Theta_0 \underline{e}'_x & - & \sin\Theta_0 \underline{e}'_y \\ \\ \underline{e}_y & = & \sin\Theta_0 \underline{e}'_x & + & \cos\Theta_0 \underline{e}'_y \end{cases} \tag{4.22}$$

where $\tan 2\Theta_0 = \frac{2C(p_0,q_0)}{1-C^2(p_0,q_0)-D^2(p_0,q_0)}$. One obtains the Cartesian equation in this new system of coordinates :

$$\left(\frac{x'}{a}\right)^2 + \left(\frac{y'}{b}\right)^2 = 1 \tag{4.23}$$

where a and b are equal to:

$$a = \frac{D(p_0, q_0)l}{\sqrt{\left(C(p_0, q_0)\sin\Theta_0 + \cos\Theta_0\right)^2 + \left(D(p_0, q_0)\sin\Theta_0\right)^2}} \tag{4.24}$$

and

$$b = \frac{D(p_0, q_0)l}{\sqrt{\left(C(p_0, q_0)\cos\Theta_0 - \sin\Theta_0\right)^2 + \left(D(p_0, q_0)\cos\Theta_0\right)^2}} \tag{4.25}$$

The crack shape can then be approximated by an ellipse whose principal axes are rotated by an angle $\Theta_0 \simeq C(p_0, q_0) \simeq \epsilon$ and whose semi-major and semi-minor axes are a and b, respectively. In the case of hydraulic fracturing, this angle is very small. One can thus approximate that the principal axes by the directions x and y, *even when the crack undergoes shear*. The crack opening $w(s)$ - in the deformed configuration - to be considered in the fluid Eq. (4.19) can be approximated by the normal displacement jump in the reference configuration: $w(s) \simeq [\![\xi_y]\!](s) = 2D(p_0, q_0)l\sqrt{1-s^2}$.

Let us now drop the restriction of constant pressure in the crack. We will consider that, as for the case of uniform loading, it is legitimate to consider that the normal displacement jump is still a good approximation of the crack opening.

For linear elastic materials, the second weak coupling problem can be broken into two sub-problems (Fig. 4-2). In the first one, a material with no crack is subjected to far field stresses $\underline{\underline{\sigma}}$ and the artificial crack is subjected to a normal stress σ_n and a shear stress τ. In the second one, a crack is subjected to a normal stress $p(s) = p_f(s) - \sigma_n$ and to a shear stress $q(s) = -\tau$ without far-field stresses. The stress field induced by the first sub-problem is uniform and does not present any singularity; only the second sub-problem is then of interest for the study of the crack propagation. This problem is purely equivalent to the one studied in Chapter 3.

Given the geometry, we have $\sigma_n = -\sigma_3\cos^2\theta - \sigma_1\sin^2\theta$ and $\tau = (\sigma_3 - \sigma_1)\cos\theta\sin\theta$. If we set $p(s,\theta) = p_f(s) + \left(\sigma_3\cos^2\theta + \sigma_1\sin^2\theta\right)$ and $q(s,\theta) = (\sigma_1 - \sigma_3)\cos\theta\sin\theta$, we can use the results from Chapter 3 to get the normal displacement jump $w(s) \simeq [\![\xi_y]\!](s)$. In fact, Eq. (3.36) and (3.52) give (we assume that the fluid pressure field is an even function:

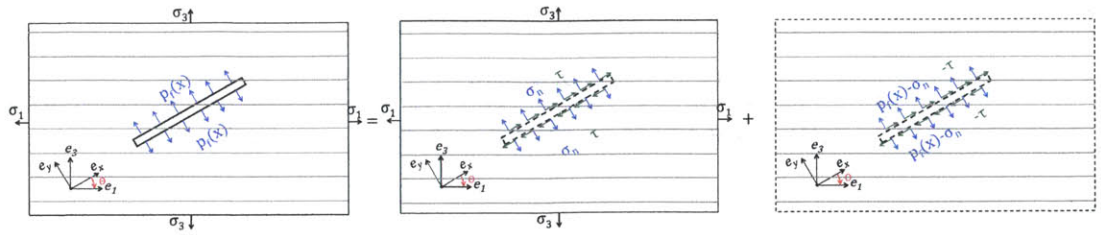

Figure 4-2: Decomposition of the problem in two sub-problems.

$p_f(u) = p_f(-u))$[2]:

$$\begin{aligned} w(s,\theta) &= -4\pi\mathcal{K}(\theta)(\sigma_1-\sigma_3)\cos\theta\sin\theta l\sqrt{1-s^2} \\ &\quad +8\pi\mathcal{H}(\theta)\int_{\tau=|s|}^{1}\frac{\tau}{\sqrt{\tau^2-s^2}}\int_{u=0}^{\tau}\frac{p_f(u)-\sigma_n}{\sqrt{\tau^2-u^2}}dud\tau \end{aligned} \tag{4.26}$$

Remark 17 *The theory developed previously is valid only if the crack is globally in traction. The effective pressure felt by the crack $p_f(x)-\sigma_n$ can be negative as long as*[3]*:*

$$\begin{cases} \int_{t=-l}^{l}(p_f(t)-\sigma_n)\sqrt{\frac{l-t}{l+t}}dt &\geq 0 \\ \int_{t=-l}^{l}(p_f(t)-\sigma_n)\sqrt{\frac{l+t}{l-t}}dt &\geq 0 \end{cases} \tag{4.27}$$

4.2.2 Crack propagation

Since we are in presence of mixed-modes, we will use the propagation criterion based on the energy release rate but without crack kinking (see Section 2.3.2). Using the even pressure field assumption, we have the following stress intensity factors (see Eq. (3.65)):

$$\begin{cases} K_I(l) &= \left(\sigma_3\cos^2\theta+\sigma_1\sin^2\theta\right)\sqrt{\pi l}+2\sqrt{\frac{l}{\pi}}\int_{t=0}^{l}\frac{p_f(t)}{\sqrt{l^2-t^2}}dt \\ K_{II}(l) &= (\sigma_1-\sigma_3)\cos\theta\sin\theta\sqrt{\pi l} \end{cases} \tag{4.28}$$

The propagation will take place only if the energy release rate $\mathcal{G}$ is equal to the fracture energy $\mathcal{G}_c$ which may depend on crack orientation. Thus, the following conditions must be

[2]We write here the crack opening as a function of the pressure as in [21]. Another possibility would have been to write the pressure in terms of the crack opening as in [10] or [11], for instance.

[3]The cases for which these two conditions are not satisfied could be tackled by allowing a crack closure and adding a sliding (without friction) between the crack lips.

satisfied:

$$\begin{cases} \mathcal{G}_c & \geq & \mathcal{G} = \pi^t \{K\} . [H] . \{K\} \\ \frac{\partial l}{\partial t}(t) & \geq & 0 \\ 0 & = & \frac{\partial l}{\partial t}(t) \left(\mathcal{G} - \mathcal{G}_c\right) \end{cases} \tag{4.29}$$

where $[H]$ is the Irwin matrix from Eq. (3.68) whose coefficients are given by Eq. (3.47).

4.2.3 Favored direction of crack propagation

In isotropy, we know that crack propagation will always be more favorable in the direction normal to the minimum far-field stress. By *more favorable* we mean that in order to propagate a crack in a specific orientation, the fluid will have to be pressurized at a lower pressure than for any other crack orientation. When considering cracks in a material where the vertical far-field stress is greater (in absolute value) than the horizontal one, the crack-propagation will be more favorable in the vertical direction.

When it comes to TI media, the favored direction of crack propagation is not that obvious since there will be a competition between two phenomena:

- The first one, also present in the isotropic case, is due to the stress anisotropy: in order to propagate the crack, the *reduced pressure* $p'_f = \frac{1}{\pi l} \int_{t=-l}^{l} p_f(t) \sqrt{\frac{l+t}{l-t}} dt$ has to be at least equal to the normal stress $\sigma_n(\theta)$. When considering cracks *in the field* conditions, we usually have:

  $$|\sigma_n(\theta = 0)| = |\sigma_3| > |\sigma_1| = |\sigma_n(\theta = \pi/2)| \tag{4.30}$$

  so that a crack in the bedding plane ($\theta = 0$) will require a greater fluid pressure to propagate compared to a vertical crack ($\theta = \pi/2$) .

- The second one, specific to the anisotropic case, is due to the difference in the compliance *felt* by the crack $\mathcal{H}(\theta)$. For instance, when considering shale materials (see Table C.3),

  $$\mathcal{H}(\theta = 0) = \mathcal{H}_1 > \mathcal{H}_2 = \mathcal{H}(\theta = \pi/2) \tag{4.31}$$

  so that it is easier to open a crack in the bedding plane ($\theta = 0$) than a vertical crack ($\theta = \pi/2$).

Below, we investigate how these two phenomena compete together. Putting together Eq.

(4.28) and (4.29), one obtains:

$$\mathcal{G}(l,\theta) = \pi^2 l \mathcal{H}_1 \left\{ \left(\cos^2\theta + \frac{\mathcal{H}_2}{\mathcal{H}_1} \sin^2\theta \right) p_f'^2 + \quad 2\left(\sigma_3 \cos^2\theta + \frac{\mathcal{H}_2}{\mathcal{H}_1} \sigma_1 \sin^2\theta \right) p_f' + \right. \\ \left. \sigma_3^2 \cos^2\theta + \frac{\mathcal{H}_2}{\mathcal{H}_1} \sigma_1^2 \sin^2\theta \right\} \tag{4.32}$$

We consider the fracture energy $\mathcal{G}_c$ independent of the crack-orientation and the mode angle (see Section 2.3.2). Thus, we rewrite Eq. (4.32) as:

$$\frac{\mathcal{G}(l,\theta) - \mathcal{G}_c}{\mathcal{G}_c} = \left(\cos^2\theta + \lambda \sin^2\theta \right) \bar{p}_f'^2 + \quad 2\left(\bar{\sigma}_3 \cos^2\theta + \lambda \bar{\sigma}_1 \sin^2\theta \right) \bar{p}_f' + \\ \bar{\sigma}_3^2 \cos^2\theta + \lambda \bar{\sigma}_1^2 \sin^2\theta - 1 \tag{4.33}$$

where we introduced the parameter $\lambda = \frac{\mathcal{H}_2}{\mathcal{H}_1}$ that quantifies the degree of anisotropy and the dimensionless fluid pressure and far-field stresses $\bar{p}_f' = \frac{p_f'}{\sigma_{3c}}$, $\bar{\sigma}_1 = \frac{\sigma_1}{\sigma_{3c}}$ and $\bar{\sigma}_3 = \frac{\sigma_3}{\sigma_{3c}}$ where $\sigma_{3c} = \sqrt{\frac{\mathcal{G}_c}{\mathcal{H}_1 \pi^2 l}}$ is the critical stress required to propagate a fracture of length $2l$ in the bedding plane.

The critical fluid pressure required to propagate a crack making an angle θ with respect to the bedding plane can be obtained by equating the energy release rate and the critical one in Eq. (4.33): $\mathcal{G}(l,\theta) = \mathcal{G}_c$.

We then introduce the dimensionless critical pressure:

$$\frac{p_f'^c(\theta)}{p_f'^c(\theta = 0)} = \mathcal{F}\left(\bar{\sigma}_1 = \frac{\sigma_1}{\sigma_{3c}}, \bar{\sigma}_3 = \frac{\sigma_3}{\sigma_{3c}}, \lambda = \frac{\mathcal{H}_2}{\mathcal{H}_1}; \theta \right) \tag{4.34}$$

that reaches its minimal value for the preferred crack orientation.

The function $\mathcal{F}$ is given by:

$$\mathcal{F}\left(\bar{\sigma}_1, \bar{\sigma}_3, \lambda; \theta\right) = \frac{\bar{\sigma}_3 \cos^2\theta + \lambda \bar{\sigma}_1 \sin^2\theta - \sqrt{\cos^2\theta + \lambda \sin^2\theta - \lambda \left(\bar{\sigma}_1 - \bar{\sigma}_3\right)^2 \sin^2\theta \cos^2\theta}}{\left(\bar{\sigma}_3 - 1\right)\left(\cos^2\theta + \lambda \sin^2\theta\right)} \tag{4.35}$$

For the sake of simplicity, we compare here only two crack orientations: $\theta = 0$ and $\theta = \pi/2$. The crack propagation will be more favorable in the vertical direction if $\mathcal{F}(\pi/2) < 1$.

This condition can be rewritten as:

$$\sqrt{\lambda}\,(|\bar{\sigma}_1| - |\bar{\sigma}_3|) < \sqrt{\lambda} - 1 \tag{4.36}$$

In isotropy, $\lambda = 1$ so that the condition (4.36) is satisfied if $|\sigma_1| < |\sigma_3|$. We thus recover the well-known result: *In isotropic media, crack propagation is more favorable in the direction normal to the minimum far-field stress.*

From now on, we assume $|\sigma_1| < |\sigma_3|$ as the general case.

Let us first consider the cases in which $\lambda \geq 1$ that is to say for materials such that $\frac{\mathcal{H}_2}{\mathcal{H}_1} = \sqrt{\frac{C_{33}}{C_{11}}} \geq 1$ or, in other terms, for materials with negative first Thomsen parameter ϵ (see Appendix B). For such materials, condition (4.36) is also always satisfied since $\sqrt{\lambda}\,(|\bar{\sigma}_1| - |\bar{\sigma}_3|) < 0 \leq \sqrt{\lambda} - 1$. This allows us to extend the previous property: *In materials having a negative first Thomsen parameter ($\epsilon \leq 0$), crack propagation is more favorable in the vertical direction than in the horizontal direction if $|\sigma_1| < |\sigma_3|$.*

If we now consider materials with a strictly positive first Thomsen parameter ($\epsilon > 0 \Leftrightarrow \lambda < 1$), the most favorable crack orientation will depend on the crack length and the fracture energy (or toughness). We introduce the reduced toughness k_c defined as:

$$k_c = \sqrt{\frac{\mathcal{G}_c}{\pi \mathcal{H}_1}} \tag{4.37}$$

If $\lambda < 1$ and $|\sigma_1| < |\sigma_3|$, there exists a critical crack half-length l_c below which the favored crack orientation is horizontal and above which the favored crack orientation is vertical. This critical crack length is equal to:

$$l_c = \frac{k_c^2}{\pi\lambda}\left(\frac{1-\sqrt{\lambda}}{|\sigma_3| - |\sigma_1|}\right)^2 \tag{4.38}$$

Remark 18 *Unless for very high fracture energies (toughnesses), the critical crack length l_c is usually small. For instance, if we take $k_c = 5$ $MPa.m^{1/2}$, $\lambda = 0.7$, $|\sigma_3| = 40$ MPa and $|\sigma_1| = 38$ MPa, one gets $l_c = 7.6$ cm. We then deduce that the favored crack orientation is, even in transverse isotropy, usually perpendicular to the minimum far-field stress, just as in isotropy.*

4.3 The strong coupling equations

4.3.1 Dimensionless equations for a viscous fluid

In the case of a constant injection rate Q_0 let us introduce $\bar{x}(t)$ and $\bar{t}$, the dimensionless abscissa and time and $\bar{w}$, $\bar{p}$, $\bar{K}$ and $\bar{l}$ the dimensionless crack opening, effective pressure, stress intensity factor (and toughness) and crack half-length defined as:

$$\left\{\begin{array}{rcl} \bar{x}(t) & = & \frac{x}{l(t)} \\ \bar{w} & = & \frac{w}{\mathcal{W}} \\ \bar{l} & = & \frac{l(t)}{\mathcal{L}} \\ \bar{t} & = & \frac{t}{\mathcal{T}} \\ \bar{p} & = & \frac{p}{\mathcal{P}} \\ \bar{K}_i & = & \frac{K_i}{\mathscr{K}} \end{array}\right. \tag{4.39}$$

with $\mathcal{P}$ a reference pressure and:

$$\left\{\begin{array}{rcl} \mathcal{T} & = & \frac{3\eta}{16\mathcal{H}^2\mathcal{P}^3} \\ \mathcal{W} & = & \sqrt{\frac{3\eta Q_0}{4\mathcal{H}\mathcal{P}^2}} \\ \mathcal{L} & = & \sqrt{\frac{3\eta Q_0}{256\mathcal{H}^3\mathcal{P}^4}} \\ \mathscr{K} & = & \left(\frac{3\eta Q_0}{16\pi^2\mathcal{H}^3}\right)^{1/4} = 2\sqrt{\frac{\mathcal{L}}{\pi}}\mathcal{P} \end{array}\right. \tag{4.40}$$

We also introduce the dimensionless horizontal and vertical far-field stresses: $\bar{\sigma}_i = \frac{\sigma_i}{\mathcal{P}}$, the dimensionless Irwin matrix: $\bar{H}_{ij} = \frac{H_{ij}}{\mathcal{H}}$ and the dimensionless fracture energy: $\bar{\mathcal{G}}_c(\theta) = \frac{\mathcal{G}_c(\theta)}{\pi\mathcal{H}\mathscr{K}^2}$. If we introduce the dimensionless parameter $\lambda = \frac{\mathcal{H}_2}{\mathcal{H}_1}$ - that catches the degree of anisotropy -, the dimensionless Irwin matrix can be written as:

$$[\bar{H}] = \frac{1}{\cos^2\theta + \lambda\sin^2\theta}\begin{bmatrix} \cos^2\theta + \lambda\sin^2\theta & (\lambda-1)\cos\theta\sin\theta \\ (\lambda-1)\cos\theta\sin\theta & \sin^2\theta + \lambda\cos^2\theta \end{bmatrix} \tag{4.41}$$

Remark 19 *Since the dimensionless abscissa $\bar{x}$ depends here on time t, one should notice that:*

$$\left.\frac{\partial f}{\partial \bar{t}}\right|_{\bar{x}}(\bar{x},\bar{t}) = \frac{\partial f}{\partial \bar{t}}(\bar{x},\bar{t}) + \frac{\partial \bar{x}}{\partial \bar{t}}\frac{\partial f}{\partial \bar{x}}(\bar{x},\bar{t}) \tag{4.42}$$

Also, as the fluid pressure $p_f(x)$ appears only through its derivative with respect to x, and as σ_n is uniform, one can replace the fluid pressure $p_f(x)$ by the effective pressure $p(x) =$

$p_f(x) - \sigma_n$.

Using the dimensionless parameters just introduced, the coupled problem can be written as:

Find $\bar{p}(\bar{x},\bar{t})$ and $\bar{l}(\bar{t})$ for $(\bar{x},\bar{t}) \in [0,1]\mathrm{x}[0,\bar{T}_f]$ such that:

$$\begin{cases} \frac{\pi}{2}\bar{H}_{12}\cos\theta\sin\theta(\bar{\sigma}_1-\bar{\sigma}_3)\bar{l}\sqrt{1-\bar{x}^2} \\ \quad +\bar{l}(\bar{t})\int_{\tau=|\bar{x}|}^{1}\frac{\tau}{\sqrt{\tau^2-\bar{x}^2}}\int_{u=0}^{\tau}\frac{\bar{p}(u,\bar{t})}{\sqrt{\tau^2-u^2}}dud\tau &=& \bar{w}(\bar{x},\bar{t}) \\ -\frac{\bar{x}}{\bar{l}(\bar{t})}\frac{d\bar{l}(\bar{t})}{dt}\frac{\partial\bar{w}}{\partial\bar{x}}(\bar{x},\bar{t})+\frac{\partial\bar{w}}{\partial\bar{t}}(\bar{x},\bar{t})-\frac{1}{\bar{l}^2(\bar{t})}\frac{\partial}{\partial\bar{x}}\left(\bar{w}^3(\bar{x},\bar{t})\frac{\partial\bar{p}}{\partial\bar{x}}(\bar{x},\bar{t})\right)(\bar{x},\bar{t}) &=& 0 \\ \bar{K}_i\bar{H}_{ij}\bar{K}_j &\leq& \bar{\mathcal{G}}_c(\theta) \\ \frac{\partial\bar{l}}{\partial\bar{t}}(\bar{t}) &\geq& 0 \\ \frac{\partial\bar{l}(\bar{t})}{\partial\bar{t}}\left(\bar{K}_i\bar{H}_{ij}\bar{K}_j-\bar{\mathcal{G}}_c(\theta)\right) &=& 0 \\ -\frac{1}{\bar{l}(\bar{t})}\left(\bar{w}^3\frac{\partial\bar{p}}{\partial\bar{x}}\right)(\bar{x}=0,\bar{t}) &=& 1 \\ \frac{1}{\bar{l}(\bar{t})}\left(\bar{w}^3\frac{\partial\bar{p}}{\partial\bar{x}}\right)(\bar{x}=1,\bar{t}) &=& 0 \\ \frac{\partial}{\partial\bar{t}}\left(\bar{l}(\bar{t})\int_{u=0}^{1}\bar{w}(u,\bar{t})du\right) &=& 1 \\ \bar{p}(\bar{x},\bar{t}=0) &=& \bar{p}_0(\bar{x}) \\ \bar{l}(\bar{t}=0) &=& \bar{l}_0 \end{cases} \tag{4.43}$$

Equation (4.43) is a highly non-linear system of equations which needs to be solved numerically.

Remark 20 *One can notice that the set of dimensionless equations to be verified depends only on six parameters: the dimensionless initial effective pressure* $\bar{p}_0(x) = \frac{p_0(x)}{\mathcal{P}}$, *the dimensionless initial crack half-length* $\bar{l}_0 = \frac{l_0}{\mathcal{L}}$, *the crack orientation* θ, *the dimensionless fracture energy* $\bar{\mathcal{G}}_c(\theta) = \frac{\mathcal{G}_c(\theta)}{\pi\mathcal{H}\mathcal{X}^2}$, *the degree of anisotropy* $\lambda = \frac{\mathcal{H}_2}{\mathcal{H}_1}$ *and the degree of stress heterogeneity* $\bar{\sigma}_1 - \bar{\sigma}_3 = \frac{\sigma_1-\sigma_3}{\mathcal{P}}$.

4.3.2 Dimensionless equations for a non-viscous fluid

If the fluid is considered as non-viscous ($\eta = 0$), then there is no flow in the crack ($Q(x,t) = 0$) and the pressure in the crack is uniform ($p(x,t) = p(t)$).

For this case, let us introduce dimensionless crack half-length, effective pressure, far-field

stresses and time defined as:

$$\begin{cases} \bar{l} &= \frac{l(t)}{\mathcal{L}'} \\ \bar{\sigma}_i &= \frac{\bar{\sigma}_i}{\mathcal{P}'} \\ \bar{p} &= \frac{p}{\mathcal{P}'} \\ \bar{t} &= \frac{t}{\mathcal{T}'} \end{cases} \tag{4.44}$$

with $\mathcal{P}'$ a reference pressure and:

$$\begin{cases} \mathcal{L}' &= l_0 \\ \mathcal{T}' &= \frac{2\pi^2 \mathcal{L}^2 \mathcal{P} \mathcal{H}}{Q_0} \end{cases} \tag{4.45}$$

Then introduce the dimensionless fracture energy $\bar{\mathcal{G}}_c = \frac{\mathcal{G}_c}{\pi^2 \mathcal{H} \mathcal{L}' \mathcal{P}'^2}$ and the dimensionless Irwin matrix from Section 4.3.1.

Using the dimensionless parameters just introduced, the coupled problem can then be written as:

Find $\bar{p}(\bar{t})$ and $\bar{l}(\bar{t})$ for $\bar{t} \in [0, \bar{T}_f]$ such that:

$$\begin{cases} \bar{l}^2(\bar{t}) \left(\bar{p}(\bar{t}) + \bar{H}_{12}\bar{q}\right) &= \bar{p}_0 + \bar{H}_{12}\bar{q} + \bar{t} \\ \bar{l} \left(\bar{p}^2(\bar{t}) + 2\bar{H}_{12}\bar{q}\bar{p}(\bar{t}) + \bar{H}_{22}\bar{q}^2\right) &\leq \bar{\mathcal{G}}_c \\ \frac{\partial \bar{l}}{\partial \bar{t}}(\bar{t}) &\geq 0 \\ \frac{\partial \bar{l}(\bar{t})}{\partial \bar{t}} \left(\bar{p}^2(\bar{t}) + 2\bar{H}_{12}\bar{q}\bar{p}(\bar{t}) + \bar{H}_{22}\bar{q}^2 - \frac{\bar{\mathcal{G}}_c}{\bar{l}}\right) &= 0 \\ \bar{q} &= (\bar{\sigma}_1 - \bar{\sigma}_3)\cos\theta \sin\theta \\ \bar{p}(\bar{t} = 0) &= \bar{p}_0 \\ \bar{l}(\bar{t} = 0) &= 1 \end{cases} \tag{4.46}$$

4.4 Numerical solution for the solid problem

Except for some specific cases, the computation of the integrals in Eq. (4.43.1) is not straightforward. We have to make use of numerical methods to solve our problem.

4.4.1 Discretization

The segment $[0, 1]$ is divided into $NN - 1$ segments of length $h = \frac{1}{NN-1}$. Given the fluid pressure at each of the NN nodes, the pressure is interpolated by the use of the hat function

$\phi(x) = (1 - |x|)\mathbb{1}_{[-1,1]}(x)$:

$$\bar{p}(\bar{x}) = \sum_{k=1}^{NN} \bar{p}_k \phi_k(\bar{x}) \tag{4.47}$$

with $\bar{x}_k = (k-1)h$; while $\phi_k(x) = \phi(\frac{x-\bar{x}_k}{h})$ is the hat function which is equal to 1 at node k and 0 at every other node.

4.4.2 First numerical integration

To be able to compute the crack opening, we first need to compute the function:

$$\bar{P}(\tau) = \tau \int_0^\tau \frac{\bar{p}(u)}{\sqrt{\tau^2 - u^2}} du \tag{4.48}$$

Substituting (4.47) into the (4.48), we obtain:

$$\bar{P}(\tau) = \sum_{k=1}^{NN} \bar{p}_k . \left(\tau \bar{P}_k(\tau)\right) \tag{4.49}$$

with:

$$\begin{aligned} \bar{P}_k(\tau) &= \int_0^\tau \frac{\phi_k(x)}{\sqrt{\tau^2 - x^2}} dx \\ &= \int_0^\tau \frac{1 - |\frac{x-\bar{x}_k}{h}|}{\sqrt{\tau^2 - x^2}} \mathbb{1}_{[-1,1]}(\frac{x - \bar{x}_k}{h}) dx \end{aligned} \tag{4.50}$$

If $\tau \leq \bar{x}_{k-1}$, then $\bar{P}_k(t) = 0$, otherwise:

$$\begin{aligned} \bar{P}_k(\tau) &= \int_{\max(0,\bar{x}_{k-1})}^{\min(\tau,\bar{x}_{k+1})} \frac{1}{h} \frac{(h - |x - \bar{x}_k|)}{\sqrt{\tau^2 - x^2}} dx \\ &= \int_{\max(0,\bar{x}_{k-1})}^{\min(\tau,\bar{x}_{k+1})} \frac{1}{\sqrt{\tau^2 - x^2}} dx + \int_{\max(0,\bar{x}_{k-1})}^{\min(\tau,\bar{x}_k)} \frac{1}{h} \frac{x - \bar{x}_k}{\sqrt{\tau^2 - x^2}} dx \\ &\quad - \int_{\bar{x}_k}^{\min(\max(\tau,\bar{x}_k),\bar{x}_{k+1})} \frac{1}{h} \frac{x - \bar{x}_k}{\sqrt{\tau^2 - x^2}} dx \\ &= \int_{\max(0,\bar{x}_{k-1})}^{\min(\tau,\bar{x}_k)} \frac{1}{h} \frac{h - \bar{x}_k}{\sqrt{\tau^2 - x^2}} dx + \int_{\bar{x}_k}^{\min(\max(\tau,\bar{x}_k),\bar{x}_{k+1})} \frac{1}{h} \frac{h + \bar{x}_k}{\sqrt{\tau^2 - x^2}} dx \\ &\quad + \int_{\max(0,\bar{x}_{k-1})}^{\min(\tau,\bar{x}_k)} \frac{x}{h} \frac{dx}{\sqrt{\tau^2 - x^2}} - \int_{\bar{x}_k}^{\min(\max(\tau,\bar{x}_k),\bar{x}_{k+1})} \frac{x}{h} \frac{dx}{\sqrt{\tau^2 - x^2}} \end{aligned} \tag{4.51}$$

Finally we have:

$$\begin{aligned}\bar{P}_k(\tau) &= \mathbb{1}_{]\bar{x}_{k-1},+\infty[}(\tau)\left\{\left(1-\frac{\bar{x}_k}{h}\right)I^{\min(\tau,\bar{x}_k)}_{\max(0,\bar{x}_{k-1})}(\tau)+(1+\frac{\bar{x}_k}{h})I^{\min(\max(\tau,\bar{x}_k),\bar{x}_{k+1})}_{\bar{x}_k}(\tau)\right. \\ &\left.+\frac{1}{h}\left(J^{\min(\tau,\bar{x}_k)}_{\max(0,\bar{x}_{k-1})}(\tau)-J^{\min(\max(\tau,\bar{x}_k),\bar{x}_{k+1})}_{\bar{x}_k}(\tau)\right)\right\} \qquad (4.52)\end{aligned}$$

with:

$$I^b_a(\tau)=\int_a^b\frac{1}{\sqrt{\tau^2-x^2}}dx=\left[\arcsin\frac{x}{\tau}\right]^b_a \qquad (4.53)$$

and:

$$J^b_a(\tau)=\int_a^b\frac{x}{\sqrt{\tau^2-x^2}}dx=\left[-\sqrt{\tau^2-x^2}\right]^b_a \qquad (4.54)$$

Using Eq. (4.49) - (4.54), one can then compute the function $\bar{P}(\tau)=\tau\int_0^\tau\frac{\bar{p}(u)}{\sqrt{\tau^2-u^2}}du$.

4.4.3 Computation of dimensionless crack opening

We saw in the previous Section that the first integral in Eq. (4.43) can be analytically computed when the pressure field is interpolated from the values of $\bar{p}$ at NN nodes by means of hat function. However, the computation of the crack opening involving the integration of functions of the form $\sqrt{\frac{\tau^2-\alpha^2}{\tau^2-x^2}}$ and $\frac{\arcsin\alpha/\tau}{\sqrt{\tau^2-x^2}}$ is much more complicated.
Indeed, we have to compute for $\bar{x}\in[0,1]$:

$$\begin{aligned}\bar{w}(\bar{x}) &= \bar{l}\int_{\bar{x}}^1\frac{\bar{P}(\tau)}{\sqrt{\tau^2-\bar{x}^2}}d\tau \\ &= \bar{l}\sum_{k=1}^{NN}p_k\int_{\bar{x}}^1\frac{\tau\bar{P}_k(\tau)}{\sqrt{\tau^2-\bar{x}^2}}d\tau \qquad (4.55)\end{aligned}$$

so that:

$$\bar{w}(\bar{x})=\bar{l}\sum_{k=1}^{NN}\bar{p}_k\frac{1-\bar{x}}{2}\int_{-1}^1\frac{\tau(u)\bar{P}_k(\tau(u))}{\sqrt{\tau(u)^2-\bar{x}^2}}du \qquad (4.56)$$

with $\tau(u)=\frac{1-\bar{x}}{2}u+\frac{1+\bar{x}}{2}$.
The integral appearing in Eq. (4.56) can be computed using Gauss-Legendre's method (for more details, the reader is directed to Ref. [25], for instance) approximating the integral of a function f on the segment $[-1,1]$ by:

$$\int_{-1}^1 f(u)du\simeq\sum_{i=1}^{NG}\omega_i f(y_i) \qquad (4.57)$$

where y_i are the roots of the NG-th Legendre's polynomial $P_{NG}(x)$ and the weight $\omega_i = \frac{-2}{(NG+1)P'_{NG}(y_i)P_{NG+1}(y_i)}$. The computation of the roots y_i can be done using Laguerre's method.

Knowing the value of the fluid pressure at each node, one can deduce the value of the crack opening at each node using the relationship:

$$\{\bar{w}\} = \bar{l}\,[M]\,.\,\{\bar{p}\} \tag{4.58}$$

where:

$$\begin{cases} M_{ij} &= \frac{1-\bar{x}_i}{2}\int_{-1}^{1}\frac{\tau_i(u)\bar{P}_j(\tau_i(u))}{\sqrt{\tau_i(u)^2-\bar{x}_i^2}}du & (i,j)\in[\![1,NN]\!]\times[\![1,NN]\!] \\ \tau_i(u) &= \frac{1-\bar{x}_i}{2}u+\frac{1+\bar{x}_i}{2} & i\in[\![1,NN]\!] \\ \{\bar{w}\}_i &= \bar{w}(\bar{x}_i) & i\in[\![1,NN]\!] \\ \{\bar{p}\}_i &= \bar{p}(\bar{x}_i) & i\in[\![1,NN]\!] \end{cases} \tag{4.59}$$

4.4.4 Computation of the dimensionless Mode I stress intensity factor

One can notice that the algorithm developed in Section 4.4.2 allows the computation of the stress intensity factor $\bar{K}_I(\bar{l})$ as well:

$$\bar{K}_I(\bar{l}) = \sqrt{\bar{l}}\int_{u=0}^{1}\frac{\bar{p}(u)du}{\sqrt{1-u^2}} = \sqrt{\bar{l}}\sum_{k=1}^{NN}\bar{p}_k.\bar{P}_k(\tau=1) \tag{4.60}$$

We define $[A]$ the $1\text{x}NN$ matrix such that $A_{1,k} = \bar{P}_k(\tau=1)$, leading to:

$$\bar{K}_I(\bar{l}) = \sqrt{\bar{l}}\,[A]\,.\,\{\bar{p}\} \tag{4.61}$$

4.5 Numerical solution for the strong coupling

Because of the first weak coupling (the fluid problem) and the crack-propagation criterion, the strong coupling is highly non-linear. While the second weak coupling could be linearized (Eq. (4.58)), solving the strong coupling requires the use of numerical methods. We here chose to use an improved Newton's method: Broyden's method, sometimes used in fluid/solid coupling problems [3].

4.5.1 Solving a non-linear problem

We have to solve an equation of the type $\{F\}(\{X\}) = \{0\}$ where $\{X\}$ is a nx1 vector containing the unknowns and $\{F\}$ a nx1 vector to be vanished.

The classical Newton method involves the (expensive) computation at each iteration i of the Jacobian: $[J]_i = \left[\frac{\partial\{F\}}{\partial\{X\}}\right](\{X\}_i)$ or of its inverse. Indeed, while some norm of the vector $\{F\}(\{X\}_i)$ to be vanished is greater than a certain value ϵ, Newton's method requires the computation of $\{X\}_{i+1}$ using:

$$[J]_i.(\{X\}_{i+1} - \{X\}_i) = -\{F\}(\{X\}_i) \tag{4.62}$$

As for Broyden's method [9], it only computes the Jacobian $[J]_0^{-1}$ once and then uses the following approximation for the Jacobian at the next iteration:

$$[J]_{i+1}^{-1} = [J]_i^{-1} + \frac{\{\Delta X\}_{i+1} - [J]_i^{-1}\{\Delta F\}_{i+1}}{{}^t\{\Delta X\}_{i+1}.[J]_i^{-1}.\{\Delta F\}_{i+1}}\left({}^t\{\Delta X\}_{i+1}[J]_i^{-1}\right) \tag{4.63}$$

where $\{\Delta X\}_{i+1} = \{X\}_{i+1} - \{X\}_i$ and $\{\Delta F\}_{i+1} = \{F\}(\{X\}_{i+1}) - \{F\}(\{X\}_i)$.
The vector $\{X\}_{i+1}$ is then computed as follows:

$$\{X\}_{i+1} = \{X\}_i - [J]_i^{-1}.\{F\}(\{X\}_i) \tag{4.64}$$

4.5.2 Implementation

To solve the strong coupling using the method presented in the previous section, we need to define the vector $\{F\}(\{X\})$ to be vanished.
We denote by $\{V^j\}$ any vector $\{V\}$ at time $\bar{t}_j$, and by Δt^j the time step $\Delta\bar{t}^j = \bar{t}_{j+1} - \bar{t}_j$.

Here, the unknowns are the pressure at each of the NN nodes and the crack half-length at time $\bar{t}_j$, knowing these quantities at time $\bar{t}_{j-1}$. Thus, the unknown vector $\{X\}$ is such that: $X_k^j = \bar{p}_k^j$ for $k \in \{1, ..., NN\}$ and $X_{NN+1}^j = \bar{l}^j$. The vector $\{F\}$ will have to regroup the information contained in the equations of the two weak couplings. We can already remark that the boundary condition (4.43_7) is verified provided that the crack opening verifies Eq.

(4.43_1), and provided that $\frac{\partial \bar{p}}{\partial \bar{x}}$ is not singular at $\bar{x} = 1$.

Equation (4.43_2) can then be discretized as follows:

$$\begin{aligned} -\frac{\bar{l}^j - \bar{l}^{j-1}}{\Delta \bar{t}^{j-1}} \frac{\{\bar{x}\}}{\bar{l}^j} * [D_x] \left\{\bar{w}^j\right\} + \frac{\left\{\bar{w}^j\right\} - \left\{\bar{w}^{j-1}\right\}}{\Delta \bar{t}^{j-1}} \\ - \frac{1}{(\bar{l}^j)^2} [D_x] \quad \left\{ \left(\left\{\bar{w}^j\right\}\right)^3 * [D_x] \left\{\bar{p}^j\right\} \right\} = \{0\} \end{aligned} \tag{4.65}$$

with $[D_x]$ the NNxNN space differentiation matrix defined by $[D_x]_{ij} = \frac{1}{h}\left(-\delta_{i,j} + \delta_{i,j+1}\right)$ ($\delta_{i,j}$ being the Kronecker delta). The spatial derivative is here defined as $\frac{\partial f}{\partial \bar{x}}(\bar{x}_k) = \frac{f(\bar{x}_{k+1}) - f(\bar{x}_k)}{h}$; $*$ is the term by term multiplication: $\{\{a\} * \{b\}\}_i = a_i b_i$ and $(\{a\})^3 = \{a\} * \{a\} * \{a\}$.

Substituting Eq. (4.58) into (4.65), one obtains:

$$\begin{aligned} -\frac{\bar{l}^j - \bar{l}^{j-1}}{\Delta \bar{t}^{j-1}} \frac{\{x\}}{\bar{l}^j} * [D_x] [M] \left\{\bar{p}^j\right\} + \quad & \frac{[M]\left(\left\{\bar{p}^j\right\} - \left\{\bar{p}^{j-1}\right\}\right)}{\Delta \bar{t}^{j-1}} \\ - \quad & \frac{1}{(\bar{l}^j)^2} [D_x] \left\{ \left([M] \left\{\bar{p}^j\right\}\right)^3 * [D_x] \left\{\bar{p}^j\right\} \right\} = \{0\} \end{aligned} \tag{4.66}$$

One may think that Eq. (4.66), containing NN independent equations, would be enough to define the first NN components of the vector $\underline{F}$. However, the last equation cannot be used since the derivative at $\bar{x} = \bar{x}_{NN} = 1$ is ill defined. The NN-th component of the $\{F\}$ vector can be obtained from condition (4.43_8):

$$\frac{\partial \bar{\mathcal{V}}}{\partial \bar{t}} - 1 = 0 \tag{4.67}$$

or,

$$\frac{\bar{\mathcal{V}}^j - \bar{\mathcal{V}}^{j-1}}{\Delta \bar{t}^{j-1}} - 1 = 0 \tag{4.68}$$

where $\bar{\mathcal{V}}^j$ is the volume of the half-crack at time $\bar{t}_j$ approximated, for instance, by the relationship:

$$\bar{\mathcal{V}}^j = \bar{l}^j \left[\frac{h}{2}\ h\ \ldots\ h\ \frac{h}{2}\right] . \left\{\bar{w}^j\right\} \tag{4.69}$$

For the last component of $\{F\}$, we will use the propagation criterions (4.43_3)-(4.43_5). If the crack does not propagate, then $F_{NN+1}(\{X^j\}) = \bar{l}^j - \bar{l}^{j-1}$. If the crack propagates, then $F_{NN+1}(\{X^j\}) = \bar{K}_m(\bar{l}^j)\bar{H}_{mn}\bar{K}_n(\bar{l}^j) - \bar{\mathcal{G}}_c$, with $\bar{K}_I(\bar{l}^j) = \sqrt{\bar{l}^j}\,[A]\left\{\bar{p}^j\right\}$.

Let $\left\{\tilde{X}\right\}$ be the NNx1 vector containing the NN first components of $\{X\}$ $(X_k = \bar{p}_k)$.

We then have at each time step:

$$\begin{cases} F_k(\{X^j\}) = \left\{ -\frac{X^j_{NN+1}-X^{j-1}_{NN+1}}{\Delta\bar{t}^{j-1}} \frac{\{\bar{x}\}}{X^j_{NN+1}} * [D_x][M]\left\{\tilde{X}^j\right\} + \frac{[M](\{\tilde{X}^j\}-\{\tilde{X}^{j-1}\})}{\Delta\bar{t}^{j-1}} \right. \\ \qquad \left. - \frac{1}{(X^j_{NN+1})^2}[D_x]\left\{\left([M]\left\{\tilde{X}^j\right\}\right)^3 * [D_x]\left\{\tilde{X}^j\right\}\right\}\right\}_k \\ \qquad\qquad \text{for } k \in \{1...NN-1\} \\ F_{NN}(\{X\}^j) = \left[\frac{h}{2}\ h\ ...\ h\ \frac{h}{2}\right].[M]\frac{X^j_{NN+1}\{\tilde{X}^j\}-X^{j-1}_{NN+1}\{\tilde{X}^{j-1}\}}{\Delta\bar{t}^{j-1}} - 1 \\ F_{NN+1}(\{X\}^j) = X^j_{NN+1} - X^{j-1}_{NN+1} \qquad \text{if the crack does not propagate} \\ F_{NN+1}(\{X\}^j) = \bar{K}_m(\bar{l}^j)\bar{H}_{mn}\bar{K}_n(\bar{l}^j) - \bar{\mathcal{G}}_c \qquad \text{if the crack propagates} \end{cases}$$

4.5.3 Solving scheme

We consider the following problem: *Given the dimensionless initial half-length $\bar{l}_0$ of a plane-strain crack oriented by angle θ with respect to the plane of isotropy, the dimensionless fracture energy $\bar{\mathcal{G}}_c$, the dimensionless initial effective pressure $\bar{p}_0$, the degree of anisotropy $\lambda = \frac{\mathcal{H}_2}{\mathcal{H}_1}$ and the stress heterogeneity $\bar{\sigma}_3 - \bar{\sigma}_1$, find the dimensionless crack opening, pressure field and half-crack-length at the dimensionless time $\bar{T}_f$.*

To solve this problem, we will have to:

1. Discretize the space segment $[0,1]$ into $NN-1$ segments of length $h = \frac{1}{NN-1}$.
2. Compute *once* the NNxNN matrix M with NG Gauss points.
3. Initialize the time increment j at $j=0$, the time step $\Delta\bar{t}^j = \frac{\bar{p}^j}{10}$, the X-vector at $X^j_k = \bar{p}^j_k$ for $k \in \{1,...,NN\}$ and $X^j_{NN+1} = \bar{l}^j$ and the prediction of the unknown vector at $\left\{X^{*j+1}\right\} = \left\{X^j\right\}$.
4. Get the predicted X-vector $\left\{X^{*j+1}\right\}$ at time step $\bar{t}_{j+1}$ solving the nonlinear problem $\{F\}\left(\left\{X^{*j+1}\right\}\right) = \{0\}$ without allowing crack propagation ($F_{NN+1}(\{X\}^j) = X^j_{NN+1} - X^{j-1}_{NN+1}$).
5. Compute the stress intensity factor $\bar{K}^{*j+1}_I = \bar{K}_I(\left\{X^{*j+1}\right\})$,

   if $\bar{K}^{*j+1}_m \bar{H}_{mn} \bar{K}^{*j+1}_n < \bar{\mathcal{G}}_c$ then $\left\{X^{j+1}\right\} = \left\{X^{*j+1}\right\}$,

else get the X-vector $\{X^{j+1}\}$ at time step $\bar{t}_{j+1}$ solving the non linear problem $\{F\}(\{X^{j+1}\}) = \{0\}$ enforcing the crack propagation ($F_{NN+1}(\{X\}^j) = \bar{K}_m(\bar{l}^j)\bar{H}_{mn}\bar{K}_n(\bar{l}^j) - \bar{\mathcal{G}}_c$).

6. $j \leftarrow j+1$, $\{X^{*j+1}\} = \{X^{*j}\}$, $\Delta\bar{t}^j = \frac{\bar{\nu}^j}{10}$; and goto step 4 if $\bar{t} < \bar{T}_f$;

4.6 Numerical results

4.6.1 Comparison to Carbonell's self-similar solution

We first benchmark our simulator by comparing our numerical solution to a self-simular solution given in Ref. [11] (in the small toughness regime). We employ similar parameters to those given in this paper. Specifically, the fluid injection rate, fluid dynamic viscosity, elastic coefficient, fracture toughness, initial length and final time are taken equal to:

$$\begin{cases} Q_0 &= 4.10^{-3}\ \text{m}^2.\text{s}^{-1} \\ \eta &= 853.10^{-3}\ \text{Pa.s}^{-1} \\ \mathcal{H} &= 0.012\ \text{GPa}^{-1} \\ K_{Ic} &= 0.14\ \text{MPa.m}^{1/2} \\ l_0 &= 0.4\ \text{m} \\ t_f &= 1000\ \text{s} \end{cases} \tag{4.70}$$

This comparison is displayed in Fig. 4-3 to 4-5, showing an excellent agreement of our results with the benchmark results. In Fig. 4-3, the crack-half length is plotted as a function of time. Figure 4-4 (4-5) shows the crack-opening (effective pressure) at the injection point and close to the crack-tip.

4.6.2 On the influence of the problem parameters

The numerical results presented below inverstigate the influence on the crack propagation of the elastic coefficient $\mathcal{H}$, the fracture toughness K_{Ic} and the dynamic viscosity η.

The fixed parameters are the flow rate $Q_0 = 4.10^{-3}\ \text{m}^2.\text{s}^{-1}$, the initial pressure $p_0 = 20$ MPa and the initial crack length $l_0 = 0.4$ m.

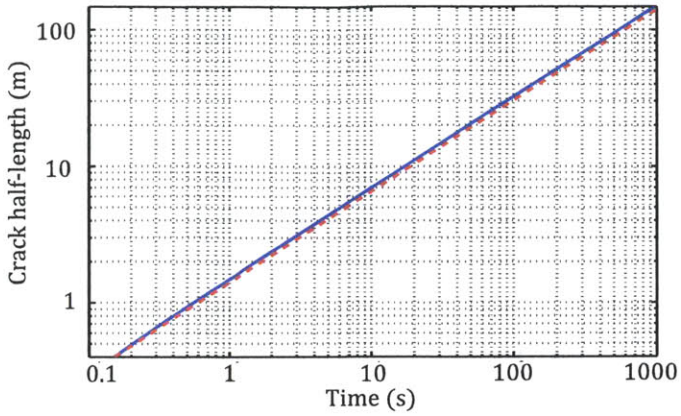

Figure 4-3: Crack half-length as a function of time computed numerically (solid blue) and from the self-similar solution (dashed red).

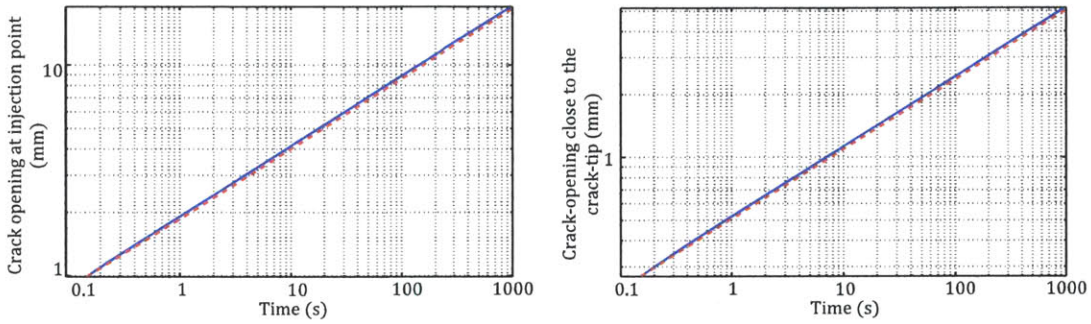

(a) At injection point.

(b) Close to the crack-tip.

Figure 4-4: Crack-opening as functions of time computed numerically (solid blue) and from the self-similar solution (dashed red).

Influence of the elastic coefficient $\mathcal{H}$

We consider two materials of different elastic coefficients $\mathcal{H}$: $\mathcal{H} = 0.012$ GPa^{-1} and $\mathcal{H}' = 0.015$ GPa^{-1}. The apparent stiffness of the first material is greater than the second one. Since the crack volume is equal to the volume of the (incompressible) fluid, a crack in the first material tends to propagate while a crack in the second one tends to *inflate* (see Fig. 4-6 and 4-7).

Influence of the fracture toughness K_{Ic}

We consider two materials of different fracture toughness K_{Ic}: $K_{Ic} = 1$ MPa.m$^{1/2}$ and $K'_{Ic} = 10$ MPa.m$^{1/2}$. Irwin's criterion $K_I = K_{Ic}$ is first reached in the material with the lower toughness and the crack should thus propagate faster (see Fig. 4-8 and 4-9).

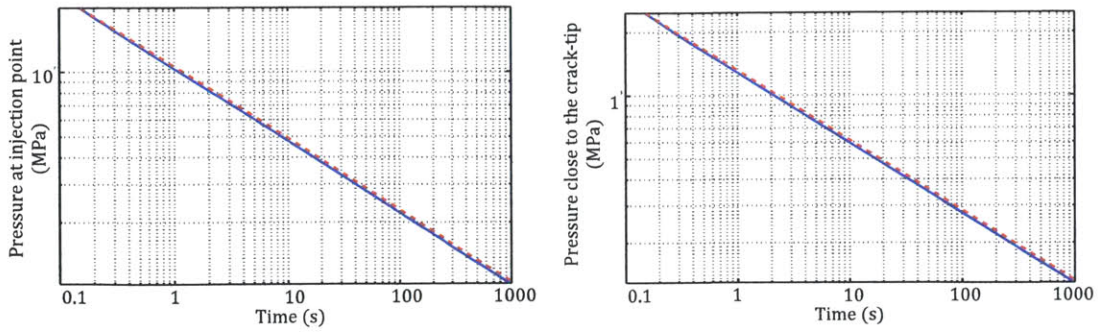

(a) At injection point.

(b) Close to the crack-tip.

Figure 4-5: Fluid pressure as function of time computed numerically (solid blue) and from the self-similar solution (dashed red).

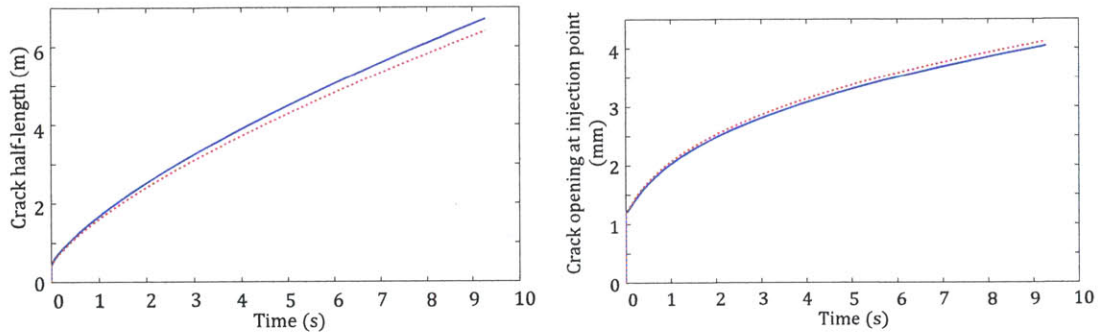

Figure 4-6: Crack half-length (left) and crack-opening at injection point (right) as functions of time for different elastic coefficients $\mathcal{H}$ (in solid blue: $\mathcal{H} = 0.012$ GPa^{-1}, in dashed red: $\mathcal{H} = 0.015$ GPa^{-1}). The fracture toughness was taken equal to 1 MPa.m$^{1/2}$ and the dynamic viscosity to 0.8 Pa.s^{-1}.

Influence of the dynamic viscosity η

Numerical simulations are performed for several dynamic viscosities. The results show that the higher the viscosity, the lower the pressure at the crack tip. As a consequence, the stress intensity factor (which depends strongly on the pressure at the crack tip) is lower for high viscosities. Thus, a crack propagates faster at low viscosities (see Fig. 4-10 and 4-11).

Application to gas shale, the effect of anisotropy

Shale materials can be considered as transversely isotropic [37]. The toughnesses in the principal directions 1, 2 and 3 can be estimated experimentally. Furthermore, the indentation moduli in directions 1 and 3 can also be measured. To determine the coefficients $\mathcal{H}_i$, $i = 1$, 2 and 3 of shale, we also need the ratio C_{11}/C_{33} which we do not have *a priori*. This ratio

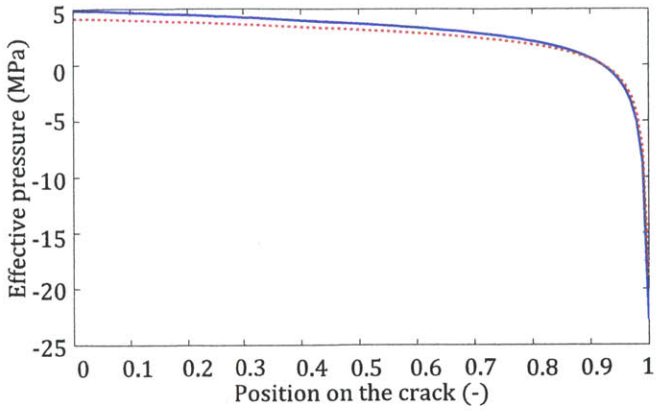

Figure 4-7: Effective pressure distribution along the crack (0 corresponds to the injection point and 1 to the crack-tip) for different elastic coefficients $\mathcal{H}$ (in solid blue: $\mathcal{H} = 0.012$ GPa^{-1}, in dashed red: $\mathcal{H} = 0.015$ GPa^{-1}). The fracture toughness was taken equal to 1 MPa.m$^{1/2}$ and the dynamic viscosity to 0.8 Pa.s^{-1}.

can however be expressed in terms of the first Thomsen parameter ϵ as: $C_{33}/C_{11} = 1 + 2\epsilon$.

Except for a non-viscous fluid, we cannot directly conclude in which direction the crack will propagate faster. For a non-viscous fluid, let us consider two materials such that $\mathcal{H} > \mathcal{H}'$ and $K_{Ic} < K'_{Ic}$. Comparing two cracks propagating in these different materials (with the same initial conditions), we have: $l'^{3/2}(t) - l^{3/2}(t) = at + b$ where a and b are two constants. It can be shown that a is such that:

$$a \propto 1 - \frac{\mathcal{H}' K'_{Ic}}{\mathcal{H} K_{Ic}} \tag{4.71}$$

We then conclude that, eventually (i.e. for a large enough time t), the crack with the smaller $\mathcal{H}K_{Ic}$ value will propagate faster. To compare two cracks, we then have to compare the product $\mathcal{H}K_{Ic}$. For viscous fluids, numerical computations lead to a similar conclusion.

4.7 Chapter summary

In this Chapter, we modelled the fluid-driven crack propagation in anisotropic materials, and possibly under shear conditions.

It was shown that, provided that the right elastic parameters are used, one could take advantage of the work already done in the isotropic case.

We also introduced a critical crack length below which the crack propagation will be more

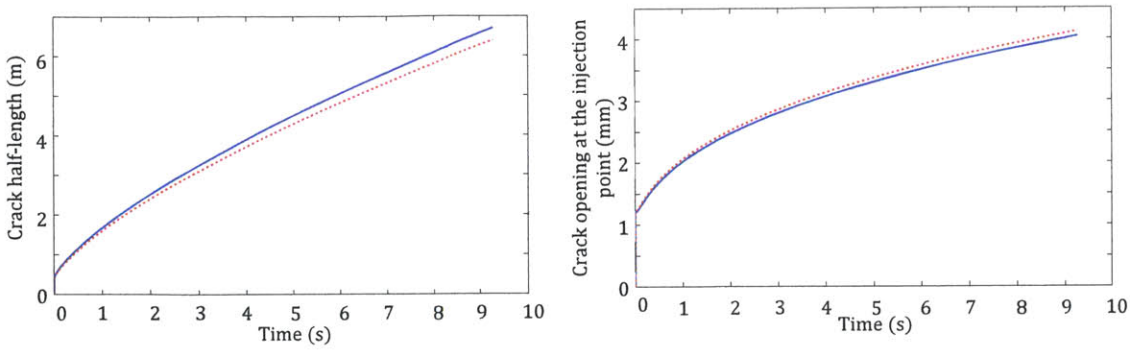

Figure 4-8: Crack half-length and crack opening at the injection point as functions of time for different fracture toughnesses K_{Ic} (in solid blue: $K_{Ic} = 1$ MPa.m$^{-1/2}$, in dashed red: $K_{Ic} = 10$ MPa.m$^{1/2}$). The elastic coefficient was taken equal to 0.012 GPa^{-1} and the dynamic viscosity to 0.8 Pa.s^{-1}.

favorable in the direction for which the stiffness felt by the crack is smaller. However, above this critical crack length, the favored direction of crack-propagation is, as in the isotropic case, perpendicular to the minimum far-field stress.

The governing equations of the problem were written in a dimensionless form.

A possible way to solve numerically the non-linear solid/fluid coupled problem was also suggested. Our numerical results were compared to an existing self-similar solution for the case of small toughness. The role played by the different parameters of the problem was identified.

What thus emerges is that the existing scholarly work developed for the isotropic case acan be applied to the anisotropic case provided that the right elastic parameters (identified in the previous Chapter) are employed. In addition, the simulator developed for the fluid-driven crack propagation problem is a viable (i.e. efficient) alternative to those already existing in industry.

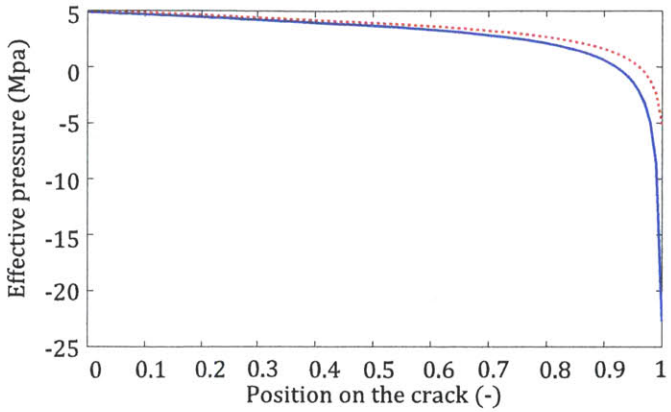

Figure 4-9: Effective pressure distribution along the crack (0 corresponds to the injection point and 1 to the crack-tip) for different fracture toughnesses K_{Ic} (in solid blue: $K_{Ic} = 1$ MPa.m$^{-1/2}$, in dashed red: $K_{Ic} = 10$ MPa.m$^{1/2}$). The elastic coefficient was taken equal to 0.012 GPa^{-1} and the dynamic viscosity to 0.8 Pa.s^{-1}.

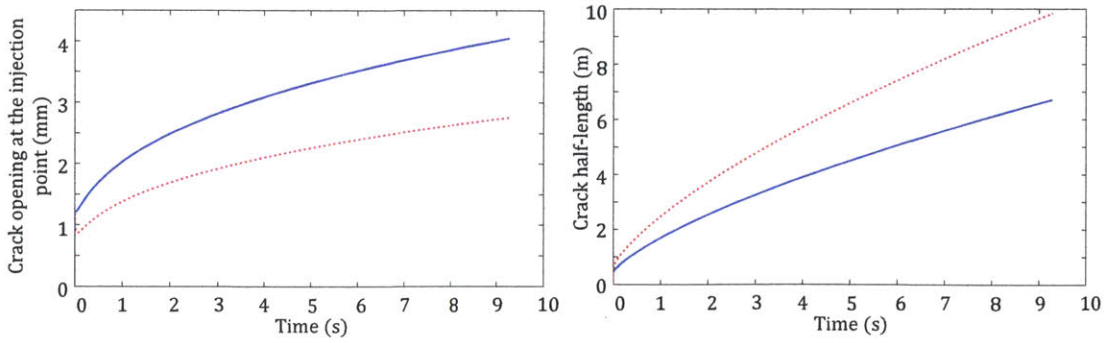

Figure 4-10: Crack half-length and crack opening at the injection point as functions of time for different viscosities η (in solid blue: $\eta = 0.8$ Pa.s^{-1}, in dashed red: $\eta = 0.08$ Pa.s^{-1}). The elastic coefficient was taken equal to 0.012 GPa^{-1} and the fracture toughness to 1 MPa.m$^{1/2}$.

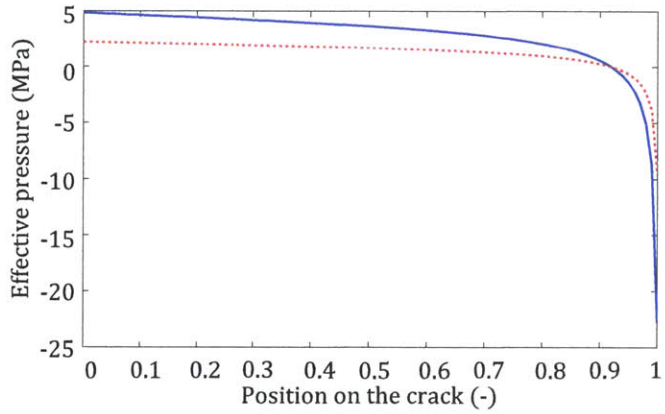

Figure 4-11: Effective pressure distribution along the crack (0 corresponds to the injection point and 1 to the crack-tip) for different viscosities η (in solid blue: $\eta = 0.8$ Pa.s^{-1}, in dashed red: $\eta = 0.08$ Pa.s^{-1}). The elastic coefficient was taken equal to 0.012 GPa^{-1} and the fracture toughness to 1 MPa.m$^{1/2}$.

Chapter 5

On flat ellipsoidal cracks in anisotropy and crack-shape adaptability

So far, we focused on two-dimensional plane-strain cracks. This type of cracks is well suited to model, for instance, magma-driven crack propagation such as in dykes [43]. However, when considering the hydraulic fracturing problem, three-dimensional models are more relevant. In this Chapter, we focus on elliptical cracks in a general anisotropic solid subjected to a uniform internal pressure and possibly to a uniform shear stress. We specify the model for the case of transverse isotropy. Finally, we study how cracks can adapt their shape to the elastic anisotropy.

5.1 Elliptical cracks in general anisotropy

In this Section, the problem of an elliptical crack subjected to a uniform loading is addressed. The parameterization of the problem is given in Section 5.1.1 and the solution from Hoenig [26] is summarized in Section 5.1.2.

5.1.1 Problem statement

We consider elliptical cracks (see Fig. 5-1) of semi-major axis a (aligned with the direction $\underline{e}_x$) and semi-minor axis b (aligned with the direction $\underline{e}_y$). Introduce the (inverse of the)

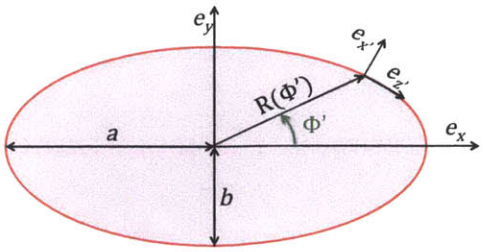

Figure 5-1: Elliptical crack geometry.

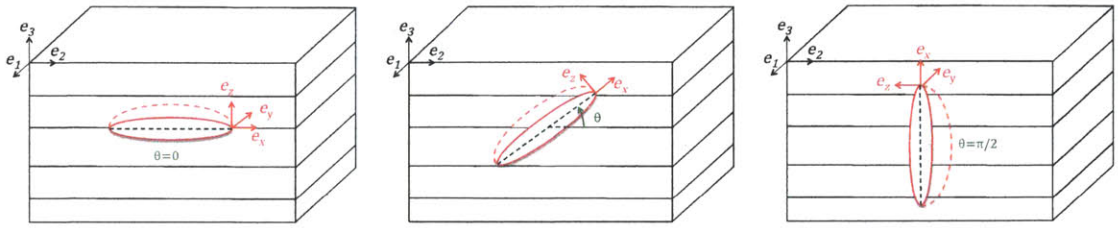

Figure 5-2: Definition of the θ-angle for a penny-shaped crack. On the left, crack in the bedding plane, in the middle, inclined crack, on the right, vertical crack.

aspect ratio $\gamma = b/a \leq 1$. If $\gamma = 1$, these cracks are often referred to as *penny-shaped cracks* [40]. The crack-edge can be parameterized either by the polar angle ϕ' (see Fig. 5-1) or by the angle ϕ satisfying $\tan\phi' = \gamma \tan\phi$:

$$\left\{ \begin{array}{rcccl} x & = & a\cos\phi & = & R(\phi')\cos\phi' \\ y & = & b\sin\phi & = & R(\phi')\sin\phi' \end{array} \right. \tag{5.1}$$

where $R(\phi')$ is the distance from the origin to the crack edge (see Fig. 5-1).

The crack so-defined is lying in an anisotropic material (the canonical orthonormal basis of the material is $(\underline{e}_1, \underline{e}_2, \underline{e}_3)$) and the crack-plane makes an angle θ with the plane $(\underline{e}_1, \underline{e}_2)$ (Fig. 5-2). In the case of an elliptical crack ($\gamma < 1$), we also have to define the angle $\alpha = \widehat{(\underline{e}_1, \underline{e}_x)}$ (Fig. 5-3). We then have:

$$\begin{pmatrix} \underline{e}_x \\ \underline{e}_y \\ \underline{e}_z \end{pmatrix} = \begin{bmatrix} \cos\alpha & \sin\alpha\cos\theta & \sin\alpha\sin\theta \\ -\sin\alpha & \cos\alpha\cos\theta & \cos\alpha\sin\theta \\ 0 & -\sin\theta & \cos\theta \end{bmatrix} \begin{pmatrix} \underline{e}_1 \\ \underline{e}_2 \\ \underline{e}_3 \end{pmatrix} \tag{5.2}$$

The crack is subjected to far-field stresses $\underline{\underline{\sigma}}$, and we want to find all the relevant quantities of a fracture mechanics problem: crack opening displacement $[\![\underline{\xi}]\!]$, stress intensity factors K_i

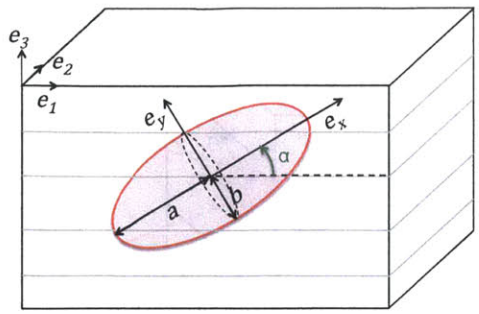

Figure 5-3: Definition of the α-angle for an elliptical vertical-crack ($\theta = \pi/2$).

($i = I$, II or III)[1] and energy release rate $\mathcal{G}$. These quantities will only depend on the stresses $\sigma_{\delta z}$ ($\delta = x$, y or z) or in an equivalent manner, $\sigma_{\delta y'}$ ($\delta = x'$, y' or z', see Fig. 5-1).

For isotropic materials subjected to a Mode I loading ($\sigma_{x'y'} = \sigma_{z'y'} = 0$), the solution of this problem was presented by Irwin [30]; and for general anisotropy and possibly mixed-mode loadings by Hoenig [26]. The following Section presents the main results from Hoenig. To keep consistent with the notations from the previous Chapters, some notations from Hoenig's original paper have been changed.

5.1.2 Main results from Hoenig [26]

Hoenig's solution is based on Eshelby's theorem [17] on ellipsoidal inclusions in anisotropic media. From this theorem, the displacement discontinuity can be written as:

$$[\![\xi_\delta]\!](r,\phi') = 2\beta_\delta\sqrt{ab}\sqrt{1-\left(\frac{r}{R(\phi')}\right)^2}, \delta = x, y \text{ or } z \tag{5.3}$$

where r and ϕ' are the polar coordinates (see Fig. 5-1), β_δ some dimensionless coefficients that are linked to the far-field stresses through a 3x3 matrix, $[\mathcal{C}]$, by means of the relationship:

$$\beta_\delta = \mathcal{C}^{-1}_{\delta\gamma}\sigma_{\gamma y'} \tag{5.4}$$

The main idea of Hoenig's solution is to consider that locally (see Fig. 5-4), each point along the crack edge (parameterized by angle ϕ) behaves as a point at the crack-tip of a

[1] Indeed, we deal here with a fully three-dimensional problem. We then have to account for all three fracture modes.

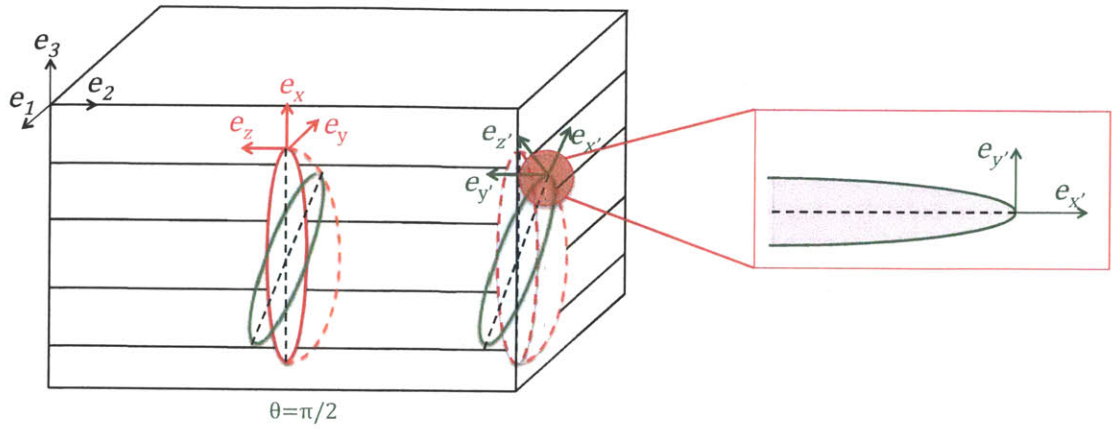

Figure 5-4: Zoom at the crack-tip.

crack in a plane anisotropic elastic body. The *two-dimensional equivalent crack* belongs to the plane $(\underline{e}_{x'}, \underline{e}_{z'})$ such that $\underline{e}_{\delta'} = \mathcal{P}_{\delta' i}\underline{e}_i$ ($\delta' = x'$, y' or z' and $i = 1$, 2 or 3) with:

$$[\mathcal{P}] = \begin{bmatrix} \cos(\alpha+\Psi) & \sin(\alpha+\Psi)\cos(\theta) & \sin(\alpha+\Psi)\sin(\theta) \\ 0 & -\sin\theta & \cos\theta \\ \sin(\alpha+\Psi) & -\cos(\alpha+\Psi)\cos(\theta) & -\cos(\alpha+\Psi)\sin(\theta) \end{bmatrix} \tag{5.5}$$

where $\tan\Psi = \frac{1}{\gamma}\tan\phi$.

The stiffness constants to be considered for the study of this two-dimensional crack are defined in the orthonormal basis $(\underline{e}_{x'}, \underline{e}_{y'}, \underline{e}_{z'})$ as follows:

$$S'_{\alpha'\beta'} = (\mathcal{R}_\epsilon)_{\alpha' i}\, S_{ij}\, \left({}^t\mathcal{R}_\epsilon\right)_{j\beta'} \tag{5.6}$$

(see Section 2.1.2 and Appendix D).

We define a *local* energy release rate $\mathcal{G}_\phi(\phi)$ that can be written in terms of the *local* stress intensity factor vector $\{K_\phi(\phi)\} = {}^t[K_I(\phi) \quad K_{II}(\phi) \quad K_{III}(\phi)]$ as:

$$\mathcal{G}_\phi(\phi) = \pi {}^t\{K_\phi(\phi)\}\,.\,[H_\phi(\phi)]\,.\,\{K_\phi(\phi)\} \tag{5.7}$$

where $[H_\phi(\phi)]$ is the *local* three-dimensional Irwin matrix[2] given in Appendix H, Eq. (H.5).

[2]Again, the name *Irwin matrix* is not standard. However, since this matrix seems to play an important role in any fracture mechanics problem, we found it convenient to give it a name.

The local stress intensity factors can be deduced from the coefficients β_δ through:

$$K_i(\phi) = \frac{1}{2}\sqrt{\frac{a}{\pi}}\left(H_\phi^{-1}(\phi)\right)_{ij} T_{jk} R_{kl}(\phi)\beta_l \tag{5.8}$$

where $[T]$ is defined in Appendix H, Eq. (H.6), while $[R]^{-1}$ is the inverse of the $[R]$ matrix defined as[3]:

$$[R(\phi)] = \frac{1}{\sqrt[4]{\sin^2\phi + \gamma^2\cos^2\phi}} \begin{bmatrix} \gamma\cos\phi & \sin\phi & 0 \\ 0 & 0 & \sqrt{\sin^2\phi + \gamma^2\cos^2\phi} \\ -\sin\phi & \gamma\cos\phi & 0 \end{bmatrix} \tag{5.9}$$

Remark 21 *Exactly as in the two-dimensional case, the near-tip displacement jump can be written in terms of the stress intensity factors as:*

$$[\![\begin{pmatrix} \xi_n \\ \xi_t \\ \xi_b \end{pmatrix}]\!](\epsilon,\phi) = [\![\begin{pmatrix} \xi_{y'} \\ \xi_{x'} \\ \xi_{z'} \end{pmatrix}]\!](\epsilon,\phi) \underset{\epsilon\to 0}{\sim} 8\sqrt{\frac{\pi\epsilon}{2}}\,[H_\phi(\phi)]\,.\,\{K_\phi\} \tag{5.10}$$

where $\epsilon = R(\phi) - r$.

The global energy release rate defined as[4] $\mathcal{G} \equiv -\left.\frac{\partial \mathcal{E}_p}{\partial \Gamma}\right|_{\gamma,\alpha}$ (where $\Gamma = \pi ab$ is the crack area) can be deduced from the local energy release rate:

$$\mathcal{G} = \frac{1}{2\pi}\int_{\phi=0}^{2\pi} \mathcal{G}_\phi(\phi)d\phi \tag{5.11}$$

Remark 22 $\mathcal{G}$ *is nothing else but the average of the local energy release rate* $\mathcal{G}_\phi(\phi)$ *along the crack edge. In the plane-strain case, we actually used in Eq.* (3.69) *the two-dimensional analogous formula* $\mathcal{G} = \frac{1}{2}\left(\mathcal{G}^{left} + \mathcal{G}^{right}\right)$.

Combining Eq. (5.7)-(5.8)-(5.11), one can obtain a first expression for the energy release rate. A second expression can be obtained from the displacement jump given by Eq. (5.3) (this method is similar to what is presented in Appendix F for the two-dimensional case). Equating the two[5], Hoenig found the following expression for the $[\mathcal{C}]$ matrix introduced in

[3]There is actually a misprint in the definition of $[R]$ given in Hoenig's original paper [26].

[4]We consider here that when the crack propagates, it keeps its *shape*, that is to say that the ratio $\gamma = b/a$ and the angle α remain constant.

[5]The very same method (equating two expressions of the potential energy) was actually used by Irwin

Eq. (5.4):

$$[\mathcal{C}] = \frac{1}{8\pi\sqrt{\gamma}} \int_{\phi=0}^{2\pi} {}^{t}([T].[R(\phi)]).[H_\phi(\phi)]^{-1}.([T].[R(\phi)])\, d\phi \tag{5.13}$$

Remark 23 *Fabrikant [18] studied the problem of a vertical elliptical crack in a vertically transversely isotropic material using a completely different approach. While Hoenig solved the problem by identifying two different expressions of the potential energy, Fabrikant used the complex potential theory. Hoenig's and Fabrikant's solutions were compared for the case of elliptical cracks subjected to a pure Mode I loading. Both solutions match.*

5.2 Specification to isotropy and transverse isotropy

In this Section, we specify the solution presented in Section 5.1 for isotropic and transversely isotropic (TI) media. We will first (Section 5.2.1) consider elliptical cracks in isotropy. We will then (Section 5.2.2) focus on penny-shaped cracks in a TI material.

Before doing this, it is important to mention that for cracks belonging to a plane of material symmetry, the local Irwin matrix $[H_\phi]$ is diagonal. Indeed, for such cracks, the three fracture modes are (at least locally) separable: a normal displacement jump induces only a Mode I stress intensity factor; and the same for Mode II or Mode III. For cracks belonging to a plane of material symmetry, we then have:

$$H_{ii}^{-1} = \frac{1}{H_{ii}} \tag{5.14}$$

for $i \in \{1,2,3\}$, all the other components H_{ij}^{-1} being null.

5.2.1 The specific case of elliptical cracks in isotropic media

Let us first focus on cracks in isotropic media. Since the Irwin matrix $[H_\phi]$ is diagonal, the $[\mathcal{C}]$ matrix defined by (5.13) is also diagonal.

[30] in the case of an isotropic material. The only difference comes that in isotropy, the Irwin matrix is independent of ϕ:

$$[H] = \begin{bmatrix} \frac{1-\nu^2}{\pi E} & 0 & 0 \\ 0 & \frac{1-\nu^2}{\pi E} & 0 \\ 0 & 0 & \frac{1+\nu}{\pi E} \end{bmatrix} \tag{5.12}$$

As in the case of plane-strain cracks, this is the limit case of a material having elastic constants such that $\mu_1 = -\epsilon + i$, $\mu_2 = \epsilon + i$, $\mu_3 = i$, $\lambda_1 = -\alpha - i\beta$, $\lambda_2 = \alpha - i\beta$, $\lambda_3 = -i\gamma$ with $(\epsilon, \alpha, \beta, \gamma) \in \mathbb{R}^4$ and $\{\epsilon, \alpha, \beta, \gamma\} \to \{0,0,0,0\}$.

Remark 24 *The fact that both $[H_\phi]$ and $[C]$ are diagonal has important consequences. Far-field stresses of the form:*

$$\underline{\underline{\sigma}} = \sigma_{zz}\underline{e}_z \otimes \underline{e}_z \tag{5.15}$$

induce neither Mode II nor Mode III stress intensity factors ($K_{II} = K_{III} = 0$); while far-field stresses of the form:

$$\underline{\underline{\sigma}} = \sigma_{xz}(\underline{e}_x \otimes \underline{e}_z + \underline{e}_z \otimes \underline{e}_x) + \sigma_{yz}(\underline{e}_y \otimes \underline{e}_z + \underline{e}_z \otimes \underline{e}_y) \tag{5.16}$$

induce no Mode I stress intensity factor ($K_I = 0$).

If the crack is subjected to a pure Mode I loading ($\sigma_{y'x'} = \sigma_{y'z'} = 0$), only the coefficient C_{33} is of interest, and is equal to:

$$C_{33} = \frac{1}{8\pi\sqrt{\gamma}} \frac{\pi E}{1-\nu^2} 4\mathbb{E}(e) \tag{5.17}$$

where $e = \sqrt{1-\gamma^2}$ is the eccentricity of the ellipse and $\mathbb{E}(k) = \int_{\phi=0}^{\pi/2} \sqrt{1-k^2\sin^2\phi}d\phi$ is the complete elliptic integral of the second kind, that has to be numerically computed.

Remark 25 *The complete elliptic integral of the second kind is actually proportional to the circumference, c, of the crack: $c = 4a\mathbb{E}(e)$. C_{33} can then be written in terms of the crack area $\Gamma = \pi ab$ and the crack circumference c as :*

$$C_{33} = \frac{c}{8\sqrt{\Gamma\pi}} \frac{\pi E}{1-\nu^2} \tag{5.18}$$

We then deduce that the Mode I stress intensity factor of an elliptical crack subjected to a uniform normal far-field stress $\sigma_{y'y'} = \sigma_{zz}$ is equal to:

$$K_I(\phi) = \sqrt[4]{\sin^2\phi + \gamma^2\cos^2\phi} \frac{\sqrt{a\pi\gamma}}{\mathbb{E}(e)} \sigma_{y'y'} \tag{5.19}$$

Remark 26 *Just as in the plane-strain case, the Mode I stress intensity factor is independent of the elastic properties of the material. In the particular case of a penny-shaped crack ($\gamma = 1$), it is constant along the crack tip and equal to:*

$$K_I^{penny-shaped} = 2\sqrt{\frac{a}{\pi}}\sigma_{y'y'} = \frac{2}{\pi} K_I^{plane-strain}(l \leftarrow a) \tag{5.20}$$

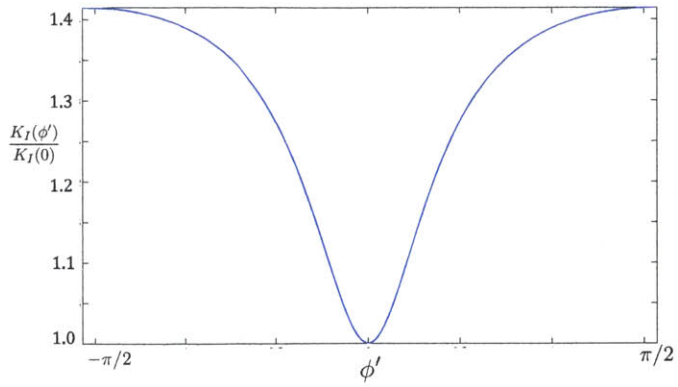

Figure 5-5: Dimensionless Mode I stress intensity factor as a function of ϕ' for an elliptical crack such that $\gamma = 1/2$ in an isotropic medium.

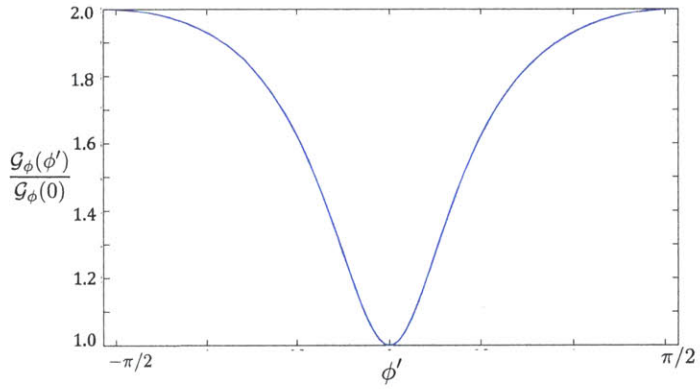

Figure 5-6: Dimensionless local energy release rate as a function of ϕ' for an elliptical crack such that $\gamma = 1/2$ in an isotropic medium.

For an elliptical crack characterized by $\gamma = 1/2$, the dimensionless Mode I stress intensity factor and local energy release rate are plotted as functions of the angle ϕ' (see Fig. 5-1) in Fig. 5-5 and 5-6.

5.2.2 The specific case of penny-shaped cracks in transverse isotropy

We saw in the previous Section that in isotropy, a penny-shaped crack subjected to a normal far-field stress $\underline{\underline{\sigma}} = \sigma_{zz}\underline{e}_z \otimes \underline{e}_z$ has three properties:

- The Mode I stress intensity factor does not vary along the crack front.

- Mode II and Mode III stress intensity factors are zero.
- The Mode I stress intensity factor is independent of the (isotropic) elastic properties of the material.

When considering anisotropic media, we will see that - unless for some specific crack orientations - none of these properties shall be true anymore.

We introduce the dimensionless stress intensity factors, Irwin matrix, energy release rate and displacement jumps defined as:

$$\left\{ \begin{array}{rcl} \bar{K}_i & = & \frac{\sqrt{\pi}}{2\sigma_{y'y'}\sqrt{a}} K_i \\ [\bar{H}_\phi] & = & \frac{1}{\mathcal{H}_1} [H_\phi] \\ \bar{\mathcal{G}}_\phi^{ad} & = & {}^t\{\bar{K}_\phi\} . [\bar{H}_\phi] . \{\bar{K}_\phi\} \\ [\![\begin{pmatrix} \bar{\xi}_n \\ \bar{\xi}_t \\ \bar{\xi}_b \end{pmatrix}]\!] & = & [\bar{H}_\phi] . \{\bar{K}_\phi\} \end{array} \right. \tag{5.21}$$

Study of inclined penny-shaped cracks in a transversely isotropic medium

We consider here penny-shaped cracks in a TI medium. The crack-plane makes an angle θ with respect to the plane of isotropy of the material (see Fig. 5-2) and the crack front is parameterized by angle $\phi = \phi'$ (see Fig. 5-1). This crack is subjected to a uniform far-field stress $\underline{\underline{\sigma}} = \sigma_{zz} \underline{e}_z \otimes \underline{e}_z$.

Figures 5-7, 5-9 and 5-8, 5-10 show how respectively the Mode I stress intensity factor and the energy release rate evolve along the crack front for different crack orientations ($\theta \in [0, \pi/2]$) for different materials. They highlight the fact that for any crack orientation other than for cracks in the bedding-plane ($\theta = 0$), both the stress intensity factor and the energy release rate vary along the crack front. In isotropic media, this was the case only for crack parameters γ strictly lower than 1, while we find this here for penny-shaped cracks ($\gamma = 1$) in TI materials.

For the clay model and for the reference TI material (see Appendix C), when considering vertical cracks ($\theta = \pi/2$), both the Mode I stress intensity factor K_I and the local energy release rate $\mathcal{G}_\phi$ reach a maximum for $\phi = \pm \pi/2$ and $\phi = 0$, respectively[6].

[6] α was taken equal to $\pi/2$ and $\gamma = 1$.

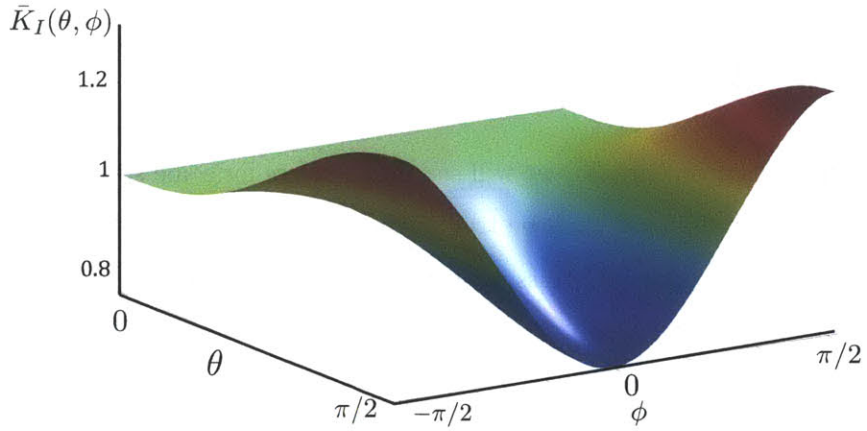

Figure 5-7: Dimensionless Mode I stress intensity factor $\bar{K}_I(\theta,\phi)$ for a penny-shaped crack subjected to a normal far-field stress (for the clay model (see Appendix C)).

Figures 5-11 and 5-12 show that the three (dimensionless) stress intensity factors and their *associated* displacement jump evolve along the crack front for different crack orientations and for different materials. It is interesting to notice that, contrary to the isotropic case, there exists a Mode II and a Mode III stress intensity factor, as well as a tangential and an out-of-plane displacement jump even if the loading is purely normal to the original crack surface $\underline{\underline{\sigma}} = \sigma_{zz}\underline{e}_z \otimes \underline{e}_z$. However, these two non-normal displacement jumps vanish when the crack belongs to a plane of material symmetry ($\theta \equiv 0\,[\pi/2]$), just as in the plane-strain case. As mentioned in Remark 24, this is due to the fact that the $[\mathcal{C}]$ matrix is diagonal for $\theta \equiv 0\,[\pi/2]$. When $\bar{K}_{II}$ and $\bar{K}_{III}$ exist, they are both of similar order of magnitude, and about one order of magnitude smaller than $\bar{K}_I$. Contrary to the isotropic case (see Remark 26), the stress intensity factors are no more independent of the elasticity.

Study of penny-shaped cracks belonging to a plane of material symmetry

We focus on two specific cases, $\theta = 0$ and $\theta = \pi/2$; that is, the cases for which the crack belongs to a plane of material symmetry.

For $\theta = 0$ (crack in the bedding-plane), the crack does not *feel* any anisotropy: the compliance matrix $[S']$ (see Eq. (5.6)) intervening in the calculation of the Irwin matrix, $[H_\phi]$, is the same for every angle ϕ, so that $[H_\phi]$ is constant along the crack front. The

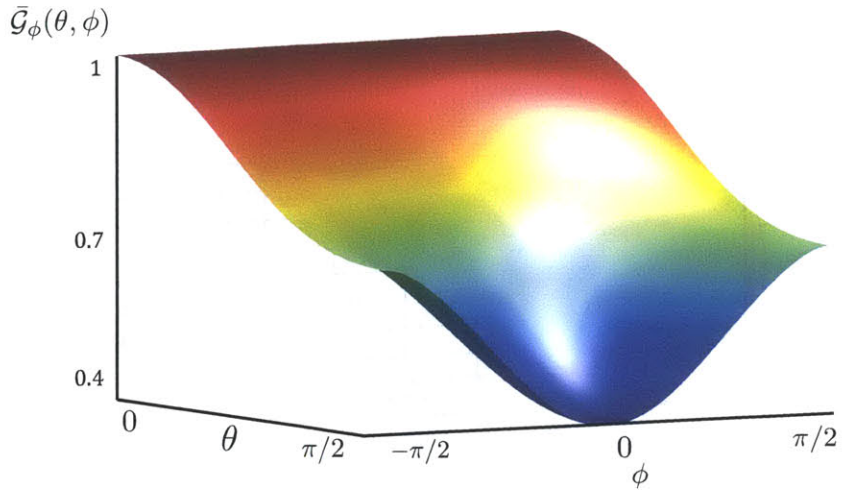

Figure 5-8: Dimensionless energy release rate $\bar{\mathcal{G}}_\phi^{penny}(\theta,\phi)$ for a penny-shaped crack subjected to a normal far-field stress (for the clay model (see Appendix C)).

Mode I stress intensity factor is then also constant and independent of the elastic properties (see Remark 26). The energy release rate is constant along the crack front and equal to $\mathcal{G}^{penny}(\theta=0) = \pi\mathcal{H}_1 K_I^2$, where $\mathcal{H}_1 = (H_\phi)_{11}$ was introduced by Eq. (3.45). According to Eq. (3.49), it can be written in terms of the vertical indentation modulus M_3 in the following form:

$$\mathcal{G}^{penny}(\theta=0) = \frac{4a\sigma_{zz}^2}{\pi M_3} \tag{5.22}$$

In return, for $\theta = \pi/2$ (vertical crack), the crack fully *feels* the anisotropy of the TI material. Indeed, the compliance $[S']$ now depends on ϕ so that the coefficient $(H_\phi)_{11} = \mathcal{H}$ (the only coefficient that is relevant to this crack orientation and this type of loadings) varies along the crack front. For $\phi = 0$, it is obviously equal to the coefficient $\mathcal{H}_2$ introduced in Eq. (3.45); and for $\phi = \pm\pi/2$, it is equal to coefficient $\mathcal{H}_3$ also introduced in Eq. (3.45).

While the exact expression for $(H_\phi(\phi))_{11} = \mathcal{H}(\phi)$ can be found in Eq. (3.37) - provided that the compliance matrix from Section 2.1.3 is used[7] - there is no easy formula for $\mathcal{H}(\phi)$. However, a satisfactory approximation having the wanted π-periodicity was proposed by Delafargue et al. [14]:

$$\mathcal{H}(\phi) \simeq \mathcal{H}_2 \cos^2\phi + \mathcal{H}_3 \sin^2\phi \tag{5.23}$$

An even more satisfactory approximation (notably for materials such as shale, see Table

[7]The θ in Section 2.1.3 then corresponds to the ϕ in this Section.

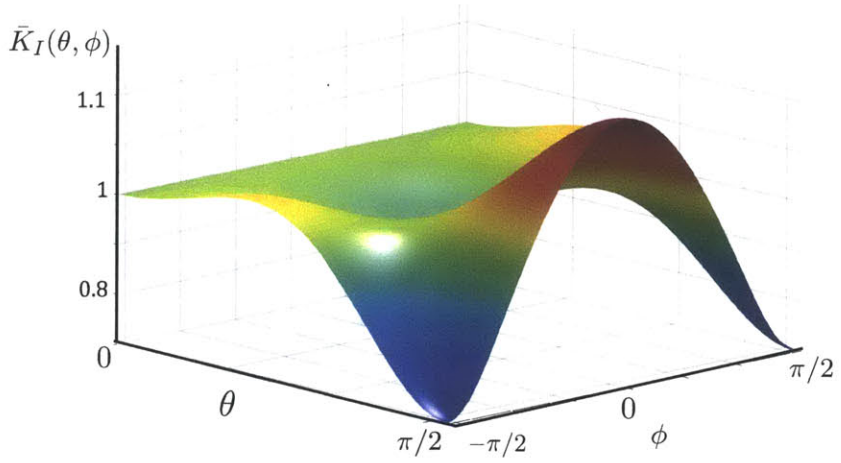

Figure 5-9: Dimensionless Mode I stress intensity factor $\bar{K}_I(\theta,\phi)$ for a penny-shaped crack subjected to a normal far-field stress (for a reference TI medium (see Appendix C)).

C.1) is suggested here:

$$\mathcal{H}(\phi) \simeq \left(\frac{\cos^2\phi}{\mathcal{H}_2} + \frac{\sin^2\phi}{\mathcal{H}_3}\right)^{-1} \tag{5.24}$$

Comparisons of approximations (5.23) and (5.24) with the real values of $\mathcal{H}(\phi)$ given by Eq. (H.5) in Appendix H are given on Fig. 5-13, 5-14 and 5-15 for different materials. Except for Apatite, approximation (5.24) and (5.23) seem pretty good. The same type of comparison was made for different shale materials and was also found to be satisfactory.

Given the quality of the approximations, one can explicitly estimate the coefficient $\mathcal{C}_{33} = \frac{1}{8\pi}\int_{\phi=0}^{2\pi}\frac{d\phi}{\mathcal{H}(\phi)}$ (where we implicitly used Eq. (5.14)). Using approximation (5.23), one obtains:

$$\mathcal{C}_{33} \simeq \frac{1}{4\sqrt{\mathcal{H}_2\mathcal{H}_3}} \tag{5.25}$$

while the use of approximation (5.24) yields:

$$\mathcal{C}_{33} \simeq \frac{1}{8}\left(\frac{1}{\mathcal{H}_2} + \frac{1}{\mathcal{H}_3}\right) \tag{5.26}$$

The *global* energy release rate for a vertical penny-shaped crack can then be estimated using Eq. (5.25) or (5.26). Using (5.25) yields:

$$\mathcal{G}^{penny}(\theta = \pi/2) \simeq 4a\sigma_{zz}^2\sqrt{\mathcal{H}_2\mathcal{H}_3} \tag{5.27}$$

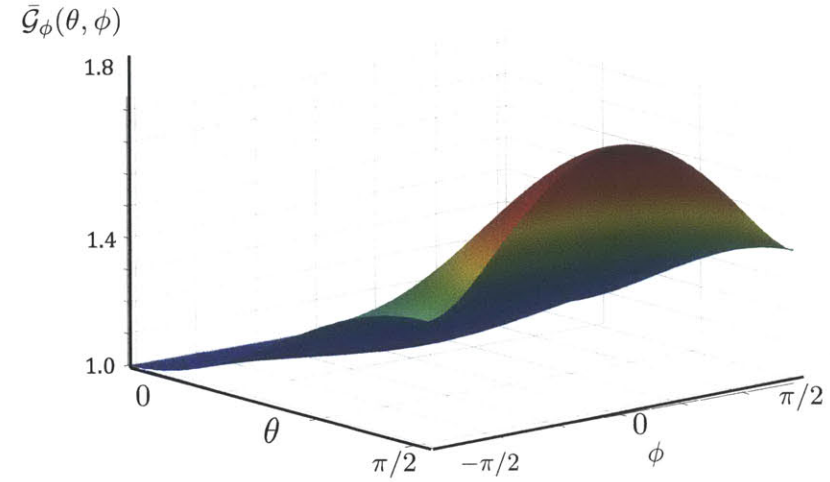

Figure 5-10: Dimensionless energy release rate $\bar{\mathcal{G}}_\phi^{penny}(\theta,\phi)$ for a penny-shaped crack subjected to a normal far-field stress (for a reference TI medium (see Appendix C)).

while using (5.26) entails:

$$\mathcal{G}^{penny}(\theta=\pi/2) \simeq 4a\sigma_{zz}^2 \frac{2}{\frac{1}{\mathcal{H}_2}+\frac{1}{\mathcal{H}_3}} \tag{5.28}$$

Remark 27 *According to [14], the coefficient $\mathcal{C}_{33}$ can actually be written in terms of the indentation modulus in the horizontal direction $\mathcal{M}_1$:*

$$\mathcal{C}_{33} \simeq \frac{1}{4}\frac{1}{\pi M_1} \tag{5.29}$$

so that the global energy release rate can also be approximated in terms of M_1:

$$\mathcal{G}^{penny}(\theta=\pi/2) \simeq \frac{4a\sigma_{zz}^2}{\pi M_1} \tag{5.30}$$

The ratio of the global energy release rate of a vertical crack over the energy release rate of a horizontal crack is then found to be approximately equal to the ratio of the indentation moduli:

$$\frac{\mathcal{G}^{penny}(\theta=\pi/2)}{\mathcal{G}^{penny}(\theta=0)} \simeq \frac{M_3}{M_1} \tag{5.31}$$

Another approximation than the one developed here was given in Ref. [33]:

$$\mathcal{G}^{penny}(\theta=\pi/2) \simeq a\sigma_{zz}^2 \frac{4(1-\nu_{13}^2)}{\pi E_1} \tag{5.32}$$

The three approximations of the *global* energy release rate are compared for different materials and the results are summarized in Table 5.1. The approximations (5.27) and (5.28) are satisfactory for most of the materials considered, especially for shale; which is not the case for approximation (5.32) showing a poor performance.

Approximation of the global energy release rate for inclined penny-shaped cracks

Consider now crack orientations $\theta \in [0, \pi/2]$. Due to the symmetries of TI materials, one knows that function $\mathcal{G}^{penny}$ has to be π-periodic. Possible approximations for the *global* energy release rate should be of the form:

$$\mathcal{G}^{penny}(\theta) \simeq \mathcal{G}^{penny}(0)\cos^2\theta + \mathcal{G}^{penny}(\pi/2)\sin^2\theta \tag{5.33}$$

or:

$$\mathcal{G}^{penny}(\theta) \simeq \left(\frac{\cos^2\theta}{\mathcal{G}^{penny}(0)} + \frac{\sin^2\theta}{\mathcal{G}^{penny}(\pi/2)}\right)^{-1} \tag{5.34}$$

The true dimensionless *global* energy release rate and its approximations based on Eq. (5.33) and (5.34) (using approximation (5.28) for the estimated value of $\mathcal{G}^{penny}(\pi/2)$) are plotted for different materials in Fig. 5-16 and 5-17. For the clay model and shale in general, the approximation (5.33) gives satisfactory results.

5.2.3 The specific case of vertical elliptical cracks

Consider now vertical elliptical cracks. Taking advantage of Eq. (5.14), we write the local energy release rate as follows:

$$\mathcal{G}_\phi(\theta = \pi/2; \gamma, \phi) = 4a\sigma_{zz}^2 \frac{\sqrt{\sin^2\phi + \gamma^2\cos^2\phi}}{16H_{11}(\phi)} \frac{1}{\left(\frac{1}{8\pi\sqrt{\gamma}}\int_{\phi=0}^{2\pi} \frac{\sqrt{\sin^2\phi+\gamma^2\cos^2\phi}}{H_{11}(\phi)}d\phi\right)^2} \tag{5.35}$$

and the global energy release rate as:

$$\mathcal{G}(\theta = \pi/2; \gamma) = 4a\sigma_{zz}^2 \frac{2\pi\gamma}{\int_{\phi=0}^{2\pi} \frac{\sqrt{\sin^2\phi+\gamma^2\cos^2\phi}}{H_{11}(\phi)}d\phi} \tag{5.36}$$

5.3 On crack-shape adaptability

Except for crack kinking, the crack-shape of two-dimensional cracks (studied in Chapters 3 and 4) after *unloading* is entirely determined by its half-length l. In contrast, for three-dimensional cracks, an infinity of possibilities of shapes is conceivable. However, depending on the loading, some shapes may be more favorable than others. Due to the restrictions of the model introduced in Section 5.1, we will look for the most favorable crack-shape only among the possible elliptical shapes. We will introduce three possible criteria for crack shape adaptability in isotropy and in anisotropy.

5.3.1 Crack-shape adaptability in isotropy

As we saw in Section 5.2.1, except for $\gamma = 1$ (i.e. for penny-shaped cracks), the Mode I local stress intensity factor K_I and the local energy release rate G_ϕ vary along the crack front. Interestingly, they reach a maximum for $\phi = \phi' = \pi/2$ (see Figs 5-5 and 5-6). Based on this observation, Irwin deduced that: *'[...] with increase of tension on a flat elliptical crack, the crack-extension, barring anisotropy, tend to produce a circular crack-boundary shape'* [30].

This reasoning is valid whether one opts for a crack-propagation criterion based on fracture toughness and stress intensity factors - $K_I \leq K_{Ic}$ - or on fracture energy and energy release rate - $\mathcal{G} \leq \mathcal{G}_c$ - (see Section 2.3).

Furthermore, one can show that the global energy release rate $\mathcal{G}$ (see Eq. (5.11)) of an elliptical crack (of crack parameter $\gamma = b/a$) subjected to a pure Mode I is equal to:

$$\mathcal{G}(\gamma) = a\sigma_{y'y'}^2 \mathcal{H} \frac{\gamma}{\mathbb{E}(\sqrt{1-\gamma^2})} \tag{5.37}$$

where $\mathcal{H} = H_{11} = \frac{1-\nu^2}{\pi E}$. The function $\frac{\mathcal{G}(\gamma)}{a\sigma_{y'y'}^2 \mathcal{H}}$ is plotted in Fig. 5-18. Interestingly, the global energy release rate reaches a maximum for $\gamma = 1$; that is, for a penny-shaped crack. Irwin deduced that the favored crack shape was a circular shape. He based his reasoning on the fact that only this shape ensures constant Mode I stress intensity factor K_I and local energy release rate $\mathcal{G}_\phi$ along the crack front. An alternative to Irwin's reasoning could be based on the fact that this shape is the one that dissipates the more energy when it propagates (at constant crack parameter γ).

Furthermore, in the case of mixed-modes II and III loading conditions (due to the crack geometry, one of these two modes cannot be separated from the other), irrespective of the crack parameter γ, neither the stress intensity factors $K_{II}(\phi)$ and $K_{III}(\phi)$, nor the local energy release rate $\mathcal{G}_\phi(\phi)$ along the crack front will be constant. In fact, the ratio $\frac{\mathcal{G}_{shear}(\gamma,\phi=\pi/2)}{\mathcal{G}_{shear}(\gamma,\phi=0)}$ is equal to:

$$\frac{\mathcal{G}_{shear}(\gamma,\pi/2)}{\mathcal{G}_{shear}(\gamma,0)} = \frac{1}{\gamma(1-\nu)} \tag{5.38}$$

It cannot be equal to unity since $\gamma \leq 1$ (at least with positive Poisson's ratios, ν). It reaches a maximum for $\gamma = 1$.

Under this type of loadings, the maximum local energy release rate occurs (again) for $\phi = \phi' = \pi/2$, and the maximum global energy release rate is obtained for $\gamma = 1$ (see Fig. 5-19). This suggests that the favored crack-shape under mixed-mode conditions would also be of circular shape.

5.3.2 Crack-shape adaptability in anisotropy

Things are somewhat different when it comes to anisotropic solids. We saw previously (Section 5.2.2) that cracks belonging to the bedding plane behaved exactly as cracks in isotropy. Everything derived in Section 5.3.1 is then still valid, provided that the right elastic coefficients are used. We will now consider vertical elliptical cracks ($\theta = \pi/2$); that is, cracks belonging to the other plane of material symmetry, the plane $(\underline{e}_1, \underline{e}_3)$. Then, we can play with the two parameters determining the crack shape. The first one is the ratio $\gamma = b/a$ and the second one is the angle α between the semi-major axis of the ellipse and direction $\underline{e}_1$ (see Fig. 5-3).

We propose here three criteria for the crack-shape adaptability. The first one is based on the global energy release rate, the second one on the Mode I stress intensity factor while the third one is based on the local energy release rate.

Global energy release rate based crack-shape adaptability criterion

A possible criterion for crack-shape adaptability can be based on the global energy release rate. It considers that the optimal crack-shape is the shape that maximizes the global energy

release rate and thus the dissipation (see Section 2.3). The *optimal* crack parameters (α, γ) are then determined by solving the maximization problem:

$$(\alpha, \gamma) = \arg\max_{(\alpha,\gamma)} \mathcal{G}(\alpha, \gamma) \tag{5.39}$$

under the constraint that $(\alpha, \gamma) \in [0, \pi/2] \times (0, 1]$.

Figures 5-20 and 5-21 show for respectively the clay model and the reference TI material the global energy release rate in function of the crack-shape parameters α and γ. The *Maximum Global Energy Release Rate Criterion* predicts that, for a crack subjected to a pure pressure loading, the *optimal* crack shape would always be obtained for $\gamma = 1$ (and thus for any α).

One can also remark that at fixed aspect ratio γ, the global energy release rate is a decreasing (respectively increasing) function of α for the clay model (respectively for the reference TI material). The main difference between the two is that $\mathcal{H}_2$ is greater than $\mathcal{H}_3$ for the first, and it is the inverse for the second.

However, as shown in Fig. 5-9 and 5-10, a vertical penny-shaped crack has varying Mode I stress intensity factor and local energy release rate along the crack front. Following Irwin's reasoning, one would then expect the crack to propagate in the direction of the maximum stress intensity factor or the maximum local energy release rate. This motivates the consideration of other crack-shape adaptability criteria.

Stress intensity based crack-shape adaptability criterion

If one considers Irwin's crack propagation criterion based on the Mode I stress intensity factor (see Section 2.3.2), the favored crack-shape should be such that $K_I(\phi)$ is equal, at each point along the crack front, to the fracture toughness $K_{Ic}(\phi)$. If K_{Ic} is isotropic, the crack shape that ensures a constant Mode I stress intensity factor along the crack, is the most favorable.

Such a constraint is, however, usually impossible to be satisfied if we restrict ourselves to elliptical cracks. Still, we can try to minimize the magnitude of the variations of the stress intensity factor. The parameters (α, γ) of the favored crack-shape are then determined by solving the minimization problem:

$$(\alpha,\gamma) = \arg\min_{(\alpha,\gamma)} \left\{ \max_{\phi} \frac{|K_I(\alpha,\gamma,\phi) - K_I(\alpha,\gamma,\phi=0)|}{K_I(\alpha,\gamma,\phi=0)} \right\} \tag{5.40}$$

under the constraint that $(\alpha,\gamma) \in [0,\pi/2] \times (0,1]$.

Using the approximation (5.24) for $\mathcal{H}(\phi)$, we then find that the preferred crack shape using the *Constant Stress Intensity Factor Criterion* was entirely determined by the ratio $\mathcal{H}_2/\mathcal{H}_3$, where $\mathcal{H}_2$ and $\mathcal{H}_3$ are given by Eq. (3.45). That is, the crack shape adapts to the elastic content. Specifically, if we remind ourselves that the ratio $\mathcal{H}_3/\mathcal{H}_2$ can be written in terms of the first Thomsen parameter and the indentation moduli in the horizontal and vertical direction:

$$\frac{\mathcal{H}_3}{\mathcal{H}_2} = (1+2\epsilon)\left(\frac{M_3}{M_1}\right)^2 \tag{5.41}$$

If $\mathcal{H}_2/\mathcal{H}_3 \leq 1$, the *Constant Stress Intensity Factor Criterion* predicts that the preferred crack shape is such that:

$$\begin{cases} \gamma &= \left(\frac{\mathcal{H}_2}{\mathcal{H}_3}\right)^2 \\ \alpha &= \frac{\pi}{2} \end{cases} \tag{5.42}$$

Otherwise, if $\mathcal{H}_2/\mathcal{H}_3 > 1$,

$$\begin{cases} \gamma &= \left(\frac{\mathcal{H}_3}{\mathcal{H}_2}\right)^2 \\ \alpha &= 0 \end{cases} \tag{5.43}$$

Table 5.2 gives the preferred crack shapes for different TI crystals and shale using the *Constant Stress Intensity Factor Criterion.* They also give a measure of the amplitude of the variations of the local Mode I stress intensity factor along the crack front for the preferred shape.

One can notice that for all the shale materials considered, the preferred crack shape has always an α equal to zero: the crack propagates in a horizontal direction.

Local energy release rate based crack-shape adaptability criterion

If now, one considers Griffith's crack propagation criterion based on the energy release rate (see Section 2.3.2), the favored crack-shape should be such that $\mathcal{G}_\phi(\phi)$ is equal, at each point along the crack front, to the fracture energy $\mathcal{G}_c(\phi)$. If the fracture energy is assumed to be constant along the crack-front, one should consider that the crack shape that ensures

a constant local energy release rate $\mathcal{G}_\phi$ along the crack-front is the most favorable.

Again, such a constraint is usually impossible to be satisfied if we restrict ourselves to elliptical cracks. However, we can try to minimize the amplitude of the variations of local energy release rate. The parameters (α, γ) of the favored crack-shape are then determined by solving the minimization problem:

$$(\alpha, \gamma) = \arg\min_{(\alpha,\gamma)} \left\{ \max_{\phi} \frac{|\mathcal{G}_\phi(\alpha, \gamma, \phi) - \mathcal{G}_\phi(\alpha, \gamma, \phi = 0)|}{\mathcal{G}_\phi(\alpha, \gamma, \phi = 0)} \right\} \tag{5.44}$$

under the constraint that $(\alpha, \gamma) \in [0, \pi/2] \times (0, 1]$.

Using the approximation (5.24) for $\mathcal{H}(\phi)$, we found out that the preferred crack shape using the *Constant Local Energy Release Rate Criterion* is also entirely determined by the ratio $\mathcal{H}_2/\mathcal{H}_3$.

However, in contrast to the constant stress intensity factor criterion, the crack shape scales linearly with $\mathcal{H}_2/\mathcal{H}_3$, not quadratic. That is, if $\mathcal{H}_2/\mathcal{H}_3 \leq 1$:

$$\begin{cases} \gamma &= \frac{\mathcal{H}_2}{\mathcal{H}_3} \\ \alpha &= \frac{\pi}{2} \end{cases} \tag{5.45}$$

Otherwise, if $\mathcal{H}_2/\mathcal{H}_3 > 1$,

$$\begin{cases} \gamma &= \frac{\mathcal{H}_3}{\mathcal{H}_2} \\ \alpha &= 0 \end{cases} \tag{5.46}$$

Table 5.3 gives the preferred crack shapes for different TI crystals and shale using the *Constant Local Energy Release Rate Criterion.* They also give a measure of the amplitude of the variations of the local energy release rate along the crack front for the preferred crack shape.

One can notice that for all materials considered, the (dimensionless) magnitude of the variations of the local energy release rate using this criterion is lower than the (dimensionless) magnitude of the variations of the Mode I stress intensity factor using the *Constant Local Energy Release Rate Criterion.* Again, for shale, the angle α is always equal to 0.

Using Eq. (5.35), one can see that for the local energy release rate to be constant, we must have $H_{11}(\phi) \propto \sqrt{\sin^2\phi + \gamma^2 \cos^2\phi}$. For $\alpha = 0$, we must have $H_{11}(0) = \mathcal{H}_3$ and

$H_{11}(\pi/2) = \mathcal{H}_2$ so that for the preferred crack shape,

$$\mathcal{G}_\phi(\theta = \pi/2, \gamma = \mathcal{H}_3/\mathcal{H}_2; \phi) \simeq \mathcal{G}(\theta = \pi/2, \gamma = \mathcal{H}_3/\mathcal{H}_2) \simeq 4a\sigma_{zz}^2\mathcal{H}_3 \tag{5.47}$$

As for $\alpha = \pi/2$, we must have $H_{11}(0) = \mathcal{H}_2$ and $H_{11}(\pi/2) = \mathcal{H}_3$ so that for the preferred crack shape,

$$\mathcal{G}_\phi(\theta = \pi/2, \gamma = \mathcal{H}_2/\mathcal{H}_3; \phi) \simeq \mathcal{G}(\theta = \pi/2, \gamma = \mathcal{H}_2/\mathcal{H}_3) \simeq 4a\sigma_{zz}^2\mathcal{H}_2 \tag{5.48}$$

5.4 Chapter summary

In this Chapter, we studied three-dimensional cracks subjected to uniform loading conditions. We restricted ourselves to flat ellipsoidal cracks, making extensive use of Hoenig's work.

In order to keep consistency with the developments in previous Chapters, we introduced the three-dimensional Irwin matrix having the same role as in the case of two-dimensional cracks.

We identified two specificities of cracks in anisotropic media. The first one is that, except for cracks belonging to a plane of material symmetry, there exists a Mode II and a Mode III stress intensity factor even for pure pressure loadings. The second one is that the local stress intensity factors and the local energy release rate can vary along the crack front of penny-shaped cracks.

We introduced several criteria to predict how an initially penny-shaped crack could adapt its shape to the elasticity. An appealing criterion based on Griffith's crack-propagation criterion predicts that an initially penny-shaped crack subjected to a pure pressure loading should first reach an *optimal* elliptical shape and then grow self-similarly, keeping constant its aspect ratio. In a first approximation this crack shape scales as a power function of the elasticity constant, the power exponent being somewhat between *one* and *two*.

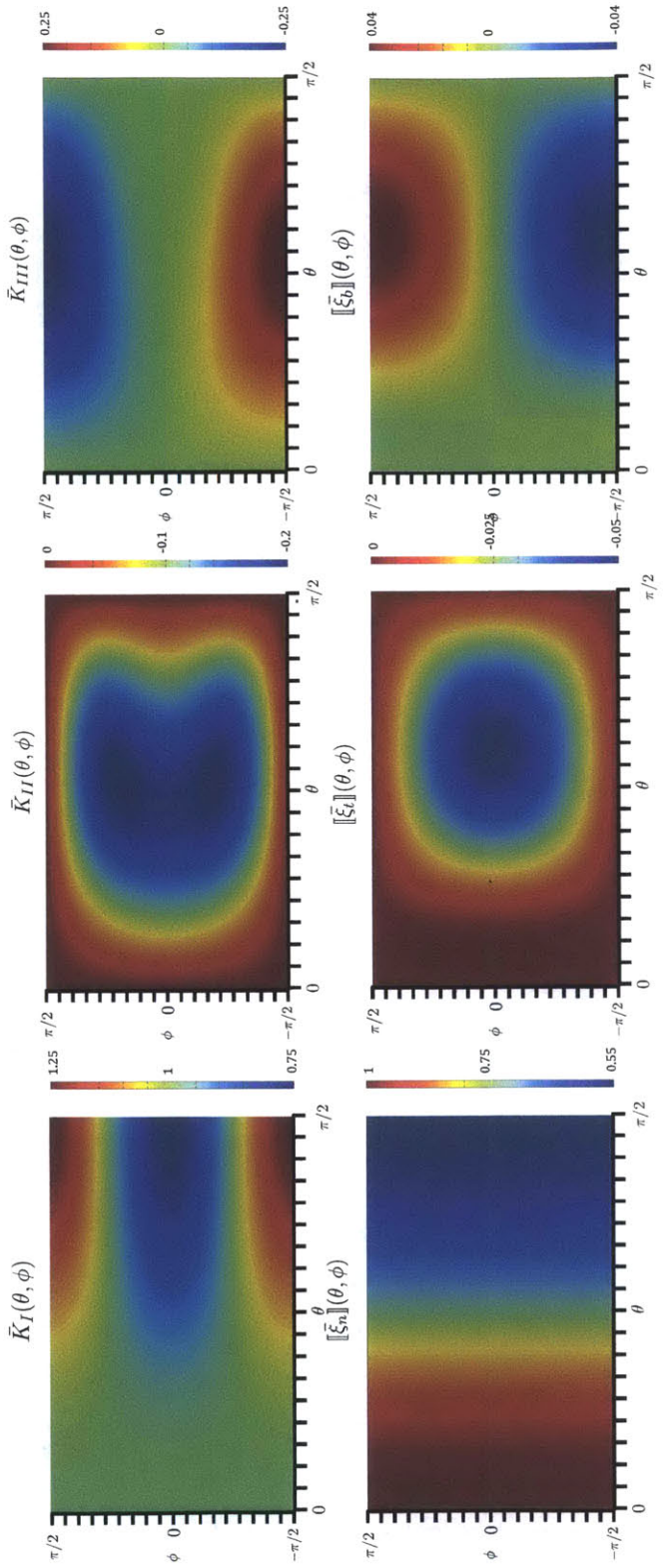

Figure 5-11: Dimensionless stress intensity factors and displacement jumps as functions of θ and ϕ for a penny-shaped crack subjected to a normal far-field stress (for the clay model, see Appendix C).

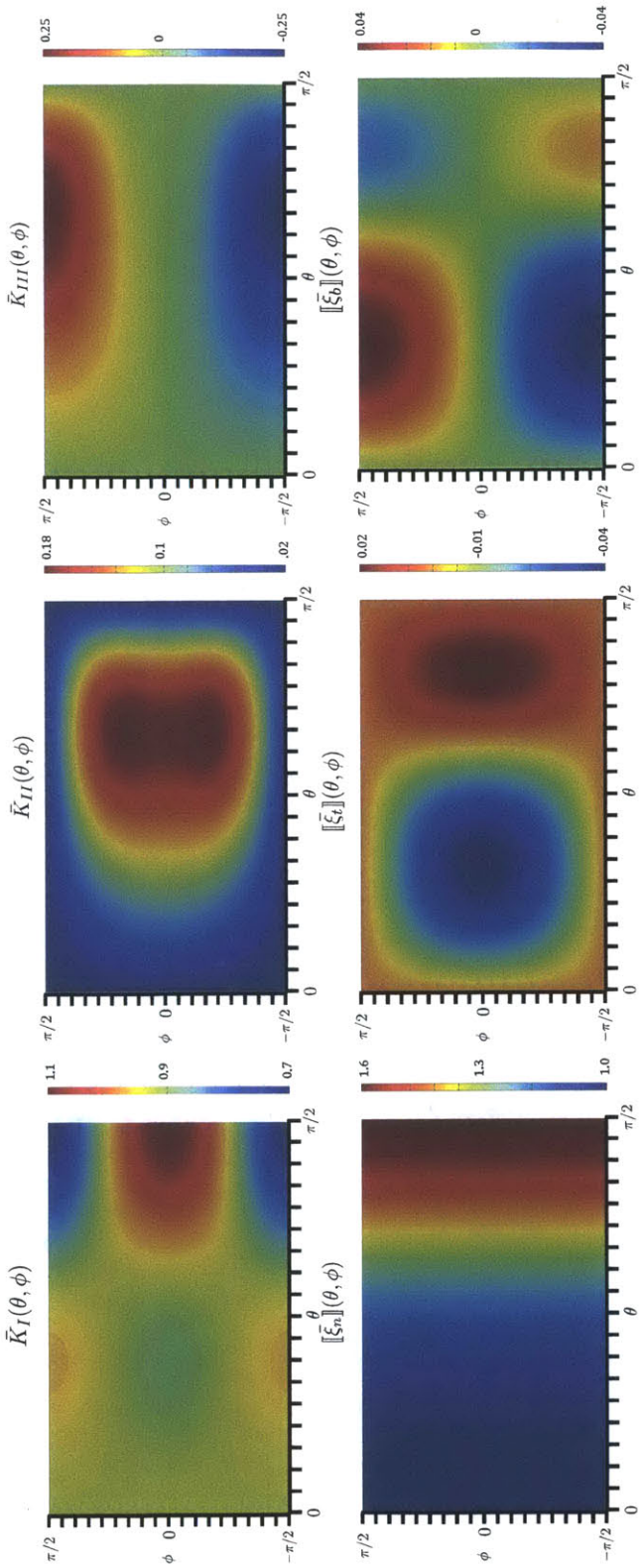

Figure 5-12: Dimensionless stress intensity factors and displacement jumps as functions of θ and ϕ for a penny-shaped crack subjected to a normal far-field stress (for a reference TI medium, see Appendix C).

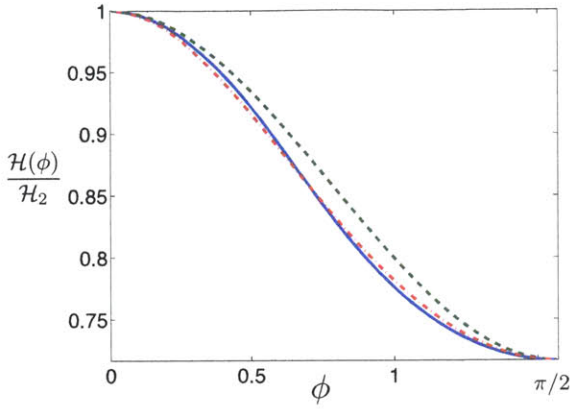

Figure 5-13: Comparison of the dimensionless $\mathcal{H}(\phi)$ (blue solid line), its approximation (5.23) (green dashed) and its approximation (5.24) (red dash-dotted) for the Zinc material studied in [14].

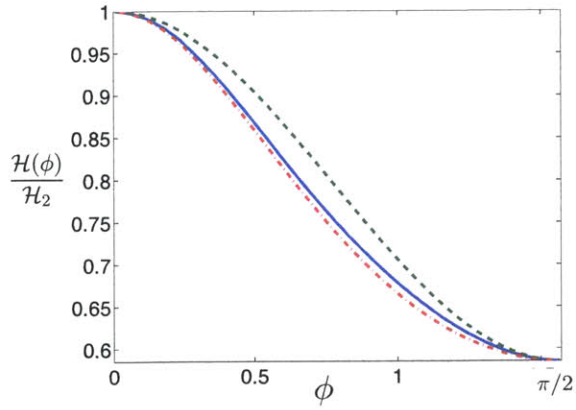

Figure 5-14: Comparison of the dimensionless $\mathcal{H}(\phi)$ (blue solid line), its approximation (5.23) (green dashed) and its approximation (5.24) (red dash-dotted) for the clay model (see Appendix C).

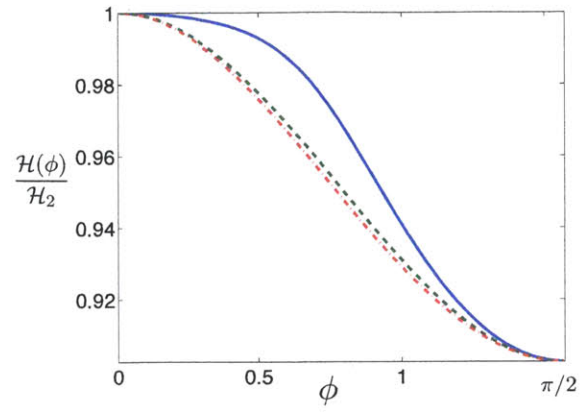

Figure 5-15: Comparison of the dimensionless $\mathcal{H}(\phi)$ (blue solid line), approximation (5.23) (green dashed) and approximation (5.24) (red dash-dotted) for Apatite crystal (see Appendix C).

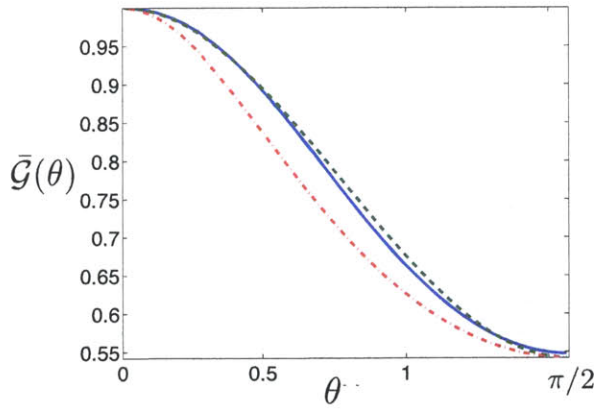

Figure 5-16: Dimensionless global energy release rate $\bar{\mathcal{G}}^{penny}(\theta)$ (blue solid line) and its approximations based on Eq. (5.33) (green dashed) and Eq. (5.34) (red dash-dotted) for the clay model (see Appendix C).

	Approximation from Eq (5.27)	Approximation from Eq (5.28)	Approximation from Eq (5.32)
Isotropic	**0.00** %	**0.00** %	**0.00** %
Magnesium	0.44 %	0.45 %	**0.05** %
Rhenium	0.77 %	0.78 %	**0.38** %
Apatite	**0.83** %	0.96 %	1.41 %
Yttrium	**0.48** %	0.49 %	0.54 %
Ice	**0.84** %	**0.84** %	1.30 %
Hafnium	**0.25** %	0.29 %	1.62 %
Cadmium	1.69 %	**0.01** %	2.77 %
Zinc	1.36 %	**0.04** %	2.89 %
Baryllium	0.27 %	**0.23** %	3.40 %
Cobalt	**1.39** %	1.60 %	3.63 %
Beryl	**0.52** %	0.62 %	4.61 %
Titanium	**0.31** %	0.84 %	8.23 %
Composite2	2.41 %	**0.86** %	20.43 %
Composite1	1.35 %	**1.32** %	25.48 %
Thallium	**3.69** %	5.83 %	45.10 %
Reference TI	0.62 %	**0.43** %	6.48 %
Woodford56	0.38 %	**0.29** %	3.87 %
Woodford40	**0.23** %	0.47 %	4.69 %
Woodford47	0.37 %	**0.12** %	4.51 %
Woodford51	0.48 %	**0.30** %	5.85 %
Woodford53	0.53 %	**0.38** %	8.22 %
Kimmeridge clay	0.96 %	**0.75** %	9.27 %
Muderong shale	0.87 %	**0.84** %	10.33 %
Cretaceous shale	**0.41** %	0.55 %	10.08 %
Clay model [37]	2.57 %	**1.00** %	14.47 %

Table 5.1: Relative error for the *global* energy release rate $\frac{|\mathcal{G}-\mathcal{G}^{app}|}{\mathcal{G}}$ for the different approximations made from Eq. (5.27), (5.28) and (5.32).

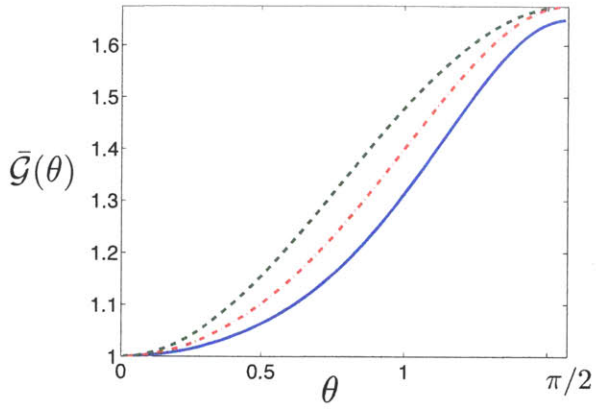

Figure 5-17: Dimensionless global energy release rate $\bar{\mathcal{G}}^{penny}(\theta)$ (blue solid line) and its approximations based on Eq. (5.33) (green dashed) and Eq. (5.34) (red dash-dotted) for the reference TI medium (see Appendix C).

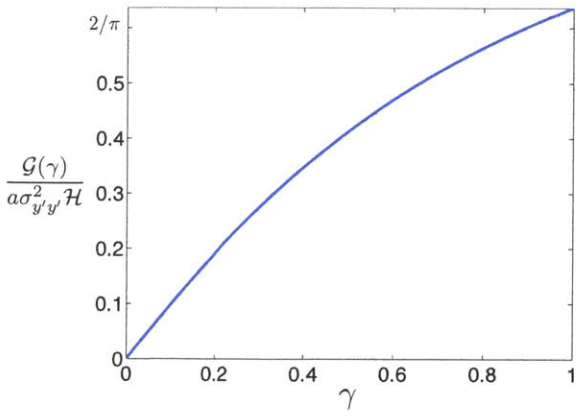

Figure 5-18: Dimensionless energy release rate as a function of the crack parameter γ for a pure Mode I loading.

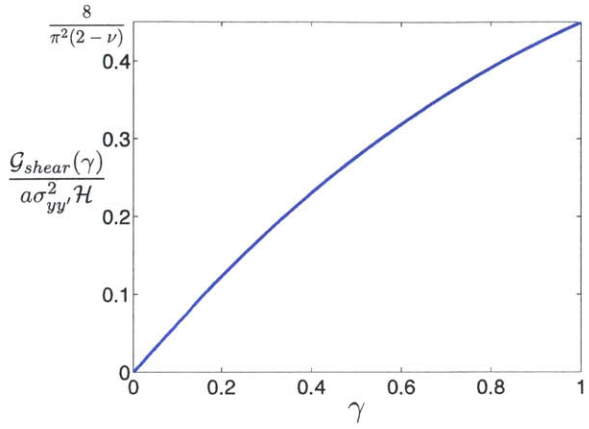

Figure 5-19: Dimensionless energy release rate as a function of the crack parameter γ for a mixed-mode II and III loading.

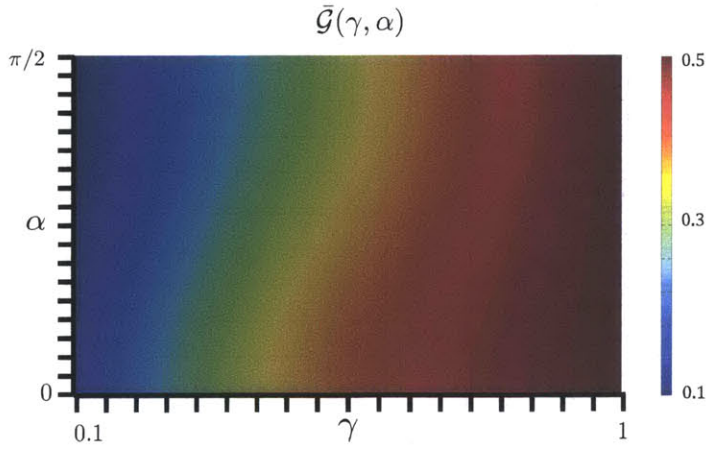

Figure 5-20: Dimensionless global energy release rate as a function of $\gamma = b/a$ and the angle α for a crack subjected to a pure pressure loading, for the clay model (see Appendix C).

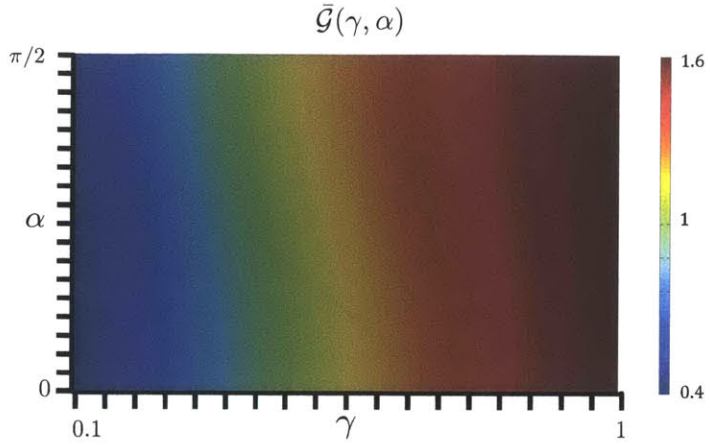

Figure 5-21: Dimensionless global energy release rate as a function of $\gamma = b/a$ and the angle α for a crack subjected to a pure pressure loading, for the reference TI material (see Appendix C).

	γ	α	$Max_\phi \left(\frac{\lvert K_I(\phi) - K_I(0) \rvert}{K_I(0)} \right)$
Isotropic	1.00	$\pi/2$	0 %
Magnesium	0.95	$\pi/2$	0.9 %
Rhenium	0.94	$\pi/2$	1.6 %
Apatite	0.81	0	2.6 %
Yttrium	0.95	$\pi/2$	1 %
Ice	0.97	$\pi/2$	1.7 %
Hafnium	0.89	$\pi/2$	0.7 %
Cadmium	0.48	0	5.0 %
Zinc	0.51	0	4.6 %
Beryllium	0.88	$\pi/2$	0.31 %
Cobalt	0.76	$\pi/2$	3.8 %
Beryl	0.84	0	1.5 %
Titanium	0.66	$\pi/2$	3.2 %
Woodford56	0.63	0	2.5 %
Woodford40	0.62	0	2.9 %
Woodford47	0.67	0	1.6 %
Woodford51	0.61	0	2.9 %
Woodford53	0.58	0	3.3 %
Kimmeridge clay	0.48	0	6.0 %
Muderong shale	0.48	0	6.4 %
Cretaceous shale	0.58	0	3.6 %
Clay model [37]	0.34	0	10.8 %

Table 5.2: Preffered crack shape (α and γ) and measure of the maximum amplitude of the Mode I stress intensity factor along the crack front ($Max_\phi \left(\frac{\lvert K_1(\phi) - K_1(0) \rvert}{K_I(0)} \right)$) for some TI crystals and shale materials using the *Constant Stress Intensity Factor Criterion*.

	γ	α	$Max_\phi\left(\frac{\lvert\mathcal{G}_\phi(\phi)-\mathcal{G}_\phi(0)\rvert}{\mathcal{G}_\phi(0)}\right)$
Isotropic	1.00	$\pi/2$	0 %
Magnesium	0.98	$\pi/2$	0.9 %
Rhenium	0.97	$\pi/2$	1.5 %
Apatite	0.90	0	2.3 %
Yttrium	0.98	$\pi/2$	1 %
Ice	0.98	$\pi/2$	1.7 %
Hafnium	0.94	$\pi/2$	0.6 %
Cadmium	0.69	0	1.8 %
Zinc	0.72	0	2 %
Beryllium	0.94	$\pi/2$	0.4 %
Cobalt	0.88	$\pi/2$	3.4 %
Beryl	0.91	0	1.3 %
Titanium	0.81	$\pi/2$	2.2 %
Woodford56	0.79	0	1.2 %
Woodford40	0.79	0	1.5 %
Woodford47	0.82	0	0.6 %
Woodford51	0.78	0	1.4 %
Woodford53	0.76	0	1.5 %
Kimmeridge clay	0.69	0	2.9 %
Muderong shale	0.69	0	3.3 %
Cretaceous shale	0.76	0	1.8 %
Clay model [37]	0.59	0	4.9 %

Table 5.3: Preffered crack shape (α and γ) and measure of the maximum amplitude of the local energy release rate along the crack front ($Max_\phi\left(\frac{\lvert\mathcal{G}_\phi(\phi)-\mathcal{G}_\phi(0)\rvert}{\mathcal{G}_\phi(0)}\right)$) for some TI crystals and shale materials using the *Constant Local Energy Release Rate Criterion.*

Chapter 6

Conclusion

6.1 Summary and main findings

We studied in this thesis how cracks propagate in anisotropic media. The problem was formulated for the case of general anisotropy, and specified for transversely isotropic media. This type of anisotropy is often used to model rock-like materials.

We first focused on cracks belonging to a plane of material symmetry which, in the case of transverse isotropy, reduces to three crack orientations: cracks in the bedding plane (horizontal cracks), cracks normal to the bedding plane (vertical cracks) and orthogonal cracks. Three elastic constants quantifying the compliance *felt* by the crack were identified. Interestingly, these elasticity constants play a role of the same importance in the indentation problem. They can be related to the indentation moduli in the vertical and horizontal directions and to the first Thomsen parameter, accessible e.g. through ultrasonic measurements.

We looked for the preferred crack orientation in the case of transverse isotropy, to answer the question in which direction is it easier to propagate an already existing crack. In isotropy, it is readily known that a crack should propagate in the direction normal to the minimum far-field stress. In anisotropy, we identified a critical crack-length below which the favored crack-orientation should be in the direction of the minimal stiffness *felt* by the crack. However, in the case of deep cracks in shale rocks, this critical crack-length is usually very small. Moreover, a stability analysis using the maximum energy release rate criterion as a kinking criterion revealed that vertical cracks were not stable for shale-like materials. This could mean that even if vertical cracks are more likely to be seen in the field, their surfaces should

exhibit a pronounced roughness.

The fluid/solid coupled crack-propagation problem was rewritten for the anisotropic case. We also accounted for the possibility of having some shear acting on the crack. This shear is due to the far-field stress anisotropy (the vertical far-field stress is usually greater in absolute value than the horizontal one). It was shown that, provided that the right elastic coefficients are used, one could take advantage of the work done on fluid-driven crack propagation in isotropic media.

We finally focused on three-dimensional cracks. We identified the relevant elastic constants for the study of a pressurized crack. These parameters are directly related to the indentation moduli in the horizontal and vertical directions. We introduced the concept of crack-shape adaptability: the ability of cracks to shape with the elasticity. An appealing criterion based on Griffith's crack propagation criterion revealed that, contrary to the isotropic case, the penny-shape might not be the preferred shape in a transversely isotropic medium. Instead, the crack shape scales linearly to quadratically with the elasticity content.

6.2 Limitations and possible future perspectives

When considering two-dimensional cracks, we saw that the work done in isotropic LEFM could be used, provided that the right elastic parameters were used. However, we did not consider at all the anisotropy of the fracture properties, that is, the variation of the fracture energy (or fracture toughness) along the crack front. We did not account for this type of anisotropy that should definitely play an important role, in addition to the elastic anisotropy.

A new way to evaluate fracture toughness at the scale of the constituents by means of molecular simulations was proposed by Brochard et al. in [8]. This approach might be a good start to assess the importance of this fracture anisotropy. Of course, more conventional experiments such a three-point bending tests could be used to investigate the fracture properties of materials depending on crack orientation, provided that large enough samples can be tested.

When considering three-dimensional cracks, the limitation of the model used in this thesis is that, contrary to the two-dimensional case, we cannot account for varying pressure on the crack-surface. Though, this is usually the case when considering a crack propagation

driven by a Newtonian fluid. Another limitation is that we can only study flat ellipsoidal cracks. These restrictions are due to the fact that Eshelby's theorem has been derived only for ellipsoidal inclusions subjected to uniform loadings. This theorem allows us to deduce how the crack displacement jump evolves on the crack surface. An extension to arbitrary crack-shapes could be of interest in order to apply more rigorously the three criteria ruling the crack-shape adaptability in anisotropy. Indeed, when considering elliptical cracks, we were not able to impose an exactly constant local energy release rate or stress intensity factor along the crack front.

A possible way to fix these drawbacks would be the use of the *boundary element method.* Lin et al. [33] provides relevant equations for the study of vertical cracks in a transversely isotropic material. This method does not have any restriction on the pressure distribution on the crack surface, nor restriction on the crack shape. Still, the boundary element method would not be able to give directly an estimation of the local energy release rate nor of the stress intensity factors. However, since it is recognized to give a pretty accurate measure of the displacements jumps, by using an Irwin matrix similar to the one introduced in this thesis, one should be able to estimate both the local energy release rate and the local stress intensity factors in terms of the displacement jumps.

Finally, it would also be of high interest to perform experiments on transversely isotropic materials to validate, if possible, the ability of cracks to shape with the elasticity.

Appendix A

Nomenclature

Symbol	Units	Description
$(\underline{e}_1, \underline{e}_2, \underline{e}_3)$	–	Canonical orthonormal basis of the material
$(\underline{e}_x, \underline{e}_y, \underline{e}_z)$	–	Orthonormal basis relevant to the problem considered
$(\underline{e}_{x'}, \underline{e}_{y'}, \underline{e}_{z'})$	–	Local crack-tip orthonormal basis when considering elliptical cracks
$\underline{v}(\underline{x}) = v_i(\underline{x})\underline{e}_i$	$[v]$	Vector field
$\underline{\underline{t}}(\underline{x}) = t_{ij}(\underline{x})\underline{e}_i \otimes \underline{e}_j$	$[t]$	Second order tensor field
$\underline{\underline{\underline{t}}}(\underline{x}) = t_{ijkl}(\underline{x})\underline{e}_i \otimes \underline{e}_j \otimes \underline{e}_k \otimes \underline{e}_l$	$[t]$	Fourth order tensor field
$[\mathcal{P}]$	–	First order tensor transformation matrix
$[\mathcal{R}]$,$[\mathcal{R}_\epsilon]$,$[\mathcal{R}_\sigma]$	–	Second order tensor transformation matrices
$\underline{\underline{\nabla v}}(\underline{x}) = \frac{\partial v_i}{\partial x_j}(\underline{x})\underline{e}_i \otimes \underline{e}_j$	$[v].\mathrm{m}^{-1}$	Gradient of a vector field
$\mathrm{div}\ \underline{\underline{t}}(\underline{x}) = \frac{\partial t_{ij}}{\partial x_j}(\underline{x})\underline{e}_i$	$[t].\mathrm{m}^{-1}$	Divergence of a second order tensor field
$\delta_{ij} = \begin{cases} 1 & \text{if } i = j \\ 0 & \text{if } i \neq j \end{cases}$	–	Kronecker delta
$\mathbb{1}$ s.t. $\mathbb{1}_{ij} = \delta_{ij}$	–	Identity matrix

$[M]^{-1}$ s.t. $[M]^{-1}.[M] = [M].[M]^{-1} = \mathbb{1}$	$[M_{ij}]$	Inverse of $[M]$
${}^t[M]$	$[M_{ij}]$	Transpose of $[M]$
$[\![X]\!](x) = X(x^+) - X(x^-)$	$[X_i]$	Jump of the field X on a plane of discontinuity
$\mathbb{R} =]-\infty, +\infty[$	–	Set of real numbers
$\mathbb{C}$	–	Set of imaginary numbers
$\mathbb{Z}$	–	Set of integers
$i \in \mathbb{C}$ s.t. $i^2 = -1$	–	Imaginary unit
$i\mathbb{R}$	–	Set of purely imaginary numbers
$\mathrm{Re}[z = a + ib] = a \in \mathbb{R}$	$[z]$	Real part of z
$\mathrm{Im}[z = a + ib] = b \in \mathbb{R}$	$[z]$	Imaginary part of z
ϵ	–	Infinitesimally small number
$\underline{\xi}(\underline{x})$	m	Displacement field
$\underline{\underline{\epsilon}}(\underline{x}) = \frac{1}{2}\left(\underline{\underline{\nabla\xi}}(\underline{x}) + {}^t\underline{\underline{\nabla\xi}}(\underline{x})\right)$	–	Strain field tensor
$\{\epsilon'\} = {}^t[\epsilon_{xx}, \epsilon_{yy}, 2\epsilon_{xy}]$	–	Plane-strain strain vector
$\underline{\underline{\sigma}}(\underline{x})$	Pa	Stress field tensor
$\{\sigma'\} = {}^t[\sigma_{xx}, \sigma_{yy}, \sigma_{xy}]$	Pa	Plane-strain stress vector
$\underline{\underline{\underline{\underline{S}}}}$ s.t. $\underline{\underline{\epsilon}} = \underline{\underline{\underline{\underline{S}}}} : \underline{\underline{\sigma}}$	Pa^{-1}	Compliance tensor
S_{ij}	Pa^{-1}	Compliance constants using Voigt notation
$[f]$	Pa^{-1}	Plane-strain compliance matrix
$\underline{\underline{\underline{\underline{C}}}}$ s.t. $\underline{\underline{\sigma}} = \underline{\underline{\underline{\underline{C}}}} : \underline{\underline{\epsilon}}$	Pa	Stiffness tensor
C_{ij}	Pa	Stiffness constants using Voigt notation
$C_{31} = \sqrt{C_{11}C_{33}} \neq C_{13}$	Pa	Definition of a *reduced* stiffness constant
E_i	Pa	Young's moduli
G_i	Pa	Shear moduli

ν_{ij}	–	Poisson's ratios
ϵ, δ and γ	–	Thomsen's parameters
Γ	m^2	Crack area
l	m	Half-length of a plane-strain crack
K_I, K_{II}, K_{III}	$\mathrm{Pa.m}^{1/2}$	Mode I, II and III stress intensity factors
$\{K\} = {}^t[K_I, K_{II}(, K_{III})]$	$\mathrm{Pa.m}^{1/2}$	Stress intensity factors vector
K_{Ic}	$\mathrm{Pa.m}^{1/2}$	Fracture toughness in Mode I
K_c	$\mathrm{Pa.m}^{1/2}$	Generalized fracture toughness
K_s, K'_s	$\mathrm{Pa.m}^{1/2}$	Scratch toughness
$\mathcal{E}_p$	J	Potential energy
$\mathcal{G} = -\frac{\partial \mathcal{E}_p}{\partial \Gamma}$	$\mathrm{J.m}^{-2}$	Energy release rate
J	$\mathrm{J.m}^{-2}$	J-integral
$\mathcal{G}_c$	$\mathrm{J.m}^{-2}$	Fracture energy
$[H]$	Pa^{-1}	The Irwin matrix defined in Eq. (2.39)
Ω_i, Ψ_i and Φ_i	Pa.m	Complex potentials
$p = w_1$	Pa	Normal stress
$q = w_2$	Pa	Shear stress
F_i	Pa.m	Stress function defined in Eq. (3.14)
G_i	Pa	Stress function defined in Eq. (3.14)
f_i, g_i	Pa	Even and odd parts of w_i
D_i	m	Displacement jump imposed in direction i
μ_i	–	Roots of the polynomial $P_{[f]}(X)$ defined in Eq. (2.25)
p_i, q_i	Pa^{-1}	Elastic constants defined in Eq. (2.28)
$[\alpha]$	Pa	Matrix of elastic constants defined in Eq. (3.25)
$[\beta] = [\mathrm{Im}\{\alpha\}]^{-1}$	Pa^{-1}	Inverse of the imaginary part of the $[\alpha]$ matrix
$\mathcal{X}$, $\mathcal{K}$, $\mathcal{Z}$, $\mathcal{H}$, $\mathcal{X}'$, $\mathcal{Z}'$, $\mathcal{H}'$	Pa^{-1}	Elastic constants defined in Eq. (3.37) and (3.42)
A, B, C, D	–	Constants defined in Eq. (3.53)
$\mathcal{V}$	m^2	Plane-strain crack volume

θ	–	Angle defining the crack orientation
ν	–	Branching angle
$K_i^\star$	$\text{Pa.m}^{1/2}$	Kinked crack stress intensity factors
$F_{ij}(\nu)$	–	Kinked crack stress intensity factors transformation matrix
p_f	Pa	Fluid pressure
η	Pa.s	Dynamic viscosity
w	m	Crack opening
Q	$\text{m}^2.\text{s}^{-1}$	Flow in the crack
σ_1, σ_3	Pa	Horizontal and vertical far-field stresses
σ_n	Pa	Normal far-field stress
τ	Pa	Shear far-field stress
$\lambda = \frac{\mathcal{H}_2}{\mathcal{H}_1}$	–	Degree of transverse isotropy
σ_{3c}	Pa	Critical stress
l_c	m	Critical crack length
k_c	$\text{Pa.m}^{1/2}$	Reduced fracture toughness
NN	–	Number of nodes
NG	–	Number of Gauss points
$P_{NG}(X)$	–	NG-th Legendre's polynomial
y_i	–	i-th root of P_{NG}
ω_i	–	Gauss weight at y_i
$\phi_k(x)$	–	Hat function of node k
$\mathbb{1}_{[a,b]}(x)$	–	Indicator function of the segment $[a, b]$
$[M]$	–	Matrix linking the dimensionless crack opening and the dimensionless pressure
$[A]$	–	Matrix linking the dimensionless stress intensity factor and the dimensionless pressure
$[J]$	–	Jacobian matrix
$[D_x]$	–	Space differentiation matrix
$*$	–	Term-by-term multiplication operator

a, b	m	Semi-major and semi-minor axes
$\gamma = b/a$	–	Inverse of the ellipse's aspect ratio
ϕ, ϕ'	–	Angles parameterizing the crack front
$R(\phi)$	m	Distance from the origin to the crack front
α	–	Angle defining the orientation of the semi-major axis
$e = \sqrt{1-\gamma^2}$	–	Ellipse's eccentricity
c	m	Ellipse's circumference
β_i	–	Dimensionless measure of the crack-opening displacement
$[R]$	–	Transformation matrix defined in Eq. (5.9)
$[T]$	–	Transformation matrix defined in Eq. (H.6)
$[\mathcal{C}]$	Pa	Matrix linking the β_i to the loading
$\mathcal{G}_\phi$	$\mathrm{J.m^{-2}}$	Local energy release rate
$[H_\phi]$	$\mathrm{Pa^{-1}}$	The local Irwin matrix
$\mathbb{E}(k)$	–	Complete elliptic integral of the second kind

Appendix B

Elastic constants

The elastic properties of a transversely isotropic material can be fully described by means of five constants. Depending on the problem considered, it will be easier to use the five compliance constants S_{ij} or the five stiffness constants C_{ij}. When considering uniaxial problems, the most relevant elastic constants are the transverse Young's modulus: $E_1 = E_2$, the longitudinal Young's modulus: E_3, the Poisson ratio for loading along the direction 3: $\nu_{13} = \nu_{23}$, the out of plane shear modulus $G_{13} = G_{23}$ and the inplane shear modulus $G_{12} = \frac{E_1}{2(1+\nu_{12})}$.
The following sections give the relationships between the different sets of constants $\{S_{11}, S_{12}, S_{13}, S_{33}, S_{44}\}$, $\{C_{11}, C_{12}, C_{13}, C_{33}, C_{44}\}$ and $\{E_1, E_3, \nu_{12}, \nu_{13}, G_{13}\}$.

B.1 Compliance constants S_{ij}

$$\begin{pmatrix} \epsilon_{11} \\ \epsilon_{22} \\ \epsilon_{33} \\ 2\epsilon_{23} \\ 2\epsilon_{13} \\ 2\epsilon_{12} \end{pmatrix} = \begin{bmatrix} S_{11} & S_{12} & S_{13} & 0 & 0 & 0 \\ S_{12} & S_{11} & S_{13} & 0 & 0 & 0 \\ S_{13} & S_{13} & S_{33} & 0 & 0 & 0 \\ 0 & 0 & 0 & S_{44} & 0 & 0 \\ 0 & 0 & 0 & 0 & S_{44} & 0 \\ 0 & 0 & 0 & 0 & 0 & 2(S_{11} - S_{12}) \end{bmatrix} \begin{pmatrix} \sigma_{11} \\ \sigma_{22} \\ \sigma_{33} \\ \sigma_{23} \\ \sigma_{13} \\ \sigma_{12} \end{pmatrix} \tag{B.1}$$

$$\begin{cases} S_{11} &= \frac{1}{E_1} \\ S_{33} &= \frac{1}{E_3} \\ S_{12} &= -\frac{\nu_{12}}{E_1} \\ S_{13} &= -\frac{\nu_{13}}{E_3} \\ S_{44} &= \frac{1}{G_{23}} \end{cases} \tag{B.2}$$

$$\begin{cases} S_{11} &= \frac{C_{11}C_{33}-C_{13}^2}{(C_{11}-C_{12})(C_{33}(C_{11}+C_{12})-2C_{13}^2)} \\ S_{33} &= \frac{C_{11}+C_{12}}{C_{33}(C_{11}+C_{12})-2C_{13}^2} \\ S_{12} &= \frac{C_{13}^2-C_{12}C_{33}}{(C_{11}-C_{12})(C_{33}(C_{11}+C_{12})-2C_{13}^2)} \\ S_{13} &= -\frac{C_{13}}{C_{33}(C_{11}+C_{12})-2C_{13}^2} \\ S_{44} &= \frac{1}{C_{44}} \end{cases} \tag{B.3}$$

B.2 Stiffness constants C_{ij}

$$\begin{pmatrix} \sigma_{11} \\ \sigma_{22} \\ \sigma_{33} \\ \sigma_{23} \\ \sigma_{13} \\ \sigma_{12} \end{pmatrix} = \begin{bmatrix} C_{11} & C_{12} & C_{13} & 0 & 0 & 0 \\ C_{12} & C_{11} & C_{13} & 0 & 0 & 0 \\ C_{13} & C_{13} & C_{33} & 0 & 0 & 0 \\ 0 & 0 & 0 & C_{44} & 0 & 0 \\ 0 & 0 & 0 & 0 & C_{44} & 0 \\ 0 & 0 & 0 & 0 & 0 & \frac{C_{11}-C_{12}}{2} \end{bmatrix} \begin{pmatrix} \epsilon_{11} \\ \epsilon_{22} \\ \epsilon_{33} \\ 2\epsilon_{23} \\ 2\epsilon_{13} \\ 2\epsilon_{12} \end{pmatrix} \tag{B.4}$$

$$\begin{cases} C_{11} &= \frac{E_1(E_1\nu_{13}^2-E_3)}{(1+\nu_{12})(2E_1\nu_{13}^2-E_3(1-\nu_{12}))} \\ C_{33} &= \frac{E_3^2(1-\nu_{12})}{E_3(1-\nu_{12})-2E_1\nu_{13}^2} \\ C_{12} &= \frac{E_1(E_3\nu_{12}+E_1\nu_{12}^2)}{(1+\nu_{12})(E_3(1-\nu_{12})-2E_1\nu_{13}^2)} \\ C_{13} &= \frac{E_1E_3\nu_{13}}{E_3(1-\nu_{12})-2E_1\nu_{13}^2} \\ C_{44} &= G_{23} \end{cases} \tag{B.5}$$

$$\begin{cases} C_{11} &= \frac{S_{11}S_{33}-S_{13}^2}{(S_{11}-S_{12})(S_{33}(S_{11}+S_{12})-2S_{13}^2)} \\ C_{33} &= \frac{S_{11}+S_{12}}{S_{33}(S_{11}+S_{12})-2S_{13}^2} \\ C_{12} &= \frac{S_{13}^2-S_{12}S_{33}}{(S_{11}-S_{12})(S_{33}(S_{11}+S_{12})-2S_{13}^2)} \\ C_{13} &= -\frac{S_{13}}{S_{33}(S_{11}+S_{12})-2S_{13}^2} \\ C_{44} &= \frac{1}{S_{44}} \end{cases} \tag{B.6}$$

B.3 Elastic constants E_i, ν_{ij} and G_{ij}

$$\begin{cases} E_1 &= \frac{1}{S_{11}} \\ E_3 &= \frac{1}{S_{33}} \\ \nu_{12} &= -\frac{S_{12}}{S_{11}} \\ \nu_{13} &= -\frac{S_{13}}{S_{33}} \\ G_{23} &= \frac{1}{S_{44}} \end{cases} \tag{B.7}$$

$$\begin{cases} E_1 &= \frac{(C_{11}-C_{12})((C_{11}+C_{12})C_{33}-2C_{13}^2)}{C_{11}C_{33}-C_{13}^2} \\ E_3 &= \frac{(C_{11}+C_{12})C_{33}-2C_{13}^2}{C_{11}+C_{12}} \\ \nu_{12} &= \frac{C_{13}^2-C_{12}C_{33}}{C_{13}^2-C_{11}C_{33}} \\ \nu_{13} &= \frac{C_{13}}{C_{11}+C_{12}} \\ G_{23} &= C_{44} \end{cases} \tag{B.8}$$

B.4 Thomsen parameters ϵ, δ and γ

The *level* of anisotropy of a transversely isotropic material can be measured through the three Thomsen parameters introduced in Ref. [44].

Their expressions in terms of the stiffness constants are:

$$\begin{cases} \epsilon &= \frac{C_{11}-C_{33}}{2C_{33}} \\ \delta &= \frac{(C_{13}+C_{44})^2-(C_{33}-C_{44})^2}{2C_{33}(C_{33}-C_{44})} \\ \gamma &= \frac{C_{66}-C_{44}}{2C_{44}} \end{cases} \tag{B.9}$$

Appendix C

Some transversely isotropic materials' constants

C.1 Elastic constants for some shale materials

Ortega gave in Ref. [37], p.131, the macroscopic stiffness constants of some shale specimens measured by acoustic emissions (Table C.1). From these five elastic constants, we computed the compliance constants (Table C.1), the Young's moduli, Poisson ratios, shear modulus, Thomsen parameters (Table C.2) and the plane-strain elastic constants introduced in Eq. (3.45) (Table C.3).

C.2 Elastic constants for some transversely isotropic crystals

Lin et al. gave in Ref. [33] the stiffness constants of some crystals gathered from the litterature (see Table C.4). From these five elastic constants, we computed the compliance constants (Table C.4), the Young's moduli, Poisson ratios, shear modulus, Thomsen parameters (Table C.5) and the plane-strain elastic constants introduced in Eq. (3.45) (Table C.6).

	C_{11}	C_{12}	C_{13}	C_{33}	C_{44}	S_{11}	S_{12}	S_{13}	S_{33}	S_{44}
Isotropic	2.67	0.67	0.67	2.67	1.00	0.42	-0.08	-0.08	0.42	1.00
Woodford56	21.20	6.30	7.90	13.80	4.90	0.06	-0.01	-0.03	0.11	0.20
Woodford40	23.10	6.90	8.80	15.70	5.20	0.06	-0.01	-0.03	0.09	0.19
Woodford47	25.60	6.10	7.70	16.00	6.60	0.05	-0.01	-0.02	0.08	0.15
Woodford51	23.80	6.20	7.80	14.90	5.30	0.05	-0.01	-0.02	0.09	0.19
Woodford53	28.00	7.50	8.30	17.30	5.60	0.04	-0.01	-0.02	0.07	0.18
Kimmeridge clay	48.40	14.40	16.40	27.30	7.80	0.03	0.00	-0.01	0.05	0.13
Muderong shale	20.00	6.80	7.60	13.00	3.00	0.07	-0.01	-0.03	0.12	0.33
Cretaceous shale	34.30	13.10	10.70	22.70	5.40	0.04	-0.01	-0.01	0.06	0.19
Clay model [37]	44.90	21.70	18.10	24.20	3.70	0.03	-0.01	-0.02	0.07	0.27

Table C.1: Stiffness and compliance constants in GPa and GPa^{-1}, respectively, for some shale [37].

	E_1	E_3	ν_{12}	ν_{13}	G_{23}	ϵ	δ	γ
Isotropic	2.40	2.40	0.20	0.20	1.00	0.00	0.00	0.00
Woodford56	16.49	9.26	0.11	0.29	4.90	0.27	0.34	0.26
Woodford40	17.95	10.54	0.11	0.29	5.20	0.24	0.26	0.28
Woodford47	21.63	12.26	0.11	0.24	6.60	0.30	0.39	0.24
Woodford51	19.49	10.84	0.11	0.26	5.30	0.30	0.28	0.33
Woodford53	23.50	13.42	0.15	0.23	5.60	0.31	0.14	0.42
Kimmeridge clay	38.01	18.73	0.12	0.26	7.80	0.39	0.19	0.59
Muderong shale	15.20	8.69	0.15	0.28	3.00	0.27	0.05	0.60
Cretaceous shale	27.04	17.87	0.28	0.23	5.40	0.26	-0.05	0.48
Clay model [37]	29.24	14.36	0.26	0.27	3.70	0.43	0.06	1.07

Table C.2: Elastic constants constants in GPa (for E_1, E_3 and G_{23}) and Thomsen parameters for some shale [37].

	$\mathcal{H}_1$	$\mathcal{H}_2$	$\mathcal{H}_3$	$\mathcal{X}_1$	$\mathcal{X}_3$	$\mathcal{X}'_1$	$\mathcal{X}'_3$
Isotropic	0.127	0.127	0.127	0.080	0.080	0.048	0.048
Woodford56	0.026	0.021	0.016	0.017	0.011	0.006	0.006
Woodford40	0.023	0.019	0.015	0.016	0.010	0.006	0.005
Woodford47	0.020	0.016	0.013	0.013	0.008	0.006	0.005
Woodford51	0.023	0.018	0.014	0.014	0.009	0.006	0.005
Woodford53	0.020	0.016	0.012	0.012	0.008	0.005	0.004
Kimmeridge clay	0.014	0.010	0.007	0.008	0.005	0.003	0.003
Muderong shale	0.032	0.026	0.018	0.019	0.012	0.007	0.006
Cretaceous shale	0.018	0.014	0.011	0.009	0.008	0.004	0.003
Clay model [37]	0.022	0.016	0.009	0.011	0.007	0.003	0.002

Table C.3: Plane-strain elastic constants constants in GPa^{-1} for some shale [37].

	C_{11}	C_{12}	C_{13}	C_{33}	C_{44}	S_{11}	S_{12}	S_{13}	S_{33}	S_{44}
Isotropic	2.67	0.67	0.67	2.67	1.00	0.42	-0.08	-0.08	0.42	1.00
Magnesium	5.92	2.57	2.14	6.14	1.64	0.22	-0.08	-0.05	0.20	0.61
Rhenium	61.20	27.00	20.60	68.30	16.20	0.02	-0.01	0.00	0.02	0.06
Apatite	16.70	1.31	6.60	14.00	6.63	0.07	0.01	-0.04	0.11	0.15
Yttrium	7.79	2.92	2.00	7.69	2.43	0.15	-0.05	-0.03	0.14	0.41
Ice	1.35	0.65	0.52	1.45	0.32	1.02	-0.41	-0.22	0.85	3.15
Hafnium	18.10	7.70	6.60	19.70	5.57	0.07	-0.02	-0.02	0.06	0.18
Cadmium	11.60	4.23	4.14	5.10	1.95	0.12	-0.01	-0.09	0.34	0.51
Zinc	16.50	3.10	5.00	6.20	3.96	0.08	0.01	-0.07	0.27	0.25
Beryllium	29.20	2.67	1.40	33.60	16.20	0.03	0.00	0.00	0.03	0.06
Cobalt	30.70	16.50	10.40	35.80	7.55	0.05	-0.02	-0.01	0.03	0.13
Beryl	28.20	9.94	6.95	24.80	6.86	0.04	-0.01	-0.01	0.04	0.15
Titanium	16.20	9.20	6.90	18.10	4.67	0.10	-0.05	-0.02	0.07	0.21
Thallium	4.08	3.54	2.90	5.28	0.73	1.04	-0.81	-0.12	0.33	1.38
Reference TI	1.10	0.10	0.48	2.38	1.00	1.00	0.00	-0.20	0.50	1.00

Table C.4: Stiffness and compliance constants in GPa and GPa^{-1}, respectively, for some transversely isotropic crystals [33].

	E_1	E_3	ν_{12}	ν_{13}	G_{23}	ϵ	δ	γ
Isotropic	2.40	2.40	0.20	0.20	1.00	0.00	0.00	0.00
Magnesium	4.53	5.06	0.35	0.25	1.64	-0.02	-0.11	0.01
Rhenium	47.13	58.68	0.38	0.23	16.20	-0.05	-0.19	0.03
Apatite	13.35	9.16	-0.13	0.37	6.63	0.10	0.58	0.08
Yttrium	6.48	6.94	0.33	0.19	2.43	0.01	-0.10	0.00
Ice	0.98	1.18	0.40	0.26	0.32	-0.03	-0.18	0.05
Hafnium	13.99	16.32	0.35	0.26	5.57	-0.04	-0.09	-0.03
Cadmium	8.15	2.93	0.11	0.26	1.95	0.64	0.85	0.44
Zinc	12.40	3.65	-0.07	0.26	3.96	0.83	2.71	0.35
Beryllium	28.91	33.48	0.09	0.04	16.20	-0.07	0.01	-0.09
Cobalt	21.11	31.22	0.49	0.22	7.55	-0.07	-0.24	-0.03
Beryl	23.82	22.27	0.30	0.18	6.86	0.07	-0.15	0.17
Titanium	10.39	14.35	0.48	0.27	4.67	-0.05	-0.10	-0.13
Thallium	0.96	3.07	0.78	0.38	0.73	-0.11	-0.16	-0.31
Reference TI	1.00	2.00	0.00	0.40	1.00	-0.27	0.04	-0.25

Table C.5: Elastic constants constants in GPa (for E_1, E_3 and G_{23}) and Thomsen parameters for some transversely isotropic crystals [33].

	$\mathcal{H}_1$	$\mathcal{H}_2$	$\mathcal{H}_3$	$\mathcal{X}_1$	$\mathcal{X}_3$	$\mathcal{X}_1'$	$\mathcal{X}_3'$
Isotropic	0.127	0.127	0.127	0.080	0.080	0.048	0.048
Magnesium	0.064	0.065	0.066	0.041	0.048	0.019	0.019
Rhenium	0.006	0.006	0.006	0.004	0.005	0.002	0.002
Apatite	0.023	0.021	0.019	0.018	0.010	0.007	0.009
Yttrium	0.047	0.046	0.048	0.028	0.033	0.016	0.015
Ice	0.292	0.302	0.307	0.181	0.227	0.083	0.080
Hafnium	0.019	0.020	0.021	0.013	0.015	0.006	0.006
Cadmium	0.069	0.046	0.032	0.045	0.022	0.013	0.010
Zinc	0.046	0.028	0.020	0.031	0.012	0.011	0.008
Beryllium	0.010	0.010	0.011	0.005	0.006	0.005	0.005
Cobalt	0.012	0.013	0.015	0.007	0.011	0.004	0.003
Beryl	0.015	0.014	0.013	0.008	0.009	0.005	0.004
Titanium	0.022	0.024	0.029	0.016	0.023	0.007	0.006
Thallium	0.114	0.129	0.316	0.091	0.295	0.021	0.021
Reference TI	0.151	0.223	0.293	0.140	0.159	0.076	0.134

Table C.6: Plane-strain elastic constants constants in GPa^{-1} for some transversely isotropic crystals [33].

Appendix D

On the rotation of tensors

Consider two orthonormal bases $(\underline{e}_1, \underline{e}_2, \underline{e}_3)$ and $(\underline{e}_x, \underline{e}_y, \underline{e}_z)$. From now on, roman subscripts (i, j) will refer to the first basis while Greek subscripts (α, β) will refer to the second one. Define $\mathcal{P}$ the 3x3 transformation (rotation) matrix such that $\underline{e}_\alpha = \mathcal{P}_{\alpha i}\underline{e}_i$. Since $\mathcal{P}$ is a rotation matrix, $\mathcal{P}^{-1} = {}^t\mathcal{P}$ and $\underline{e}_i = \mathcal{P}_{\alpha i}\underline{e}_\alpha$.

In this Appendix, we will see how to get the expression of first, second and fourth-order tensors (in a matrix form) in the basis $(\underline{e}_x, \underline{e}_y, \underline{e}_z)$ from their expression in the basis $(\underline{e}_1, \underline{e}_2, \underline{e}_3)$.

D.1 Rotation of a first-order tensor

Let $\underline{v}$ be a first-order tensor: $\underline{v} = v_i\underline{e}_i$. It can be expressed in the basis $(\underline{e}_x, \underline{e}_y, \underline{e}_z)$ as $\underline{v} = v'_\alpha\underline{e}_\alpha$ where:

$$v'_\alpha = \mathcal{P}_{\alpha i}v_i \tag{D.1}$$

Proof:

$$\begin{aligned} \underline{v} &= v_i\underline{e}_i \\ &= v_i\mathcal{P}_{\alpha i}\underline{e}_\alpha \\ &= \mathcal{P}_{\alpha i}v_i\underline{e}_\alpha \\ &= v'_\alpha\underline{e}_\alpha \end{aligned} \tag{D.2}$$

D.2 Rotation of a symmetric second-order tensor

Let $\underline{\underline{t}}$ be a *symmetric* second-order tensor: $\underline{\underline{t}} = t_{ij}\underline{e}_i \otimes \underline{e}_j$. It can be expressed in the basis $(\underline{e}_x, \underline{e}_y, \underline{e}_z)$ as $\underline{\underline{t}} = t_{\alpha\beta}\underline{e}_\alpha \otimes \underline{e}_\beta$ with:

$$ {}^{t}[t_{xx}\ t_{yy}\ t_{zz}\ t_{yz}\ t_{xz}\ t_{yz}] = [\mathcal{R}]\,{}^{t}[t_{11}\ t_{22}\ t_{33}\ t_{23}\ t_{13}\ t_{23}] \tag{D.3} $$

and where $\mathcal{R}$ is defined as:

$$ [\mathcal{R}] = \begin{bmatrix} (\mathcal{P}_{11})^2 & (\mathcal{P}_{12})^2 & (\mathcal{P}_{13})^2 & 2\mathcal{P}_{12}\mathcal{P}_{13} & 2\mathcal{P}_{11}\mathcal{P}_{13} & 2\mathcal{P}_{11}\mathcal{P}_{12} \\ (\mathcal{P}_{21})^2 & (\mathcal{P}_{22})^2 & (\mathcal{P}_{23})^2 & 2\mathcal{P}_{22}\mathcal{P}_{23} & 2\mathcal{P}_{21}\mathcal{P}_{23} & 2\mathcal{P}_{21}\mathcal{P}_{22} \\ (\mathcal{P}_{31})^2 & (\mathcal{P}_{32})^2 & (\mathcal{P}_{33})^2 & 2\mathcal{P}_{32}\mathcal{P}_{33} & 2\mathcal{P}_{31}\mathcal{P}_{33} & 2\mathcal{P}_{31}\mathcal{P}_{32} \\ \mathcal{P}_{21}\mathcal{P}_{31} & \mathcal{P}_{22}\mathcal{P}_{32} & \mathcal{P}_{23}\mathcal{P}_{33} & \mathcal{P}_{22}\mathcal{P}_{33}+\mathcal{P}_{23}\mathcal{P}_{32} & \mathcal{P}_{21}\mathcal{P}_{33}+\mathcal{P}_{23}\mathcal{P}_{31} & \mathcal{P}_{21}\mathcal{P}_{32}+\mathcal{P}_{22}\mathcal{P}_{31} \\ \mathcal{P}_{11}\mathcal{P}_{31} & \mathcal{P}_{12}\mathcal{P}_{32} & \mathcal{P}_{13}\mathcal{P}_{33} & \mathcal{P}_{12}\mathcal{P}_{33}+\mathcal{P}_{13}\mathcal{P}_{32} & \mathcal{P}_{11}\mathcal{P}_{33}+\mathcal{P}_{13}\mathcal{P}_{31} & \mathcal{P}_{11}\mathcal{P}_{32}+\mathcal{P}_{12}\mathcal{P}_{31} \\ \mathcal{P}_{11}\mathcal{P}_{21} & \mathcal{P}_{12}\mathcal{P}_{22} & \mathcal{P}_{13}\mathcal{P}_{23} & \mathcal{P}_{12}\mathcal{P}_{23}+\mathcal{P}_{13}\mathcal{P}_{22} & \mathcal{P}_{11}\mathcal{P}_{23}+\mathcal{P}_{13}\mathcal{P}_{21} & \mathcal{P}_{11}\mathcal{P}_{22}+\mathcal{P}_{12}\mathcal{P}_{21} \end{bmatrix} \tag{D.4} $$

Proof:

$$ \begin{aligned} \underline{\underline{t}} &= t_{ij}\underline{e}_i \otimes \underline{e}_j \\ &= \sum_{1\le i\le 3} t_{ii}\underline{e}_i \otimes \underline{e}_i + \sum_{1\le i<j\le 3} t_{ij}\left(\underline{e}_i \otimes \underline{e}_j + \underline{e}_j \otimes \underline{e}_i\right) \\ &= \sum_{1\le i\le 3} t_{ii} \sum_{1\le \alpha\le 3} \mathcal{P}_{\alpha i}\underline{e}_\alpha \otimes \sum_{1\le \beta\le 3} \mathcal{P}_{\beta i}\underline{e}_\beta \\ &\qquad + \sum_{1\le i<j\le 3} t_{ij}\left(\sum_{1\le \alpha\le 3} \mathcal{P}_{\alpha i}\underline{e}_\alpha \otimes \sum_{1\le \beta\le 3} \mathcal{P}_{\beta j}\underline{e}_\beta + \sum_{1\le \alpha\le 3} \mathcal{P}_{\alpha j}\underline{e}_\alpha \otimes \sum_{1\le \beta\le 3} \mathcal{P}_{\beta i}\underline{e}_\beta\right) \\ &= \sum_{1\le i\le 3}\sum_{1\le \alpha\le 3}\sum_{1\le \beta\le 3} t_{ii}\mathcal{P}_{\alpha i}\mathcal{P}_{\beta i}\underline{e}_\alpha \otimes \underline{e}_\beta \\ &\qquad + \sum_{1\le i<j\le 3}\sum_{1\le \alpha\le 3}\sum_{1\le \beta\le 3} t_{ij}\left(\mathcal{P}_{\alpha i}\mathcal{P}_{\beta j} + \mathcal{P}_{\alpha j}\mathcal{P}_{\beta i}\right)\underline{e}_\alpha \otimes \underline{e}_\beta \\ &= \sum_{1\le \alpha\le 3}\sum_{1\le \beta\le 3}\left[\sum_{1\le i\le 3} t_{ii}\mathcal{P}_{\alpha i}\mathcal{P}_{\beta i} + \sum_{1\le i<j\le 3} t_{ij}\left(\mathcal{P}_{\alpha i}\mathcal{P}_{\beta j} + \mathcal{P}_{\alpha j}\mathcal{P}_{\beta i}\right)\right]\underline{e}_\alpha \otimes \underline{e}_\beta \end{aligned} \tag{D.5} $$

Using the engineering notation, the stresses in the basis $(\underline{e}_x, \underline{e}_y, \underline{e}_z)$ can be written as $\{\sigma\}_{\underline{e}_x,\underline{e}_y,\underline{e}_z} = [\mathcal{R}_\sigma]\{\sigma\}_{\underline{e}_1,\underline{e}_2,\underline{e}_3}$ and the strains as $\{\epsilon\}_{\underline{e}_x,\underline{e}_y,\underline{e}_z} = [\mathcal{R}_\epsilon]\{\epsilon\}_{\underline{e}_1,\underline{e}_2,\underline{e}_3}$ where $[\mathcal{R}_\sigma] = [\mathcal{R}]$ and $[\mathcal{R}_\epsilon]$ is defined as:

$$[\mathcal{R}_\epsilon] = \begin{bmatrix} (\mathcal{P}_{11})^2 & (\mathcal{P}_{12})^2 & (\mathcal{P}_{13})^2 & \mathcal{P}_{12}\mathcal{P}_{13} & \mathcal{P}_{11}\mathcal{P}_{13} & \mathcal{P}_{11}\mathcal{P}_{12} \\ (\mathcal{P}_{21})^2 & (\mathcal{P}_{22})^2 & (\mathcal{P}_{23})^2 & \mathcal{P}_{22}\mathcal{P}_{23} & \mathcal{P}_{21}\mathcal{P}_{23} & \mathcal{P}_{21}\mathcal{P}_{22} \\ (\mathcal{P}_{31})^2 & (\mathcal{P}_{32})^2 & (\mathcal{P}_{33})^2 & \mathcal{P}_{32}\mathcal{P}_{33} & \mathcal{P}_{31}\mathcal{P}_{33} & \mathcal{P}_{31}\mathcal{P}_{32} \\ 2\mathcal{P}_{21}\mathcal{P}_{31} & 2\mathcal{P}_{22}\mathcal{P}_{32} & 2\mathcal{P}_{23}\mathcal{P}_{33} & \mathcal{P}_{22}\mathcal{P}_{33} + \mathcal{P}_{23}\mathcal{P}_{32} & \mathcal{P}_{21}\mathcal{P}_{33} + \mathcal{P}_{23}\mathcal{P}_{31} & \mathcal{P}_{21}\mathcal{P}_{32} + \mathcal{P}_{22}\mathcal{P}_{31} \\ 2\mathcal{P}_{11}\mathcal{P}_{31} & 2\mathcal{P}_{12}\mathcal{P}_{32} & 2\mathcal{P}_{13}\mathcal{P}_{33} & \mathcal{P}_{12}\mathcal{P}_{33} + \mathcal{P}_{13}\mathcal{P}_{32} & \mathcal{P}_{11}\mathcal{P}_{33} + \mathcal{P}_{13}\mathcal{P}_{31} & \mathcal{P}_{11}\mathcal{P}_{32} + \mathcal{P}_{12}\mathcal{P}_{31} \\ 2\mathcal{P}_{11}\mathcal{P}_{21} & 2\mathcal{P}_{12}\mathcal{P}_{22} & 2\mathcal{P}_{13}\mathcal{P}_{23} & \mathcal{P}_{12}\mathcal{P}_{23} + \mathcal{P}_{13}\mathcal{P}_{22} & \mathcal{P}_{11}\mathcal{P}_{23} + \mathcal{P}_{13}\mathcal{P}_{21} & \mathcal{P}_{11}\mathcal{P}_{22} + \mathcal{P}_{12}\mathcal{P}_{21} \end{bmatrix} \tag{D.6}$$

Moreover, these matrices satisfy: $[\mathcal{R}_\sigma]^{-1} = {}^t[\mathcal{R}_\epsilon]$.

Proof: We know from Eq. (D.3) that:

$$\{\sigma\}_{\underline{e}_x,\underline{e}_y,\underline{e}_z} = [\mathcal{R}(\mathcal{P})]\,\{\sigma\}_{\underline{e}_1,\underline{e}_2,\underline{e}_3} \tag{D.7}$$

so that:

$$\{\sigma\}_{\underline{e}_1,\underline{e}_2,\underline{e}_3} = [\mathcal{R}(\mathcal{P})]^{-1}\,\{\sigma\}_{\underline{e}_x,\underline{e}_y,\underline{e}_z} \tag{D.8}$$

But, since $\underline{e}_i = {}^t\mathcal{P}_{i\alpha}\underline{e}_\alpha$, we also have:

$$\{\sigma\}_{\underline{e}_1,\underline{e}_2,\underline{e}_3} = \left[\mathcal{R}({}^t\mathcal{P})\right]\{\sigma\}_{\underline{e}_x,\underline{e}_y,\underline{e}_z} \tag{D.9}$$

or:

$$\left[\mathcal{R}({}^t\mathcal{P})\right] = [\mathcal{R}(\mathcal{P})]^{-1} \tag{D.10}$$

Let us decompose the 6x6 matrix $\mathcal{R}(\mathcal{P})$ in four 3x3 matrices $\mathcal{R}_i$, $1 \leq i \leq 4$ as:

$$[\mathcal{R}(\mathcal{P})] = \begin{bmatrix} \mathcal{R}_1 & 2\mathcal{R}_2 \\ \mathcal{R}_3 & \mathcal{R}_4 \end{bmatrix} \tag{D.11}$$

or:

$$[\mathcal{R}_\epsilon(\mathcal{P})] = \begin{bmatrix} \mathcal{R}_1 & \mathcal{R}_2 \\ 2\mathcal{R}_3 & \mathcal{R}_4 \end{bmatrix} \tag{D.12}$$

On can notice that $\mathcal{R}({}^t\mathcal{P})$ satisfies:

$$\left[\mathcal{R}({}^t\mathcal{P})\right] = \begin{bmatrix} {}^t\mathcal{R}_1 & 2{}^t\mathcal{R}_3 \\ {}^t\mathcal{R}_2 & {}^t\mathcal{R}_4 \end{bmatrix} \tag{D.13}$$

Since $\left[\mathcal{R}({}^t\mathcal{P})\right] = [\mathcal{R}(\mathcal{P})]^{-1}$, one deduces that:

$$ {}^t[\mathcal{R}(\mathcal{P})]^{-1} = \begin{bmatrix} \mathcal{R}_1 & \mathcal{R}_2 \\ 2\mathcal{R}_3 & \mathcal{R}_4 \end{bmatrix} = [\mathcal{R}_\epsilon(\mathcal{P})] \tag{D.14} $$

D.3 Rotation of the (fourth-order) compliance tensor

In the orthonormal basis $(\underline{e}_1, \underline{e}_2, \underline{e}_3)$, the generalized Hooke's law can be written as $\epsilon_{ij} = S_{ijkl}\sigma_{kl}$ or, using the engineering notation, $\epsilon_i = S_{ij}\sigma_j$. In the rotated basis $(\underline{e}_x, \underline{e}_y, \underline{e}_z)$, it can be written as $\epsilon_\alpha = S'_{\alpha\beta}\sigma_\beta$ where:

$$ \left[S'\right] = [\mathcal{R}_\epsilon] \,.\, [\mathcal{S}] \,.\, {}^t[\mathcal{R}_\epsilon] \tag{D.15} $$

Proof:

$$ \begin{aligned} \epsilon_\alpha &= (\mathcal{R}_\epsilon)_{\alpha i}\, \epsilon_i \\ &= (\mathcal{R}_\epsilon)_{\alpha i}\, S_{ij}\sigma_j \\ &= (\mathcal{R}_\epsilon)_{\alpha i}\, S_{ij}\, (\mathcal{R})^{-1}_{j\beta}\, \sigma_\beta \\ &= (\mathcal{R}_\epsilon)_{\alpha i}\, S_{ij}\, \left({}^t\mathcal{R}_\epsilon\right)_{j\beta}\, \epsilon_\beta \\ &= S'_{\alpha\beta}\epsilon_\beta \end{aligned} \tag{D.16} $$

Appendix E

Proof that $\mu_1 + \mu_2 \in i\mathbb{R}$ and $\mu_1\mu_2 \in \mathbb{R}$ for a crack belonging to a plane of material symmetry

We have:

$$P(X) = f_{11}\left[X^4 - \frac{2f_{13}}{f_{11}}X^3 + \frac{(2f_{12}+f_{33})}{f_{11}}X^2 - \frac{2f_{23}}{f_{11}}X + \frac{f_{22}}{f_{11}}\right] \tag{E.1}$$

in addition,

$$P(X) = f_{11}(X-\mu_1)(X-\mu_2)(X-\bar{\mu}_1)(X-\bar{\mu}_2) \tag{E.2}$$

so that:

$$\begin{aligned} P(X) \;=\; f_{11}\big[&X^4 - 2\,\mathrm{Re}\left[\mu_1+\mu_2\right]X^3 + \left(|\mu_2|^2 + 4\,\mathrm{Re}\left[\mu_1\right]\mathrm{Re}\left[\mu_2\right] + |\mu_1|^2\right)X^2 \\ &-2\left(\mathrm{Re}\left[\mu_1\right]|\mu_2|^2 + \mathrm{Re}\left[\mu_2\right]|\mu_1|^2\right)X + |\mu_1|^2|\mu_2|^2\big] \end{aligned} \tag{E.3}$$

Let's write $\mu_i = a_i + ib_i$ with $(a_i, b_i) \in \mathbb{R}\mathrm{x}\mathbb{R}_*^+$. Accounting for the fact that for a crack belonging to a plane of material symmetry, $f_{13} = f_{23} = 0$, we have:

$$\begin{cases} \mathrm{Re}\left[\mu_1+\mu_2\right] &= 0 \\ \mathrm{Re}\left[\mu_1\right]|\mu_2|^2 + \mathrm{Re}\left[\mu_2\right]|\mu_1|^2 &= 0 \end{cases} \tag{E.4}$$

or,

$$\begin{cases} a_1 + a_2 &= 0 \\ a_1\left(b_2^2 - b_1^2\right) &= 0 \end{cases} \tag{E.5}$$

This can also be written as:

$$\begin{cases} a_1 = a_2 = 0 \\ \qquad\qquad \text{or} \begin{cases} a_1 = -a_2 \\ b_1 = b_2 \end{cases} \end{cases} \tag{E.6}$$

We showed that $\mathrm{Re}\,[\mu_1 + \mu_2] = 0$ so that $\mu_1 + \mu_2 \in i\mathbb{R}$.

We now want to proove that $\mu_1\mu_2 \in \mathbb{R}$:

$$\begin{aligned} \mu_1\mu_2 &= (a_1 + ib_1)(-a_1 + ib_2) \\ &= -(a_1^2 + b_1b_2) + ia_1(b_2 - b_1) \end{aligned} \tag{E.7}$$

Since $a_1 = 0$ or $b_1 = b_2$, we always have $\mathrm{Im}\,[\mu_1\mu_2] = 0$ so that $\mu_1\mu_2 \in \mathbb{R}$.

Appendix F

Computation of the energy release rate

Clapeyron's formula [45] gives:

$$\begin{aligned}
\mathcal{E}_p(l) &= -\frac{1}{2}\left\{\int_{x=-l}^{l}\left(\underline{\underline{\sigma}}.\underline{n}\right)(x^+).\underline{\xi}(x^+)dx + \int_{x=-l}^{l}\left(\underline{\underline{\sigma}}.\underline{n}\right)(x^-).\underline{\xi}(x^-)dx\right\} \\
&= -\frac{1}{2}\int_{x=-l}^{l}\left(p(x)[\![\xi_y]\!](x) + q(x)[\![\xi_x]\!](x)\right)dx \\
&= 8\pi H_{ij}\int_{x=-l}^{l} w_i(x)\int_{|x|}^{l}\frac{F_j(t)+xG_j(t)}{\sqrt{t^2-x^2}}dtdx
\end{aligned} \tag{F.1}$$

where we used Einstein summation convention and where $H_{11} = \mathcal{H}$, $H_{12} = H_{21} = -\mathcal{K}$, $H_{22} = \mathcal{H}'$, $w_1 = p$ and $w_2 = q$.
One should remark that $\mathcal{P}_i^l(x) = \int_{|x|}^{l}\frac{F_i(t)dt}{\sqrt{t^2-x^2}}$ is an even function and that $\mathcal{I}_i^l(x) = \int_{|x|}^{l}\frac{xG_i(t)dt}{\sqrt{t^2-x^2}}$ is an odd function so that:

$$\begin{aligned}
\mathcal{E}_p(l) &= 8\pi H_{ij}\int_{x=-l}^{l}\left(f_i(x)+g_i(x)\right)\left(\mathcal{P}_j^l(x)+\mathcal{I}_j^l(x)\right)dx \\
&= 16\pi H_{ij}\int_{x=0}^{l}\left(f_i(x)\mathcal{P}_j^l(x)+g_i(x)\mathcal{I}_j^l(x)\right)dx
\end{aligned} \tag{F.2}$$

Let's write $\mathcal{E}_{p,ij}^1(l) = 2\pi\int_{x=0}^{l} f_i(x)\mathcal{P}_j^l(x)dx$ and $\mathcal{E}_{p,ij}^2(l) = 2\pi\int_{x=0}^{l} g_i(x)\mathcal{I}_j^l(x)dx$.

We then have for the first term in (F.2)[1]:

$$\begin{aligned}
\frac{\mathcal{E}^1_{p,ij}(l+dl)-\mathcal{E}^1_{p,ij}(l)}{dl} &= \frac{2\pi}{dl}\left(\int_{x=0}^{l+dl} f_i(x)\mathcal{P}_j^{l+dl}(x)dx - \int_{x=0}^{l} f_i(x)\mathcal{P}_j^{l}(x)dx\right) \\
&= \frac{2\pi}{dl}\int_{x=0}^{l} f_i(x)\left(\mathcal{P}_j^{l+dl}(x)-\mathcal{P}_j^{l}(x)\right)dx \\
&= \frac{-1}{dl}\int_{x=0}^{l} f_i(x)\int_{t=l}^{l+dl}\frac{t}{\sqrt{t^2-x^2}}\int_{u=0}^{l}\frac{f_j(u)du}{\sqrt{t^2-u^2}}dtdx \\
&= \frac{-1}{dl}\int_{x=0}^{l}\int_{t=l}^{l+dl}\int_{u=0}^{l}\frac{tf_i(x)f_j(u)dudtdx}{\sqrt{t^2-x^2}\sqrt{t^2-u^2}} \\
&= \frac{-1}{dl}\int_{t=l}^{l+dl} t\left(\int_{x=0}^{l}\frac{f_i(x)dx}{\sqrt{t^2-x^2}}\right)\left(\int_{u=0}^{l}\frac{f_j(u)du}{\sqrt{t^2-u^2}}\right)dt \qquad \text{(F.3)}
\end{aligned}$$

As for the second term in (F.2), we have:

$$\begin{aligned}
\frac{\mathcal{E}^2_{p,ij}(l+dl)-\mathcal{E}^2_{p,ij}(l)}{dl} &= \frac{2\pi}{dl}\left(\int_{x=0}^{l+dl} g_i(x)\mathcal{I}_j^{l+dl}(x)dx - \int_{x=0}^{l} g_i(x)\mathcal{I}_j^{l}(x)dx\right) \\
&= \frac{2\pi}{dl}\int_{x=0}^{l} g_i(x)\left(\mathcal{I}_j^{l+dl}(x)-\mathcal{I}_j^{l}(x)\right)dx \\
&= \frac{-1}{dl}\int_{x=0}^{l} g_i(x)\int_{t=l}^{l+dl}\frac{x}{\sqrt{t^2-x^2}}\int_{u=0}^{l}\frac{g_j u(u)du}{t\sqrt{t^2-u^2}}dtdx \\
&= \frac{-1}{dl}\int_{x=0}^{l}\int_{t=l}^{l+dl}\int_{u=0}^{l}\frac{xug_i(x)g_j(u)dudtdx}{t\sqrt{t^2-x^2}\sqrt{t^2-u^2}} \\
&= \frac{-1}{dl}\int_{t=l}^{l+dl}\left(\int_{x=0}^{l}\frac{xg_i(x)dx}{\sqrt{t^2-x^2}}\right)\left(\int_{u=0}^{l}\frac{ug_j(u)du}{\sqrt{t^2-u^2}}\right)\frac{dt}{t} \qquad \text{(F.4)}
\end{aligned}$$

Taking the limit as dl goes to 0 and using the following property:

$$\lim_{\epsilon\to 0}\frac{1}{\epsilon}\int_{t=x}^{x+\epsilon} f(t)dt = f(x) \qquad \text{(F.5)}$$

one obtains from (F.3):

$$\lim_{dl\to 0}\frac{\mathcal{E}^1_{p,ij}(l+dl)-\mathcal{E}^1_{p,ij}(l)}{dl} = -l\left(\int_{u=0}^{l}\frac{f_i(u)du}{\sqrt{l^2-u^2}}\right)\left(\int_{u=0}^{l}\frac{f_j(u)du}{\sqrt{l^2-u^2}}\right) \qquad \text{(F.6)}$$

and from (F.4):

$$\lim_{dl\to 0}\frac{\mathcal{E}^2_{p,ij}(l+dl)-\mathcal{E}^2_{p,ij}(l)}{dl} = -\frac{1}{l}\left(\int_{u=0}^{l}\frac{ug_i(u)du}{\sqrt{l^2-u^2}}\right)\left(\int_{u=0}^{l}\frac{ug_j(u)du}{\sqrt{l^2-u^2}}\right) \qquad \text{(F.7)}$$

[1]We here use twice the fact that $p = q = 0$ for $x \in]l, l+dl[$ (if the crack is filled with a fluid, the fluid does not propagate as the crack does). However, this expression is also valid if $p(x)$ and $q(x)$ are uniform on $]l, l+dl[$.

Finally, putting together Eq. (F.2), (F.6) and (F.7), we have the following expression for the energy release rate:

$$\begin{aligned}\mathcal{G}(l) &= 4\Bigg\{\mathcal{H}\left[l\left(\int_{u=0}^{l}\frac{f_1(u)du}{\sqrt{l^2-u^2}}\right)^2+\frac{1}{l}\left(\int_{u=0}^{l}\frac{ug_1(u)du}{\sqrt{l^2-u^2}}\right)^2\right]\\ &\quad+\mathcal{H}'\left[l\left(\int_{u=0}^{l}\frac{f_2(u)du}{\sqrt{l^2-u^2}}\right)^2+\frac{1}{l}\left(\int_{u=0}^{l}\frac{ug_2(u)du}{\sqrt{l^2-u^2}}\right)^2\right]\\ &\quad-2\mathcal{K}'\left[l\int_{u=0}^{l}\frac{f_1(u)du}{\sqrt{l^2-u^2}}\int_{u=0}^{l}\frac{f_2(u)du}{\sqrt{l^2-u^2}}+\frac{1}{l}\int_{u=0}^{l}\frac{ug_1(u)du}{\sqrt{l^2-u^2}}\int_{u=0}^{l}\frac{ug_2(u)du}{\sqrt{l^2-u^2}}\right]\Bigg\}\end{aligned} \tag{F.8}$$

Appendix G

Near-tip displacement jump

Equation (3.44) can be written as a function of $r = l - x$ as:

$$[\![\begin{pmatrix} \xi_n \\ \xi_t \end{pmatrix}]\!](r) = -16\pi \begin{bmatrix} \mathcal{H} & -\mathcal{K} \\ -\mathcal{K} & \mathcal{H}' \end{bmatrix} \cdot \int_{t=l-r}^{l} \frac{1}{\sqrt{t^2-(l-r)^2}} \begin{pmatrix} F_1(t)+(l-r)G_1(t) \\ F_2(t)+(l-r)G_2(t) \end{pmatrix} dt \tag{G.1}$$

where F_i and G_i are given by:

$$\begin{cases} F_i(t) &= -\frac{t}{2\pi}\int_{u=0}^{t} \frac{f_i(u)du}{\sqrt{t^2-u^2}} \\ G_i(t) &= -\frac{1}{2\pi t}\int_{u=0}^{t} \frac{ug_i(u)du}{\sqrt{t^2-u^2}} \end{cases} \tag{G.2}$$

Using the following property:

$$\lim_{\epsilon\to 0}\frac{1}{\epsilon}\int_{t=x-\epsilon}^{x} f(t)dt = f(x) \tag{G.3}$$

one gets:

$$\begin{aligned} \lim_{r\to 0}\frac{1}{r}\int_{t=l-r}^{l}\frac{F_i(t)+(l-r)G_i(t)}{\sqrt{t^2-(x-r)^2}}dt &= \lim_{r\to 0}\frac{1}{r}\int_{t=l-r}^{l}\frac{1}{\sqrt{t^2-(l-r)^2}} \\ &\quad \left(-\frac{t}{2\pi}\int_{u=0}^{t}\frac{f_i(u)du}{\sqrt{t^2-u^2}} - \frac{l-r}{2\pi t}\int_{u=0}^{t}\frac{ug_i(u)du}{\sqrt{t^2-u^2}}\right)dt \\ &= \frac{1}{\sqrt{l^2-(l-r)^2}}\left(-\frac{l}{2\pi}\int_{u=0}^{l}\frac{f_i(u)du}{\sqrt{l^2-u^2}}\right. \\ &\quad \left. -\frac{l-r}{2\pi l}\int_{u=0}^{l}\frac{ug_i(u)du}{\sqrt{l^2-u^2}}\right) \end{aligned} \tag{G.4}$$

so that we have:

$$\lim_{r\to 0}\frac{1}{r}\int_{t=l-r}^{l}\frac{F_i(t)+(l-r)G_i(t)}{\sqrt{t^2-(x-r)^2}}dt \underset{r\to 0}{\sim} \frac{1}{\sqrt{2lr}}\left(\frac{-l}{2\pi}\int_{u=0}^{l}\frac{f_i(u)du}{\sqrt{l^2-u^2}} - \frac{1}{2\pi}\int_{u=0}^{l}\frac{ug_i(u)du}{\sqrt{l^2-u^2}}\right) \tag{G.5}$$

Injecting Eq. (G.5) in (G.1), one deduces that:

$$\begin{aligned}
[\![\begin{pmatrix} \xi_n \\ \xi_t \end{pmatrix}]\!](r) &\underset{r\to 0}{\sim} -16\pi\,[H]\cdot\sqrt{\frac{r}{2}} \begin{pmatrix} \frac{-\sqrt{l}}{2\pi}\int_{u=0}^{l}\frac{f_1(u)du}{\sqrt{l^2-u^2}} - \frac{1}{2\pi\sqrt{l}}\int_{u=0}^{l}\frac{ug_1(u)du}{\sqrt{l^2-u^2}} \\ \frac{-\sqrt{l}}{2\pi}\int_{u=0}^{l}\frac{f_2(u)du}{\sqrt{l^2-u^2}} - \frac{1}{2\pi\sqrt{l}}\int_{u=0}^{l}\frac{ug_2(u)du}{\sqrt{l^2-u^2}} \end{pmatrix} \\
&\underset{r\to 0}{\sim} 8\sqrt{\frac{\pi r}{2}}\,[H]\,.\,\{K\}
\end{aligned} \tag{G.6}$$

Appendix H

The three-dimensional Irwin matrix

Let $[S']$ be the compliance matrix (using Voigt notation) in the system of coordinates $(\underline{e}_{x'}, \underline{e}_{y'}, \underline{e}_{z'})$. We introduce the new compliance matrix $[M]$ such that:

$$M_{\alpha\beta} = S'_{\alpha\beta} - \frac{S'_{\alpha 3} S'_{\beta 3}}{S'_{33}} \tag{H.1}$$

Contrary to what is stated in Hoenig's original paper [26], this new compliance matrix is the one to be used when using the plane-strain condition $\epsilon_{z'z'} = 0$. Indeed, the $M_{3\alpha}$ coefficients are null so that it ensures that $\epsilon_{z'z'} = \epsilon_3 = M_{3\alpha}\sigma_\alpha = 0$.

We introduce the *Lekhnitskii's polynomials*:

$$\left\{ \begin{array}{rcl} \mathcal{L}_2(X) & = & M_{22}X^2 - 2M_{45}X + M_{44} \\ \mathcal{L}_3(X) & = & M_{15}X^3 - (M_{14} + M_{56})X^2 + (M_{25} + M_{46})X - M_{24} \\ \mathcal{L}_4(X) & = & M_{11}X^4 - 2M_{16}X^3 + (2M_{12} + M_{66})X^2 - 2M_{26}X + M_{22} \\ \mathcal{L}_6(X) & = & \mathcal{L}_4(X)\mathcal{L}_2(X) - (\mathcal{L}_3(X))^2 \end{array} \right. \tag{H.2}$$

Lekhnitskii prooved [32] that the roots of the polynomial $\mathcal{L}_6(X)$ are imaginaries. We then introduce μ_i ($i = 1, 2$ or 3) the roots of $\mathcal{L}_6$ with positive imaginary part and $\lambda_i = -\frac{\mathcal{L}_3(\mu_i)}{\mathcal{L}_2(\mu_i)}$.

Define $[p]$ the 3x3 matrix such that:

$$\left\{ \begin{array}{rcl} p_{1i} & = & M_{11}\mu_i^2 + M_{12} - M_{16}\mu_i + \lambda_i \left(M_{15}\mu_i - M_{14}\right) \\ p_{2i} & = & M_{12}\mu_i + \frac{M_{22}}{\mu_i} - M_{26} + \lambda_i \left(M_{25} - \frac{M_{24}}{\mu_i}\right) \\ p_{3i} & = & M_{14}\mu_i + \frac{M_{24}}{\mu_i} - M_{46} + \lambda_i \left(M_{45} - \frac{M_{44}}{\mu_i}\right) \end{array} \right. \tag{H.3}$$

and $[N]$ the 3x3 matrix defined as:

$$[N] = \begin{bmatrix} 1 & 1 & 1 \\ -\mu_1 & -\mu_2 & -\mu_3 \\ -\lambda_1 & -\lambda_2 & -\lambda_3 \end{bmatrix} \tag{H.4}$$

Hoenig *indirectly*[1] prooved in Ref. [27] that the Irwin matrix $[H]$ such that $\mathcal{G} = \pi^t \{K\} . [H] . \{K\}$ was equal to:

$$[H] = -\frac{1}{2\pi} [T] . \mathrm{Im} \left\{ [p] . \left[N^{-1} \right] \right\} \tag{H.5}$$

with:

$$[T] = \begin{bmatrix} 0 & 1 & 0 \\ 1 & 0 & 0 \\ 0 & 0 & 1 \end{bmatrix} \tag{H.6}$$

If two μ_i are equal, the inverse of $[N]$ is no more defined so that in this specific case, the methodology presented here should not apply. However, just as in the two-dimensional plane-strain case, this drawback can be overcome. For instance, for isotropic media where $\mu_1 = \mu_2 = \mu_3 = i$, one can compute the Irwin matrix by doing $\mu_1 \leftarrow \hat{\mu}_1 = \epsilon + i$ and $\mu_2 \leftarrow \hat{\mu}_2 = -\epsilon + i$ and by letting ϵ go to zero.

[1]Hoenig did not write Irwin's formula in a matrix form. However, we found it convenient to introduce the $[H]$ matrix just as in the two-dimensional plane-strain case.

Bibliography

[1] J.I. Adachi and E. Detournay. Self-similar solution of a plane-strain fracture driven by a power-law fluid. International Journal for Numerical and Analytical Methods in Geomechanics, 26(6):579–604, May 2002.

[2] A.-T. Akono and F.-J. Ulm. Scratch test model for the determination of fracture toughness. Engineering Fracture Mechanics, 78(2):334–342, January 2011.

[3] S. Alben. Simulating the dynamics of flexible bodies and vortex sheets. Journal of Computational Physics, 228(7):2587–2603, April 2009.

[4] A. Azhdari. Energy-release rate and crack kinking in anisotropic brittle solids. Journal of the Mechanics and Physics of Solids, 44(6):929–951, 1996.

[5] J.R. Barber. Elasticity. Solid Mechanics and Its Applications, Volume 107. Kluwer Academic Pub, 2002.

[6] D.M. Barnett and R.J. Asaro. The fracture mechanics of slit-like cracks in anisotropic elastic media. Journal of the Mechanics and Physics of Solids, 20:353–366, 1972.

[7] M. Bonnet and A. Frangi. Analyse des solides déformables par la méthode des éléments finis. Éditions de l'École Polytechnique, 2006.

[8] L. Brochard, G. Hantal, H. Laubie, F.-J. Ulm, and R. J.-M. Pellenq. Fracture Toughness Calculation by Molecular Simulation : Cases of Silica, Microporous Carbons and their Interface. Submitted, 2013.

[9] C.G. Broyden. A class of methods for solving nonlinear simultaneous equations. Mathematics of Computation, 19(92):577, October 1965.

[10] A. Bunger and E. Detournay. Experimental validation of the tip asymptotics for a fluid-driven crack. Journal of the Mechanics and Physics of Solids, 56(11):3101–3115, November 2008.

[11] R. Carbonell and J. Desroches. A comparison between a semi-analytical and a numerical solution of a two-dimensional hydraulic fracture. International journal of solids, 36:3758–3777, 1999.

[12] B. Cotterell and J.R. Rice. Slightly curved or kinked cracks. International Journal of Fracture, 16(2):155–169, 1980.

[13] S.L. Crouch and A.M. Starfield. Boundary element methods in solid mechanics. Allen & Unwin, INC., Winchester, MA 01890, USA, 1983.

[14] A. Delafargue and F.-J. Ulm. Explicit approximations of the indentation modulus of elastically orthotropic solids for conical indenters. International Journal of Solids and Structures, 41(26):7351–7360, December 2004.

[15] E. Detournay. Propagation regimes of fluid-driven fractures in impermeable rocks. International Journal of Geomechanics, (March):35–45, 2004.

[16] A.H. England and A.E. Green. Some two-dimensional punch and crack problems in classical elasticity. In Proc. Camb. Phil. Soc, volume 59, pages 489–500. Cambridge Univ Press, 1963.

[17] J.D. Eshelby. The determination of the elastic field of an ellipsoidal inclusion, and related problems. Proceedings of the Royal Society of London. Series A, Mathematical and Physical Sciences, 241(1226):376–396, 1957.

[18] V.I. Fabrikant. Non-traditional crack problem for transversely-isotropic body. European Journal of Mechanics - A/Solids, 30(6):902–912, November 2011.

[19] D.I. Garagash. Plane-strain propagation of a fluid-driven fracture during injection and shut-in: asymptotics of large toughness. Engineering Fracture Mechanics, 73(4):456–481, March 2006.

[20] D.I. Garagash and E. Detournay. Plane-strain propagation of a fluid-driven fracture: small toughness solution. Journal of Applied Mechanics, 72(6):916, 2005.

[21] J. Geertsma and F. de Klerk. A rapid method of predicting width and extent of hydraulically induced fractures. Journal of Petroleum Technology, (December):1571–1581, 1969.

[22] A.A. Griffith. The phenomena of rupture and flow in solids. Philosophical Transactions of the Royal Society of London. Series A, Containing Papers of a Mathematical or Physical Character, 221:163–198, 1921.

[23] M.E. Gurtin, E. Fried, and L. Anand. The Mechanics and Thermodynamics of Continua. Cambridge University Press, New York, 2010.

[24] É. Guyon, J.P. Hulin, and L. Petit. Hydrodynamique physique. Savoirs actuels. EDP Sciences, 2001.

[25] F.B. Hildebrand. Introduction to numerical analysis. Dover Books on Advanced Mathematics. Dover Publ., 1987.

[26] A. Hoenig. The behavior of a flat elliptical crack in an anisotropic elastic body. International Journal of Solids and Structures, 14:925–934, 1978.

[27] A. Hoenig. Near-tip behavior of a crack in a plane anisotropic elastic body. Engineering Fracture Mechanics, 16(3), 1982.

[28] P. Huerre. Mécanique des fluides, lecture notes. École Polytechnique, Palaiseau, France, 2010.

[29] G.R. Irwin. Fracture. In Handbüche der Physik, Berlin, 1958. Springer.

[30] G.R. Irwin. Crack-extension force for a part-through crack in a plate. Journal of Applied Mechanics, pages 7–10, 1962.

[31] J.-B. Leblond. Mécanique de la rupture fragile et ductile. Lavoisier, Paris, 2003.

[32] S.G. Lekhnitskii. Theory of elasticity of an anisotropic elastic body. Mir Publishers, Moscow, 1981.

[33] W. Lin and L.M. Keer. Three-dimensional analysis of cracks in layered transversely isotropic media. Proceedings of the Royal Society A: Mathematical, Physical and Engineering Sciences, 424(1867):307–322, August 1989.

[34] J.-J. Marigo. Plasticité et rupture, lecture notes. École Polytechnique, Palaiseau, France, 2010.

[35] N.I. Muskhelishvili. Some basic problems of the mathematical theory of elasticity. Springer, 1977.

[36] M. Obata and S. Nemat-Nasser. Branched cracks in anisotropic elastic solids. Journal of applied mechanics, 56:858–864, 1989.

[37] A. Ortega. Microporomechanical modeling of shale. PhD thesis, Massachusetts Institute of Technology, 2010.

[38] J.R. Rice. A path independent integral and the approximate analysis of strain concentration by notches and cracks. Journal of Applied Mechanics, 35:379–386, 1968.

[39] G.C. Sih and P.C. Paris. On cracks in rectilinearly anisotropic bodies. International Journal of Fracture, (6), 1965.

[40] I.N. Sneddon. The distribution of stress in the neighbourhood of a crack in an elastic solid. Proceedings of the Royal Society A: Mathematical, Physical and Engineering Sciences, 187(1009):229–260, October 1946.

[41] I.N. Sneddon and M. Lowengrub. Crack problems in the classical theory of elasticity. John Wiley and Sons, Inc., 1969.

[42] D.A. Spence and P. Sharp. Self-similar solutions for elastohydrodynamic cavity flow. Proceedings of the Royal Society A: Mathematical, Physical and Engineering Sciences, 400(1819):289–313, August 1985.

[43] D.A. Spence and D.L. Turcotte. Magma-driven propagation of cracks. Journal of Geophysical Research, 90(2):575–580, 1985.

[44] L. Thomsen. Weak elastic anisotropy. Geophysics, 51(10):1954–1966, 1986.

[45] F.-J. Ulm. Micromechanics and durability of solids, lecture notes. MIT, Cambridge, MA, 2012.

[46] U.S. Energy Information Administration. Annual Energy Outlook 2012. Technical report, U.S. Department of Energy, 2012.